Technical Report ECOM-0138-21-T

Reports Control Symbol
OSD-1366
February 1971

IMPEDANCE CHARACTERIZATION OF A WAVEGUIDE MICROWAVE CIRCUIT

C.E.L. Technical Report No. 208

Contract No. DAAB07-68-C-0138

DA Project No. 1H021101 A042.01.02

Prepared by

Robert L. Eisenhart

COOLEY ELECTRONICS LABORATORY
Department of Electrical Engineering
The University of Michigan
Ann Arbor, Michigan

for

U.S. Army Electronics Command, Fort Monmouth, N.J.

DISTRIBUTION STATEMENT

This document is subject to special export controls and each transmittal to foreign governments or foreign nationals may be made only with prior approval of CG, U.S. Army Electronics Command, Fort Monmouth, N. J. Attn: AMSEL-WL-S.

ABSTRACT

The induced e.m.f. method has been extended and applied to derive the driving point impedance of a common waveguide structure used for mounting small microwave devices. The resulting mathematical relationship has been conceptually interpreted as an equivalent coupling circuit, terminated by a set of impedances which are associated with the many modes within the waveguide. Properties of this circuit and its terminations are discussed in detail. In addition the multilateral nature of the circuit allows consideration of the mount in the waveguide as an obstacle to any incident propagating mode.

The driving point impedance of this mount was also considered from the experimental viewpoint. An investigation was carried out to check and support the results of the theoretical analysis. A novel measurement technique was employed, based upon the use of subminiature coaxial line to gain electrical access to a terminal pair located inside the waveguide. An extensive model of the measurement circuit was developed, which enhanced the accuracy of the data interpretation, and provided excellent agreement between these values and the theory.

Measurements of the mount as an obstacle to the H_{10} mode were made using standard waveguide techniques, and compared favorably with the theoretical predictions.

It is anticipated that this formulation will permit accurate design of many components which previously required empirical methods based on limited experimental data.

FOREWORD

This report was prepared by the Cooley Electronics Laboratory of the University of Michigan under United States Army Electronics Command Contract No. DAAB07-68-C-0138, "Countermeasures Research."

The research under this contract consists in part of an investigation to develop operational solid-state components in microwave circuits.

The material reported herein represents a summary of a theoretical and experimental study which was made to determine the impedance characteristics of a commonly used waveguide mounting structure.

TABLE OF CONTENTS

TABLE OF CONTENTS (Cont.)

LIST OF ILLUSTRATIONS

LIST OF SYMBOLS

Symbol	Meaning	Defined by or first used in
A	Region at z = 0 containing the post	Fig. 2.1
A^+, A^-	Arbitrary coefficients	Eq. B.2
A_ℓ^y	Current y-distribution normalized expansion coefficient	Eq. 2.6b
A_f^x	Current x-distribution normalized expansion coefficient	Eq. 2.6c
a	Width of the waveguide	Fig. 2.1
B	Region at z = 0 not containing the post	Fig. 2.1
B^+, B^-	Arbitrary coefficients	Eq. B.2
B_ℓ^y	Current y-distribution normalized expansion coefficient	Eq. 2.6b
B_f^x	Current x-distribution normalized expansion coefficient	Eq. 2.6c
b	Height of waveguide	Fig. 2.1
C_1, C_2	Effective discontinuity capacitances	Fig. E.1
C_D	Discontinuity capacitance	Fig. D.1a
C_{f1}, C_{f2}	Fringing capacitances in the coaxial radial line transformation	Sec. 4.3.2
C_ℓ	Coaxial line capacitance per unit length	Eq. D.3
C_o	Gap series capacitance	Fig. C.1

LIST OF SYMBOLS (Cont.)

Symbol	Meaning	Defined by or first used in
C_p	Gap parallel capacitance	Fig. C.1
C_r	Parallel plate capacitance in the radial line	Sec. 4.3.2
d	Diameter of a circular post	Sec. 2.3.2
$\bar{E}$	Electric field vector	Eq. 2.1
$\bar{E}_A$	Gap electric field vector	Sec. 2.2
$\bar{E}_{A_n}$	n^{th} harmonic of $\bar{E}_A$	Eq. 2.14
$\bar{E}_{mn}$	Transverse magnetic mode designation	Sec. 2.3.1
$\bar{E}_n$	n^{th} harmonic of $\bar{E}$	Eq. 2.14
F(y)	General distributed quantity	Eq. 2.13
f	Frequency in GHz	Sec. 4.3
$\bar{\bar{G}}(\bar{r} \| \bar{r}')$	Dyadic Green's function	Sec. 2.2
$G(\bar{r} \| \bar{r}')$	$\hat{y}\hat{y}$ portion of $\bar{\bar{G}}(\bar{r} \| \bar{r}')$	Sec. 2.3.1
$G_E(\bar{r} \| \bar{r}')$	E_{mn} mode portion of $G(\bar{r} \| \bar{r}')$	Sec. 2.3.1
$G_H(\bar{r} \| \bar{r}')$	H_{mn} mode portion of $G(\bar{r} \| \bar{r}')$	Sec. 2.3.1
$\bar{\bar{G}}_T(\bar{r} \| \bar{r}')$	Green's function for terminated waveguide	Sec. 3.4
$G_z(z \| z')$	Factor of $G(\bar{r} \| \bar{r}')$ which is a function of z	Eq. B.12
g	Gap size	Fig. 2.1

LIST OF SYMBOLS (Cont.)

Symbol	Meaning	Defined by or first used in
g'	Normalized gap size = g/b	Fig. 2.1
$g_o(z\|z')$	Free space one-dimensional Green's function	Eq. B.11
$g_T(z\|z')$	Green's function for terminated one-dimensional line	Eq. B.1
H_{mn}	Transverse electric mode designation	Sec. 2.3.1
h	Gap position (center from bottom)	Fig. 2.1
h'	Normalized gap position = h/b	Fig. 2.1
I	Total gap current	Eq. 2.16
I_n	n^{th} harmonic gap current	Eq. 2.15
$\bar{\bar{I}}\delta(\bar{r} - \bar{r}')$	Unit dyad at $\bar{r} = \bar{r}'$	Eq. 2.4
$\bar{J}$	Current density vector	Eq. 2.1
$\bar{J}_n$	n^{th} harmonic of $\bar{J}$	Eq. 2.14
J_o	Current density scale factor	Eq. 2.6a
j	Complex coefficient = $\sqrt{-1}$	Eq. 2.1
K	Scale factor for $\sum_m$	Eq. 3.1
K'	Scale factor for $\sum_n$	Eq. 3.2
k	Wave number (phase constant)	Eq. 2.1
k_g	Waveguide wave number (phase constant)	Eq. A.20

Symbol	Meaning	Defined by or first used in
k^2_{mn}	Parameter $= k_x^2 + k_y^2$	Eq. A.9a
k_x	m - eigenvalue parameter	Eq. 2.5
k_y	n - eigenvalue parameter	Eq. 2.5
L	Gap series inductance	Fig. C.1
L_1	Effective discontinuity inductance	Fig. E.1
L_c	Transition inductance for coaxial-radial line model	Sec. 4.3.2
LEN	Measurement circuit effective line length	Fig. E.1
L_ℓ	Coaxial line inductance per unit length	Eq. D.3
L_o	Discontinuity compensating inductance	Fig. D.1a
L_r	Transition inductance for coaxial-radial line model	Sec. 4.3.2
ℓ	Compensating length	Eq. D.4
ℓ_1, ℓ_2	Distances to terminations 1 and 2 from post mount plane $z = 0$	Eq. 3.6
M	Number of terms in $\sum_m$	Sec. 3.2
$\overline{M}$	Vector function	Eq. A.5
m	x-distribution eigenvalue index	Sec. 2.3.1
$\overline{m}$	Vector function	Eq. A.9a

LIST OF SYMBOLS (Cont.)

Symbol	Meaning	Defined by or first used in
N	Number of terms in $\sum_n$	Sec. 3.2
$\bar{N}$	Vector function	Eq. A.5
n	y-distribution eigenvalue index	Sec. 2.3.1
$\bar{n}$	Vector function	Eq. A.9b
$\hat{n}$	Surface normal unit vector	Eq. A.7
$\bar{P}$	Arbitrary vector coefficient	Eq. A.10
P_n	n^{th} harmonic power flow at the gap	Eq. 2.15
P_R	Total power at the gap	Eq. 2.16
$\bar{Q}$	Arbitrary vector coefficient	Eq. A.10
R	Gap series resistance	Fig. C.1
R_R	Resistive part of Z_R	Fig. 3.2
$\bar{r}$	General field point	Sec. 2.2
$\bar{r}'$	General source point	Sec. 2.2
$\bar{S}$	General vector	Eq. A.4
S_p	$\bar{E}_A$ - field y-distribution normalized expansion coefficient	Eq. 2.10b
s	Post position (center from side)	Fig. 2.1
s'	Normalized post position = s/a	Fig. 2.1
T_{mn}	Simplifying factor	Eq. A.12
t	Time/or compensating length (use is clear from context)	Sec. 2.2/ Fig. D.2

LIST OF SYMBOLS (Cont.)

Symbol	Meaning	Defined by or first used in
u(x)	Current x-distribution function	Eq. 2.6a
u(y)	Current y-distribution function	Eq. 2.6a
V	Voltage across the gap	Sec. 2.3.4
$v(x)$	$\bar{E}_A$ - field x-distribution function	Eq. 2.10a
$v(y)$	$\bar{E}_y$ - field y-distribution function	Eq. 2.10a
w	Post width (flat strip)	Fig. 2.1
w'	Normalized post width = w/a	Fig. 2.1
X_L	Post inductive reactance for H_{10} mode	Eq. 3.10a
X'_{OBS}	Obstacle reactance in shunt across the waveguide normalized to the H_{10} mode	Fig. 5.6
X_R	Reactive part of Z_R	Fig. 3.2
$\hat{x}$	Rectangular coordinate unit vector	Fig. 2.1
Y'_G	Transformed gap admittance	Eq. 3.10b
Y_R	Gap driving point admittance	Eq. 2.17b
Y'_R	Approximate value of Y_R	Eq. 3.3
$Y'_R(n\neq 0)$	Reactive effect of $n > 0$ modes in the H_{10} obstacle circuit	Eq. 3.10c
$\hat{y}$	Rectangular coordinate unit vector	Fig. 2.1
$Z(\omega)$	General frequency dependent impedance function	Sec. 1.1

LIST OF SYMBOLS (Cont.)

Symbol	Meaning	Defined by or first used in
Z_c	Characteristic impedance of one-dimensional line	Eq. B.3
Z_{cmn}	Waveguide mode (m, n) characteristic impedance	Eq. 2.24
Z_{cs}	Stripline characteristic impedance	Eq. 2.26
Z_E	Impedance component due to E_{mn} modes	Eq. 2.21c
Z_G	Terminal impedance of device in the mount	Sec. 3.5
Z_{IN}	General input impedance at a terminal	Eq. 2.27
Z_H	Impedance component due to H_{mn} modes	Eq. 2.21b
Z_{jmn}	Terminating impedance on waveguide arm j normalized to Z_{cmn}	Eq. 3.9
$Z_{\ell 1}$	Terminating impedance at ℓ_1 on one-dimensional line	Eq. B.3
Z_{mn}	Mode pair impedance	Eq. 2.21a
Z_n	n^{th} harmonic impedance component	Sec. 2.3.5
Z'_n	Approximate value of Z_n	Eq. 3.4
Z'_{OBS}	Obstacle impedance in shunt across the waveguide, normalized to the H_{10} mode	Sec. 5.3
Z_R	Gap driving point impedance	Sec. 2.3

LIST OF SYMBOLS (Cont.)

Symbol	Meaning	Defined by or first used in
Z_{Tmn}	Terminated mode pair impedance	Eq. 3.7
$\hat{z}$	Rectangular coordinate unit vector	Fig. 2.1
α	Arbitrary scalar coefficient	Eq. A.17
β	Arbitrary scalar coefficient	Eq. A.17
Γ_g	Attenuation constant for one-dimensional transmission line	Appendix B
Γ_{mn}	Waveguide attenuation constant	Eq. 2.5
γ	General phase constant	Eq. A.4
Δ	Error in Y'_R	Eq. 3.3
Δ'	Error in Z'_n	Eq. 3.4
δ_o	Mode coefficient	Eq. 2.5
ζ	Waveguide phase parameter	Eq. A.8
η	Free-space impedance = 120π ohms	Eq. 2.9
θ_f	Post width parameter	Eq. 2.8
θ_M	Truncation parameter = argument of final term of $\sum_m$	Sec. 3.2
κ_{gn}	Gap coupling factor	Eq. 2.22b
κ_{pm}	Post coupling factor	Eq. 2.22a
λ	Free-space wavelength	Eq. 2.25

LIST OF SYMBOLS (Cont.)

Symbol	Meaning	Defined by or first used in
λ_g	Waveguide wavelength	Eq. 2.25
μ_o	Permeability of free-space	Eq. 2.1
ρ_1, ρ_2	Complex voltage reflection coefficient at terminals 1, 2 on one-dimensional line	Appendix B
ρ_{1mn}, ρ_{2mn}	Complex reflection coefficients for terminations 1 and 2	Eq. 3.6
τ	Green's function termination parameter	Eq. 3.6
τ_j	Single waveguide termination parameter	Eq. 3.8
ϕ_p	Gap size parameter	Eq. 2.12
ψ_1, ψ_2	Scalar wave equation solutions	Eq. A.6
ω	Angular frequency	Eq. 2.1

LIST OF APPENDICES

CHAPTER I

INTRODUCTION

1.1 Statement of the Problem

This report is concerned with the impedance characterization of the microwave structure shown in Fig. 1.1, commonly used for mounting small microwave devices in shunt across a waveguide. The general term "impedance characterization" implies complete knowledge of the driving point and transfer impedances associated with and between each and every entry or terminal port of the mount. This information is best displayed by development of an equivalent circuit, representing the effects of the electromagnetic fields within the region of the mount. Once such a circuit is established, standard circuit analysis techniques can be applied when using the mount.

In the theoretical analysis of parametric amplifiers and frequency converters, general impedance functions $Z(\omega)$ are assumed to be known and are utilized accordingly as parameters when determining such quantities as gain, bandwidth, stability and noise figure. When designing low frequency ($<$ 100 MHz) circuits, the determination of the various impedance functions is normally straight forward and presents no particular problem. However, this is not the case when the frequencies of interest fall within the

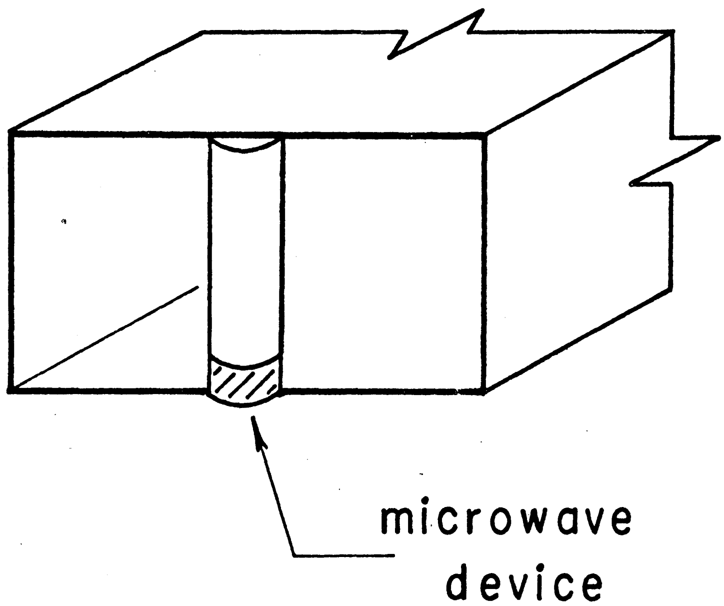

Fig. 1.1 Typical mount configuration with device mounted at the bottom of the waveguide.

microwave region. In particular, when using a structure or microwave circuit such as shown in Fig. 1.1, determination of impedance seen by the device becomes very difficult due to the complex nature of the electromagnetic fields which are involved. The question is then asked, why use such a complex structure? The answer comes from experimental work which has shown this configuration to work well for many applications because of the strong coupling between the "post" current and propagated energy within the waveguide.

The motivation for this topic came from work done by myself on parametric up-converters designed around such a waveguide circuit. It became apparent that lack of an adequate circuit description was sufficient to completely remove any chance of predictable success with the circuit.

Although initial interest in this structure was for use in parametric circuits (especially wide-band design), it was obvious a complete description would have great significance in the design of circuits for a variety of applications. In particular this method of mounting solid-state microwave source elements is very common. The mode of operation of a transferred-electron oscillator (Gunn diode) has been shown to be strongly dependent on the circuit characteristics (Ref. 1) Also, studies of the TRAPATT mode of avalanche diode operation indicate that the impedances at harmonics of the oscillation frequency affect the power output (Ref. 2). Frequency multipliers represent another area where the operation is influenced by impedances at frequencies other than the input and output (Ref. 3).

The utility and application of the work described in this report may be expressed through the following quotation, taken from a design paper by Getsinger (Ref. 4).

> "In order to reduce the approximations involved in design work it is necessary to be able to describe the circuit under consideration in mathematical terms. In order to [conceptually] relate the circuit to the real world, it is necessary to be able to interpret the circuit in terms of a physical configuration with reasonably accurate correspondence between the predicted behavior of the circuit and the measured behavior of the physical structure. This is particularly apparent in the microwave region where the electromagnetic fields are distributed throughout the entire structure constituting the circuit, rather than, as at low frequencies, being confined to individual circuit elements . . . Thus, the microwave engineer often tends to think more in terms of physical structures than in terms of conventional circuit elements. A major portion of his work is in selecting appropriate physical structures and finding dimensions which will cause the structure to yield the desired performance as a microwave component . . . Since microwave networks are made up mostly of distributed elements, impedance may be defined only at terminal surfaces. However it is possible to describe microwave network impedance variation with frequency at some terminal surface in terms of lumped-element mathematics . . ."

1.2 Topics of Investigation

The impedance characterization sought is determined by a theoretical approach, based on development of a formulation derived from a solution to Maxwell's equations. This theoretical analysis is supported by an extensive experimental effort. Both the theoretical and experimental analyses are dependent upon new techniques or procedures which are developed.

The theoretical analysis is discussed in detail. A general procedure is first developed, then applied to the specific problem outlined. All of the mount configuration parameters are left as variables, so that their significance in the resulting characterization can be determined. Of major importance in this study is the development of a thorough understanding of how these various parameters affect that characterization, allowing the possibility of some success in impedance synthesis, which is the key to successful mount design. To enhance this understanding many graphs are presented, representing various sets of parameter values, accompanied by detailed discussion of the dominant characteristics.

The initial objective was to determine the impedance seen at the terminals of the mounted device. Once completed, it was possible to interpret the resulting formulation as an equivalent circuit relating the device terminals to a set of impedances representing all the possible modes in the waveguide. The terminals associated with the propagating modes can be considered as input ports for each respective mode, thus allowing description of the mount as a load to an incident mode. This capability results in the complete characterization desired.

The experimental analysis was carried out to check and support the results of the theoretical work. Each aspect of this analysis is discussed from the design of the necessary equipment to the final results of data interpretation. Among the several items included are measurement circuit description, coaxial to radial line transformation, and multimode matching considerations.

1.3 Review of the Literature

Prior to World War II, microwave technology was not the subject of extensive research, primarily because the state of the art in frequency sources, amplifiers and other general components was not sufficiently advanced to include a wide availability of devices at such high frequencies, ($>$ 1.0 GHz). However with the advent of radar and its strong resolution dependence upon frequency, coupled to the wartime urgency, a large scale research and development requirement appeared on the scene. Through the concentrated effort of many scientists, engineers and associate co-workers the fundamentals of microwave technology as it is known today were established and documented (Ref. 5). During and following this period, very few solid-state devices were available for the microwave region. In June 1958, a paper published in the IRE Proceedings did much to introduce solid-state diodes to the microwave world (Ref. 6). This paper discussed the various properties of the diodes and uses to which their characteristics could be put.

Soon afterwards many technical papers appeared (Refs. 7 - 12). In general, these represent theoretical analyses of different types of amplifier and frequency converter circuits (includes harmonic generation) to determine characteristics such as gain, bandwidth, noise figure, stability and frequency conversion efficiency. All are quite restricted by use of many assumptions, one being the use of filters to control energy flow in the circuit.

For coaxial and stripline applications this is reasonably accurate; however, with waveguide no comprehensive circuit description has been outlined and such filters are hard to realize, presenting a major obstacle to the application of this theoretical knowledge to practical waveguide circuits. Getsinger, in 1966 and 1967 suggested a relatively simple equivalent circuit for the waveguide mount (Refs. 13, 14). A more complete description was discussed by Yamashita and Baird (Ref. 15) using the variational approach in solving for the impedance, considering the post as a radiating antenna element. Then Hanson and Rowe (Ref. 16) following a similar procedure to that of Yamashita and Baird introduced a coaxial line as a tuning stub for the circuit. An equivalent circuit was developed and used to help analyze the operation of the oscillator being investigated. These analyses have treated the impedance characterization of the mount but all have imposed unacceptable restrictions on the range of mount parameters and frequency. Usually the post is considered to be located in the center of the waveguide, and the device is positioned at the bottom of the guide. In addition the waveguide height is often reduced for matching purposes, and the frequency range is restricted to that of the dominant mode.

All of these restrictions are removed in the following analysis, which is therefore of considerable generality.

No previous work was found discussing the measurement of the device terminal impedance. This is no doubt due to the inaccessability of these terminals, using standard measurement techniques.

1.4 Report Organization

Chapter II presents the theoretical analysis both as a general procedure and as an application of this procedure towards the resolution of the impedance characterization, resulting in the determination of an equivalent circuit for the mount. This chapter is supported by Appendix A, which contains the detailed development of the waveguide dyadic Green's function. This function is necessary to describe the electric field within the guide relative to an arbitrary current element.

An interesting low frequency limiting property of the circuit is also discussed.

Chapter III points out various general properties of the equivalent circuit developed in Chapter II and considers the effect of having terminations other than a match on the waveguide ports. The necessary mathematical modifications to include the terminations are contained in Appendix B.

The chapter is concluded with a comprehensive discussion of the mount impedance as it is affected by changes in the various mount parameters, using graphs to illustrate key points. Appendix C is a short discussion of the computer program used in determining the graphs.

Chapter IV deals with the development of the equipment, techniques and procedures necessary to perform the measurement of the mount impedance. Appendices D and E support this chapter by respectively expanding the discussion of the measurement circuit and the data interpretation program.

Chapter V presents the results of the experiment and compares these results to the theoretically predicted values.

Chapter VI summarizes the report with a review consolidating the major points of the thesis to establish a perspective for the conclusions and discussion of possible areas of related future work.

CHAPTER II

THEORETICAL ANALYSIS OF THE MOUNT

2.1 Introduction

The objectives of this chapter are to 1) develop a mathematical formulation for the terminal impedance seen by a device mounted as shown in Fig. 1.1, and 2) to successfully interpret that formulation into an equivalent circuit representing the distributed circuit effects as lumped elements. It is anticipated that such an equivalent circuit will enhance understanding of the mount by providing a means to conceptually associate various circuit elements with mount characteristics.

2.2 General Analysis Procedure

The procedure utilized here is based upon an extension of the induced e.m.f. method of Carter (Ref. 17). It is presented here in a form applicable to determination of the driving point impedance of an antenna located in a region having a defined boundary, through solution of the field equation

$$\nabla \times \nabla \times \bar{E} - k^2 \bar{E} = -j \omega \mu_o \bar{J} \qquad (2.1)$$

where $\bar{E}$ and $\bar{J}$ are the electric field and current vectors and an $e^{j\omega t}$ time dependence has been assumed. For convenience, the procedure is described in the following series of steps:

Step 1: Determine the dyadic Green's function $\bar{\bar{G}}(\bar{r}|\bar{r}')$ for the region. This is expressed in the form of a series of orthogonal functions defined by the region.

Step 2: Express $\bar{J}(\bar{r})$ in a general set of orthogonal functions similar to those used in the expansion of $\bar{\bar{G}}(\bar{r}|\bar{r}')$.

Step 3: Using the equation:

$$\bar{E}(\bar{r}) = -j\,\omega\,\mu_0 \int_V \bar{\bar{G}}(\bar{r}|\bar{r}') \cdot \bar{J}(\bar{r}')\,dv' \qquad (2.2)$$

determine an expression for the electric field intensity valid anywhere within the region.

Step 4: Develop an expression for the electric field $\bar{E}_A$ at the antenna feed.

The Lorentz Reciprocity Theorem (Ref. 18) in a condensed form representing the case with perfectly conducting boundaries, establishes a direct relationship between the antenna feed $\bar{E}_A$ field expression and the general $\bar{E}(\bar{r})$ described by step 3. Consider a source current element $\bar{J}(1)$ at point 1 inside the defined region which generates a field value $\bar{E}(2)$ at point 2. Conversely if a current element $\bar{J}(2)$ aligned with $\bar{E}(2)$ generated a value $\bar{E}(1)$ at point 1, then

$$\int_V \bar{E}(1) \cdot \bar{J}(1)\, dv = \int_V \bar{E}(2) \cdot \bar{J}(2)\, dv \quad . \tag{2.3}$$

If desirable, the $\bar{E}$ - field elements can be considered the source functions and the current densities as induced, without changing the relationships in (2. 3).

Step 5: Consider then the field $\bar{E}_A$ from step 4 as the source function at point 1 and $\bar{E}(\bar{r})$ a general field value at point 2. Relating appropriate expansion terms through (2. 3) results in an infinite set of equations, each representing one of the spatial harmonic components defined by the orthogonal function expansion. These equations are individually interpreted to represent the equality between the power incident at the antenna feed point, and that radiated by the antenna for each harmonic being considered. Using the fact that the sum of each side of the infinite set of equations described represents the total power applied to the antenna terminals, an expression is found for the input impedance (antenna driving point impedance) as the sum of impedance terms representing all of the possible spatial harmonic components. An equivalent circuit is then obtained, providing interpretation of the impedance.

2.3 Post Mount Analysis

The general procedure described in the preceding section is here applied to analysis of the post mount shown in Fig. 2.1. Attention is directed initially to a mount in a waveguide which is infinite in the axial $\pm$ z directions, and the results are modified to take account of terminations in Section 3.4.

The antenna driving point impedance Z_R determined by this analysis represents the impedance seen at the terminals of a device located in the post mount.

2.3.1 Dyadic Green's Function. The dyadic Green's function $\bar{\bar{G}}(\bar{r}|\bar{r}')$ required here is the solution of the equation

$$\nabla \times \nabla \times \bar{\bar{G}}(\bar{r}|\bar{r}') - k^2 \bar{\bar{G}}(\bar{r}|\bar{r}') = \bar{\bar{I}}\, \delta(\bar{r} - \bar{r}') \qquad (2.4)$$

for the waveguide boundary conditions (Ref. 19).

$\bar{\bar{I}}\, \delta(\bar{r} - \bar{r}')$ represents the unit dyad at $\bar{r} = \bar{r}'$. Each one of the nine components of $\bar{\bar{G}}(\bar{r}|\bar{r}')$ may be interpreted as representing coupling between one component of $\bar{J}(\hat{x}, \hat{y}, \hat{z})$ and one of $\bar{E}(\hat{x}, \hat{y}, \hat{z})$. However the orientation of the post parallel to the y-axis limits $\bar{J}$ to only a y-component and also necessitates considering only the y-component of the resulting $\bar{E}$ field. Therefore only the $\hat{y}\hat{y}$-component of $\bar{\bar{G}}(\bar{r}|\bar{r}')$ is required here.

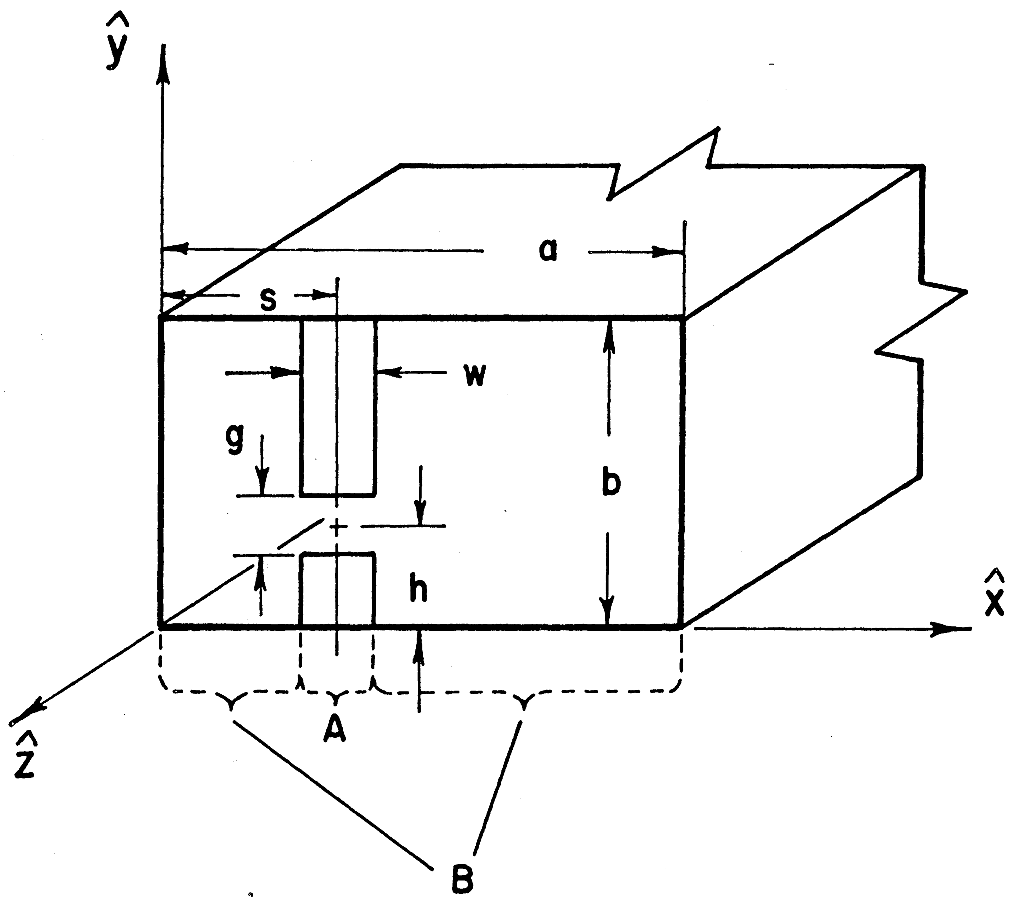

a	width of waveguide
b	height of waveguide
h	gap position (center from bottom)
s	post position (center from side)
w	post width (flat strip)
g	gap size
$s' = s/a$	normalized post position
$w' = w/a$	normalized post width
$h' = h/b$	normalized gap position
$g' = g/b$	normalized gap size

Fig. 2.1 General mount configuration with description of parameters

i.e., $$\bar{\bar{G}}(\bar{r}|\bar{r}') = \hat{y}\hat{y}\, G(\bar{r}|\bar{r}')$$

$$= \hat{y}\hat{y} \left[G_H(\bar{r}|\bar{r}') + G_E(\bar{r}|\bar{r}') \right]$$

where $G_H(\bar{r}|\bar{r}')$ represents coupling from $\bar{J}(\bar{r}')$ to H_{mn} waveguide modes and $G_E(\bar{r}|\bar{r}')$ represents coupling from $\bar{J}(\bar{r}')$ to E_{mn} waveguide modes.

This Green's function derived in Appendix A, is dependent upon two independent eigenvalues which are related to the dimensions of the waveguide. Since a complete solution requires the inclusion of all eigenvalues, a double sum results as shown in (2.5).

$$G(\bar{r}|\bar{r}') = \text{total coupling} = \sum_{m=1}^{\infty} \sum_{n=0}^{\infty} \frac{(2-\delta_o)\,(k^2-k_y^2)\, e^{-\Gamma_{mn}|z-z'|}}{ab\, k^2\, \Gamma_{mn}}$$

$$\cdot \sin k_x x \sin k_x x' \cos k_y y \cos k_y y' \qquad (2.5)$$

where

$$k_x = \frac{m\pi}{a}, \quad k_y = \frac{n\pi}{b}, \quad k = \frac{2\pi}{\lambda},$$

$$\Gamma_{mn} = (k_x^2 + k_y^2 - k^2)^{\frac{1}{2}}, \qquad \delta_o = \begin{cases} 1, & n=0 \\ 0, & n\neq 0 \end{cases}$$

with all dimensions specified in Fig. 2.1.

2.3.2 Expansion of $\bar{J}(\bar{r})$. Consider first the current density $\bar{J}(\bar{r})$. Rather than assuming a specific distribution it is more useful to expand the current in a general orthogonal set, with trigonometric functions to correspond to $G(\bar{r}|\bar{r}')$. This can be done by taking intervals $0 \rightarrow 2a$, $0 \rightarrow 2b$ for the x and y directions respectively. Then

$$\bar{J}(\bar{r}) = \hat{y}\, J_o\, u(y)\, u(x)\, \delta(z-o) \tag{2.6a}$$

$$u(y) = \sum_{\ell=o}^{\infty} \frac{2-\delta_o}{b} \left(A_\ell^y \cos \frac{\ell\pi y}{b} + B_\ell^y \sin \frac{\ell\pi y}{b}\right) \tag{2.6b}$$

$$u(x) = \sum_{f=1}^{\infty} \frac{2-\delta_o}{a} \left(A_f^x \cos \frac{f\pi x}{a} + B_f^x \sin \frac{f\pi x}{a}\right) \tag{2.6c}$$

$$\delta(z-o) = \begin{cases} 1, & z = 0 \\ 0, & \text{otherwise} \end{cases}$$

with A and B as normalized expansion coefficients.

While it is desirable to leave the y distribution in this general form, the x distribution may be specified more precisely. In particular, following the suggestion of Yamashita and Baird (Ref. 15) the circular post is here represented by an equivalent flat post or strip in the plane $z = 0$. An equivalent width (Ref. 20)

$w = 2d$, where d is the diameter of the post, was initially chosen but was subsequently reduced to $w = 1.8\,d$ because of the proximity to the waveguide walls. This effect is discussed in Section 5.3.1. The current distribution is assumed to be constant across the width of the strip, although this distribution will actually be the sum of many components related to the modes present in the surrounding region. However this assumption should yield quite good accuracy since the width will normally be small (usually $w' < 0.25$); this point is discussed further in Section 3.3. Setting

$$u(x) = \begin{cases} 1, & s - \frac{w}{2} \leq x \leq s + \frac{w}{2} \\ 0, & \text{otherwise} \end{cases} \tag{2.7}$$

results in

$$A_f^x = w \cos \frac{f\pi s}{a} \left(\frac{\sin \theta_f}{\theta_f} \right) \tag{2.8a}$$

$$B_f^x = w \sin \frac{f\pi s}{a} \left(\frac{\sin \theta_f}{\theta_f} \right) \tag{2.8b}$$

where

$$\theta_f = \frac{f\pi w}{2a} \quad .$$

2.3.3 Determination of $\bar{E}(\bar{r})$. Substituting the expanded forms for $\bar{\bar{G}}(\bar{r}|\bar{r}')$ and $\bar{J}(\bar{r})$ into (2.2), and performing the integration, yields the equation

$$\bar{E}(\bar{r}) = -\hat{y} \frac{j\eta J_o}{abk} \sum_{n=0}^{\infty} \sum_{m=1}^{\infty} \frac{(2-\delta_o)(k^2 - k_y^2)\, e^{-\Gamma_{mn}|z|}}{\Gamma_{mn}} A_n^y B_m^x$$

$$\cdot \sin k_x x \cos k_y y \,. \qquad (2.9)$$

The orthogonal properties of the integration remove dependence upon B_ℓ^y and A_f^x.

2.3.4 Expansion of $\bar{E}_A$. The assumption is made that a voltage V exists across the feed or gap g, thus specifying a constant spatial $\bar{E}$ - field $= -\frac{V}{g}$. For large gaps a set of spatially varying fields should be summed for an exact representation; however the gap considered here is sufficiently small that the approximation is good. This assumption is discussed in more detail in Section 3.3.

Considering an expansion for the field at $z = 0$ in the region A of Fig. 2.1,

$$\bar{E}_A = -\hat{y} \frac{V}{g} \, \mathfrak{v}(y) \, \mathfrak{v}(x) \, \delta(z-o) \qquad (2.10a)$$

where

$$\mathcal{v}(y) = \sum_{p=o}^{\infty} \frac{(2-\delta_o)}{b} S_p \cos \frac{p\pi y}{b} \qquad (2.10b)$$

$$\mathcal{v}(x) = 1 \qquad (2.10c)$$

S_p = normalized expansion coefficient

V = voltage across the gap .

The y-distribution function $\mathcal{v}(y)$ is expanded only in cosine terms because the rectangular waveguide will not support y-directed sinusoidally varying (with y) $\overline{E}$ - fields.

The field in region B, shown in Fig. 2.1, will not be considered further because the current $\overline{J}(\overline{r}')$ does not exist in this region - consequently the $\overline{E}$ - field there makes no contribution to the power relationship which is to be developed.

Describing the y-dependence then as

$$\mathcal{v}(y) = \begin{cases} 1, & h - \frac{g}{2} \leq y \leq h + \frac{g}{2} \quad \text{(in the gap)} \\ 0, & \text{otherwise} \quad \text{(along the strip)} \end{cases} \qquad (2.11)$$

which satisfies the zero condition along the strip, results in

$$S_p = g \cos \frac{p\pi h}{b} \left(\frac{\sin \phi_p}{\phi_p} \right) \qquad (2.12)$$

where $\phi_p = \frac{p\pi g}{2b}$, for the expansion coefficient in (2.10b).

2.3.5 Spatial Harmonic Equations. It is necessary to recognize that $\bar{E}(\bar{r})$, $\bar{E}_A$, and $\bar{J}(\bar{r})$ are all of the general form

$$F(y) = \sum_{n=0}^{\infty} F_n = \sum_{n=0}^{\infty} F' \cos \frac{n\pi y}{b} \qquad (2.13)$$

When a component $\bar{E}_j$ of $\bar{E}(\bar{r}')$ is considered as a source function at a point 1, the induced current at a point 2 must be of the same spatial harmonic, i.e., component J_j. This follows from the relationship between $\bar{E}$ and $\bar{J}$ indicated in (2.2). Therefore it follows that (2.3) holds for each spatial harmonic of the quantities involved, or

$$\int_v \bar{E}_{A_n}(1) \cdot \bar{J}_n(1)\, dv = \int_v \bar{E}_n(2) \cdot \bar{J}_n(2)\, dv$$

$$\text{for} \quad n = 0, 1, 2, \ldots \infty. \qquad (2.14)$$

The motivation for this separation of the general relationship (2.3) into a set of equations will become more apparent as the analysis proceeds.

Using (2.14), substitute in $\bar{E}(\bar{r})$, $\bar{E}_A$, and $\bar{J}(\bar{r})$ and integrate each side over the plane $z = 0$. The left hand side, representing the antenna gap field expansion becomes

$$\int_0^a \int_0^b \bar{E}_{A_n} \cdot \bar{J}_n \, dydx = - V J_o w A_n^y \left(\frac{2-\delta_o}{b}\right) \cos \frac{n\pi h}{b} \left(\frac{\sin \phi_n}{\phi_n}\right)$$

$$= - V I_n = - P_n \qquad \text{for} \quad n = 0, 1, 2, . . \infty \qquad (2.15)$$

or

$$I_n \equiv \left(\frac{2-\delta_o}{b}\right) A_n^y J_o w \cos k_y h \left(\frac{\sin \phi_n}{\phi_n}\right)$$

where P_n represents the power flow from the gap for the spatial harmonic specified by the value of n, and $\bar{J}_n$ utilizes the description in (2.7) for u(x) to correspond to $v(x)$ in $\bar{E}_{A_n}$.

The total radiated power P_R will then be equal to the sum of all of these power terms and can be represented in terms of the gap voltage and total current I as

$$P_R = V I = \sum_{n=0}^{\infty} P_n = \sum_{n=0}^{\infty} V I_n \qquad (2.16)$$

By defining

$$Z_R \equiv \text{Gap driving point impedance} = \frac{V}{I}$$

and

$$Z_n \equiv \text{Impedance related to } n^{th} \text{ harmonic} = \frac{V}{I_n} = \frac{P_n}{I_n^2} = \frac{V^2}{P_n}$$

we have

$$\frac{V^2}{Z_R} = \sum_{n=0}^{\infty} \frac{V^2}{Z_n} = V^2 \sum_{n=0}^{\infty} \frac{1}{Z_n} \tag{2.17a}$$

hence

$$\frac{1}{Z_R} = \sum_{n=0}^{\infty} \frac{1}{Z_n} = Y_R . \tag{2.17b}$$

This impedance relationship is represented by the parallel circuit of Fig. 2.2a.

<u>2.3.6 Determination of Impedance Components.</u> The values for the individual Z_n components are found by evaluating the right hand side of (2.14) by integrating to get

$$P_n = \frac{j\,\eta\, J_o^{\,2}\, w^2\, (2-\delta_o)\, (k^2 - k_y^{\,2})\, A_n^{y^2}}{a\, k\, b} \sum_{m=1}^{\infty} \frac{\sin^2 k_x s}{\Gamma_{mn}} \left(\frac{\sin \theta_m}{\theta_m}\right)^2$$

$$\text{for} \quad n = 0, 1, 2, \ldots \infty \tag{2.18}$$

this time utilizing (2.6c) for $u(x)$ to correspond to $\bar{E}(\bar{r})$. Since

$$Z_n = \frac{P_n}{I_n^{\,2}}$$

it follows that

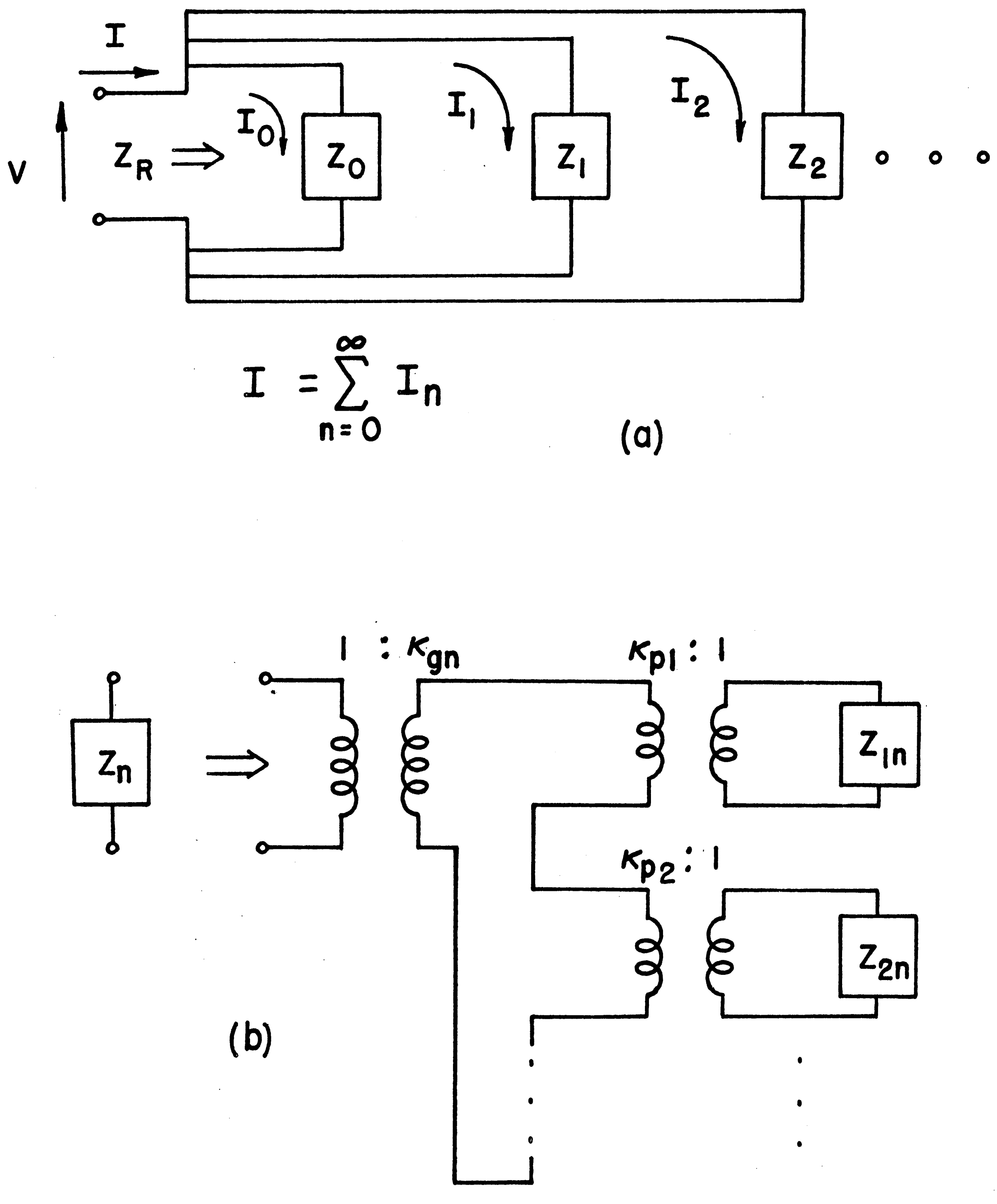

Fig. 2.2 Circuit relationships
(a) Generalized circuit for gap driving point impedance Z_R.
(b) Coupling network for a typical parallel set.

$$Z_n = \frac{j\,\eta\, b(k^2 - k_y^{\,2})}{a\,k(2-\delta_o)\cos^2 k_y h \left(\frac{\sin\phi_n}{\phi_n}\right)^2} \sum_{m=1}^{\infty} \frac{\sin^2 k_x s}{(k_x^{\,2} + k_y^{\,2} - k^2)^{\frac{1}{2}}} \left(\frac{\sin\theta_m}{\theta_m}\right)^2$$

$$\text{for} \quad n = 0, 1, 2, \ldots \infty. \qquad (2.19)$$

The required impedance Z_R is found by summation, in accord with (2.17).

It is very worthwhile to note at this time the lack of dependence of the impedance function Z_n on the assumed current distribution in the y-direction u(y). This agrees with the notion that both the current distribution and the impedance are independently determined by the physical configuration. However, as a consequence of the above development, the y-directed current expansion coefficients A^y_n, and hence the total current distribution can now be determined.

Using

$$I_n = \frac{V}{Z_n}$$

and substituting from (2.15) and (2.19) results in

$$A_n^y = \frac{V\ a\ k \cos k_y h \left(\frac{\sin \phi_n}{\phi_n}\right)}{j\,\eta\, J_o\, w(k^2 - k_y^2) \left[\sum_{m=1}^{\infty} \frac{\sin^2 k_x s}{(k_x^2 + k_y^2 - k^2)^{\frac{1}{2}}} \left(\frac{\sin \theta_m}{\theta_m}\right)^2\right]}$$

for $n = 0, 1, 2, \ldots \infty$ (2.20)

which can be substituted in (2.6b). Equation (2.20) has both real and imaginary parts representing respectively the current contributions along the post due to propagating and evanescent modes.

<u>2.3.7 Mode Pair Impedances.</u> It is clear from (2.17) that the total impedance Z_R is made up of the parallel connection of an infinite number of sets each one of which contains an infinite sum of terms, thus representing all of the possible modes in the waveguide. This formulation readily permits relating each impedance component to a specific mode pair impedance, defined as:

$$Z_{mn} \equiv \frac{j\,\eta\, b}{a\,k} \frac{(k^2 - k_y^2)}{(2-\delta_o)\,(k_x^2 + k_y^2 - k^2)^{\frac{1}{2}}} = Z_H + Z_E \quad (2.21a)$$

$$Z_H = \frac{j\,\eta\, b}{a(2-\delta_o)} \left(\frac{k}{(k_x^2 + k_y^2 - k^2)^{\frac{1}{2}}}\right)\left(\frac{k_x^2}{k_x^2 + k_y^2}\right) \quad (2.21b)$$

$$Z_E = \frac{-j\,\eta\, b}{a(2-\delta_o)} \left(\frac{(k_x^2 + k_y^2 - k^2)^{\frac{1}{2}}}{k}\right)\left(\frac{k_y^2}{k_x^2 + k_y^2}\right) \quad (2.21c)$$

representing a series combination of the H_{mn} and E_{mn} mode contributions for a (m, n) set. For frequencies below the cutoff frequency the impedance Z_H contributed by the H_{mn} mode is inductive and Z_E for the E_{mn} mode capacitive; consequently the combination has a resonant frequency, as shown in Fig. 2.3. This resonance produces the zero in the reactive region which, as seen from (2.21), occurs when $k = k_y$. Since $k_y = \frac{n\pi}{b}$, the zero is dependent only on n and the guide height b. It should also be noted that (2.21) is a function only of the waveguide dimensions a, b and the eigenvalues chosen.

The equations for Z_H and Z_E are derived separately by using $G_H(\bar{r}|\bar{r}')$ or $G_E(\bar{r}|\bar{r}')$ respectively. They are not normally considered separately however, unless it is desirable to perhaps determine power levels of distinct modes. Z_{mn} is more convenient as a composite effect in the circuit.

The remaining terms in (2.19) are then interpreted as coupling factors which determine the coupling of the strip and gap to a particular mode pair impedance, and which are a function of width and position of both strip and gap. In other words, all of the mode pair impedances Z_{mn} exist for a given waveguide, but their coupling to the mount is determined by the mount configuration. Defining

$$\text{Post coupling factor} \quad \kappa_{pm} = \sin k_x s \left(\frac{\sin \theta_m}{\theta_m} \right) \qquad (2.22a)$$

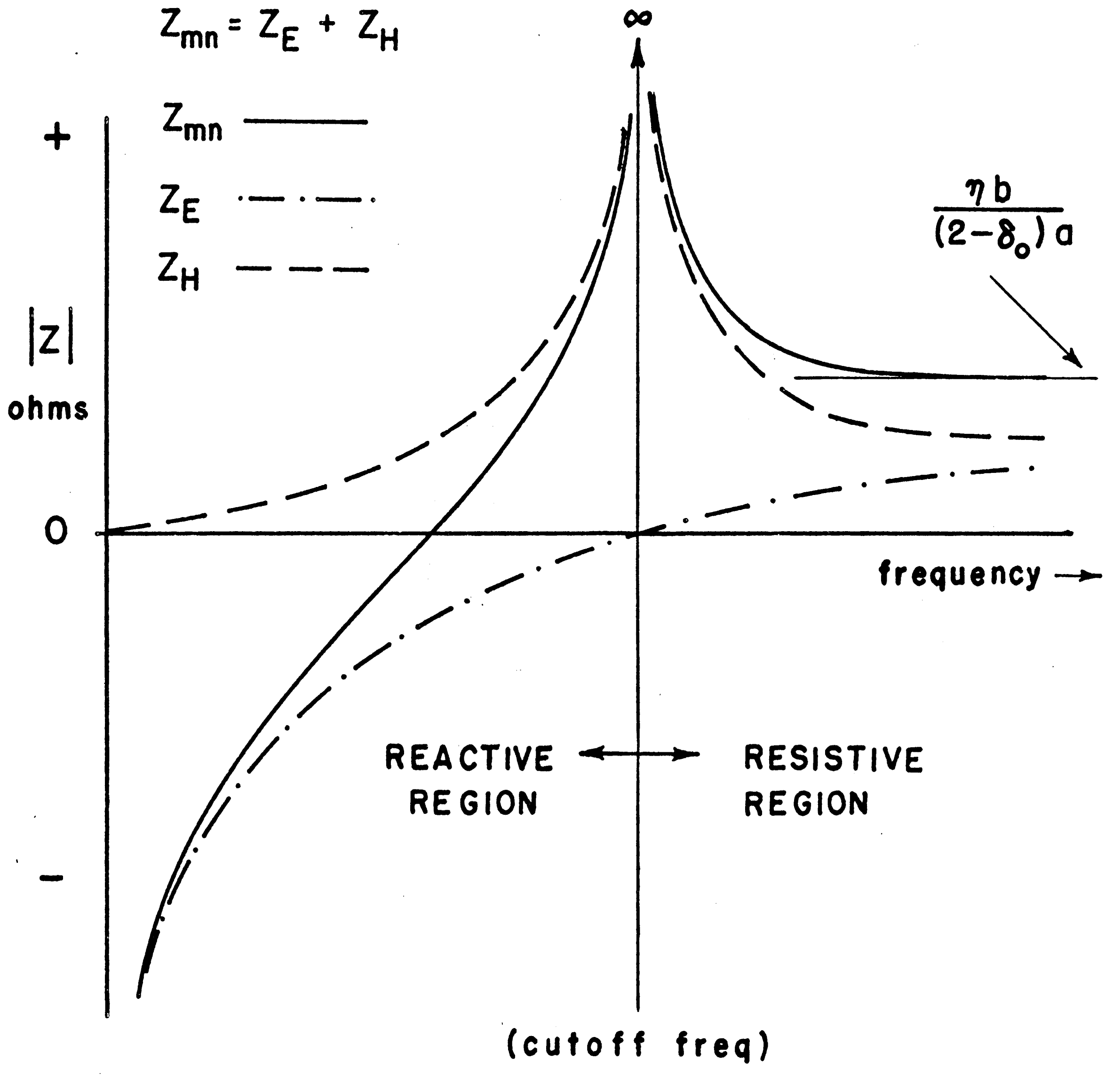

Fig. 2.3 Mode pair impedance plot.

$$\text{Gap coupling factor} \quad \kappa_{gn} = \cos k_y h \left(\frac{\sin \phi_n}{\phi_n} \right) \qquad (2.22b)$$

(2.19) may be expressed as

$$Z_n = \sum_{m=1}^{\infty} Z_{mn} \left(\frac{\kappa_{pm}}{\kappa_{gn}} \right)^2 \quad \text{for} \quad n = 0, 1, 2, \ldots \infty \qquad (2.23)$$

which is shown schematically in Fig. 2.2b.

The symmetry of the post mount about $z = 0$ along the z-axis suggests separating Z_{mn} into two parallel components, each representing the impedance associated with either the positive or negative z-direction. As shown in Fig. 2.4

$$Z_{cmn} \equiv \text{Characteristic impedance of the waveguide} = 2Z_{mn}. \qquad (2.24)$$

In particular for the dominant H_{10} mode

$$Z_{c10} = \frac{2\eta b}{a} \frac{k}{(k^2 - k_x^2)^{\frac{1}{2}}} = \frac{2\eta b}{a} \left(\frac{\lambda_g}{\lambda} \right) \qquad (2.25)$$

which agrees exactly with Schelkunoff's power-voltage definition of characteristic impedance (Ref. 21) for waveguide.

Since the mode pair impedance can be associated directly with the impedances which the waveguide presents at the plane $z = 0$ for the $\pm$ z-directions, it is most convenient to interpret Z_{mn} as

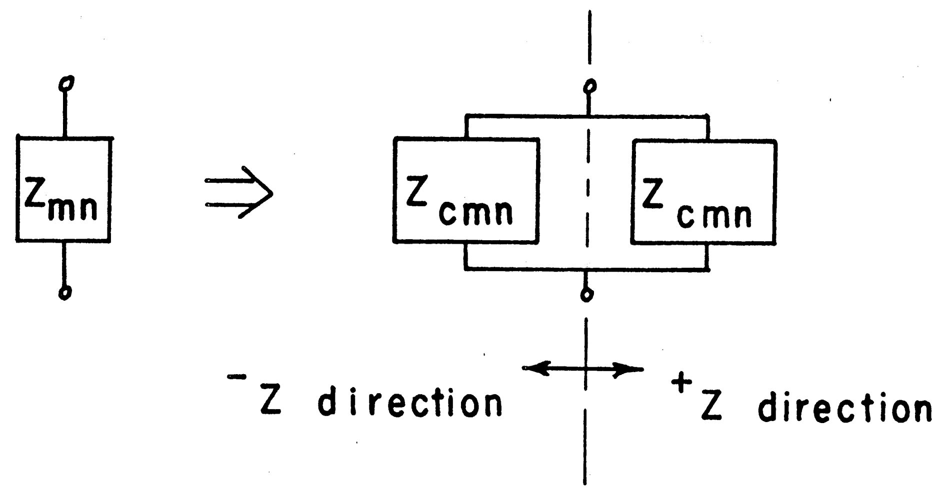

Fig. 2.4 Parallel effect of waveguide arms.

being a termination on the mount. With this in mind the equivalent circuit of the post mount is defined as that portion of the total circuit consisting only of the parallel sets of ideal coupling transformers which provide connection between the gap-post and all of the individual ports of the modes, exclusive of the terminations. In other words the equivalent circuit is strictly a coupling circuit defined at the plane $z = 0$ and therefore not containing any energy storage or dissipative capability. This equivalent circuit is shown in Fig. 2.5.

2.4 Z_R Low Frequency Limit

If the gap position is chosen to be adjacent to the bottom of the the waveguide, it is possible to consider the mount as a short length of transmission line with its axis in the y-direction, terminated by a short circuit at $y = b$ (i.e., the top of the waveguide) (Ref. 22). The cross-section of this line would be represented by two infinite ground planes with a thin post as center conductor, as seen in Fig. 2.6a. Standard strip-line, having a characteristic impedance of

$$Z_{cs} \cong 60 \ln \left(\frac{8a}{\pi w}\right) \tag{2.26}$$

for $\frac{a}{w} > 2.0$, is shown in Fig. 2.6b (Ref. 23). Fortunately, for such a restriction on w, the characteristic impedance is relatively

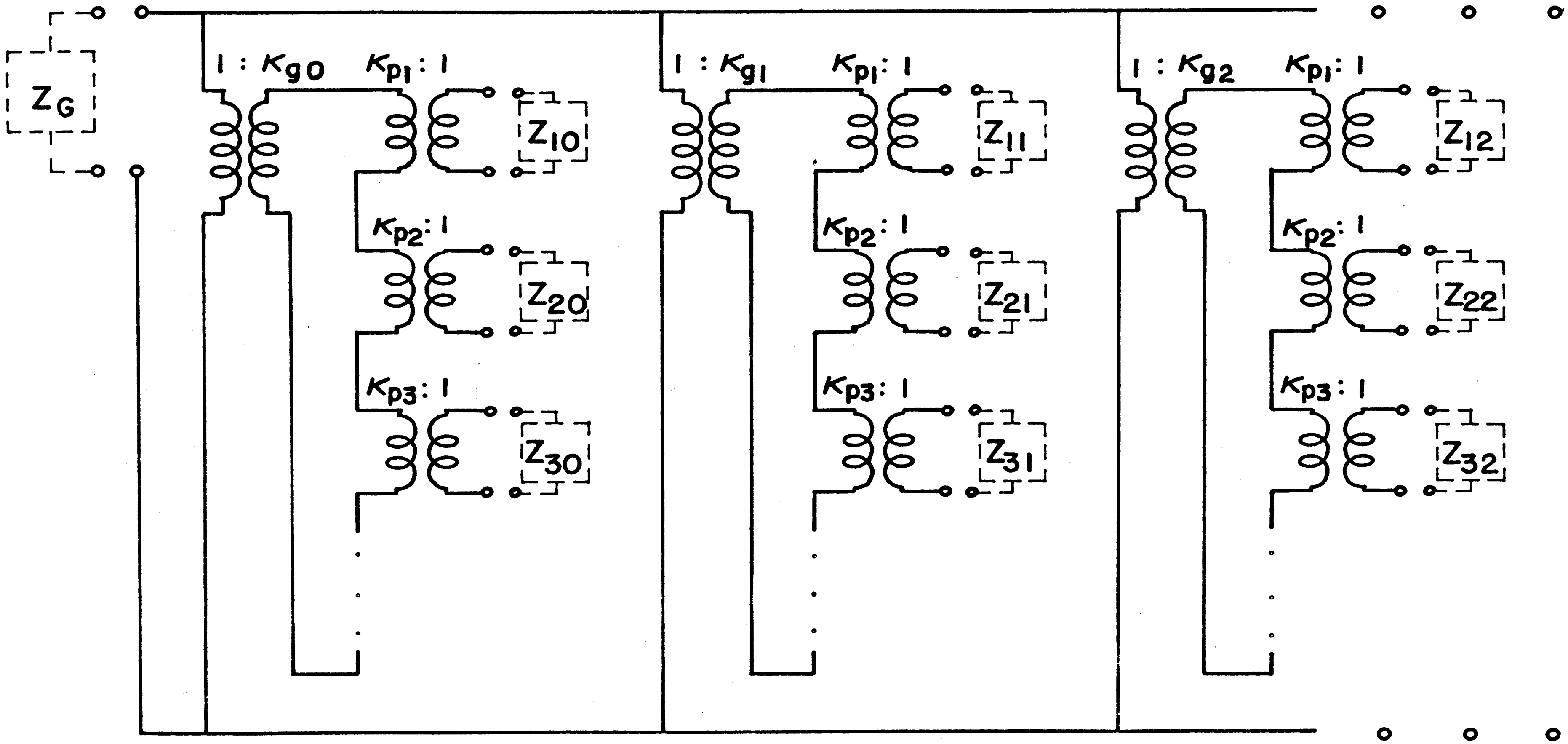

Fig. 2.5 Equivalent circuit of post mount

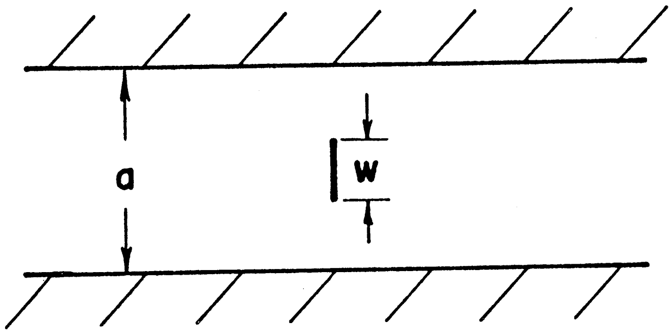

(a)

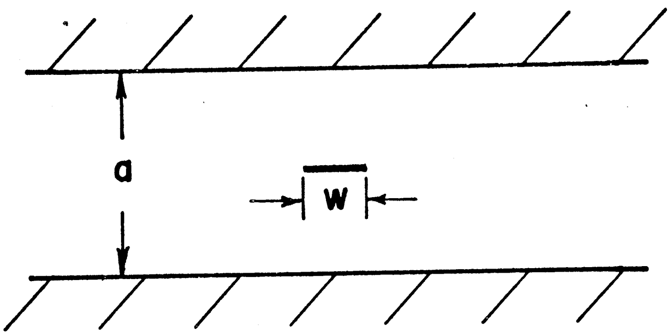

(b)

Fig. 2.6 Cross-sectional view of
(a) Waveguide mount for TEM mode
(b) Standard stripline

independent (error $< 3\%$) of the angular orientation of the center conductor with respect to the sides, so that (2.26) also represents the characteristic impedance of Fig. 2.6a. The impedance at the gap is then equivalent to the input impedance of this shorted transmission line, or

$$Z_{IN} = j\, Z_c \tan(k\,l) \tag{2.27}$$

which becomes

$$Z_{IN} = j\, \frac{\eta\, b}{\lambda}\, \ln\left(\frac{8a}{\pi w}\right) \tag{2.28}$$

for $l = b$ and $kb << 1.0$ in the low frequency case.

Looking next at Z_R we find that for k very small, Z_n for $n \geq 1$ becomes very large relative to Z_o (i.e., $n = 0$) such that the parallel effects of Z_n, $n \geq 1$, can be neglected in Fig. 2.2a. Therefore

$$Z_R \cong Z_o = \frac{j\,\eta\, b\, k}{a} \sum_{m=1}^{\infty} \frac{\sin^2 k_x s}{k_x} \left(\frac{\sin \theta_m}{\theta_m}\right)^2 \tag{2.29}$$

Placing the center conductor at $s = a/2$ to correspond to Fig. 2.6a gives a further reduction of

$$Z_R \cong \frac{j\,\eta\, b\, 8}{\lambda} \left(\frac{a}{\pi w}\right)^2 \sum_{\substack{m=1,\,3 \\ \text{odd}}}^{\infty} \frac{\sin^2 \theta_m}{m^3}\,. \tag{2.30}$$

Using the trigonometric identity

$$\sin^2 \gamma = \tfrac{1}{2}(1 - \cos 2\gamma) \tag{2.31}$$

and the necessary series expansion relationship (Ref. 18, p. 580) results in

$$Z_R \cong \frac{j\eta b}{\lambda} \ln\left(\frac{9a}{\pi w}\right), \tag{2.32}$$

showing very good agreement with (2.28). This demonstrates that the reactive energy stored in this physical structure is, as expected, independent of the method of analysis.

CHAPTER III

PROPERTIES OF THE EQUIVALENT CIRCUIT

3.1 Introduction

The objective of this chapter is to develop familiarity with the equivalent circuit through discussion of the various properties. Initially we review the more general properties such as convergence, error and reciprocity; then we conclude by considering the effect of variation in the circuit parameter values on the detailed impedance behavior.

3.2 Convergence Properties

Since the developed circuit (Fig. 2.5) is made up of a double-infinite number of terms, convergence of the various impedance functions must be insured before practical application is possible.

First consider the convergence of the set Z_n for arbitrary n. For large values of m the terms in the series decrease as

$$\lim_{m \to \infty} Z_n \longrightarrow K\left(\frac{1}{m}\right)\left(\frac{\sin \frac{m\pi w'}{2}}{\frac{m\pi w'}{2}}\right)^2 \qquad (3.1)$$

which is determined by the value of the argument $\frac{m\pi w'}{2}$. The significance of width w must be noted at this time. As long as $w \neq 0$ the series eventually converges as $1/m^3$, but an increasing number of terms must be included as $w \rightarrow 0$. Consider M to be the number of terms included in the summation. Then $\theta_M = \frac{M\pi w'}{2}$ is the argument of the final term. Fig. 3.1 shows the error due to truncation of the summation as a function of θ_M. This curve was obtained by calculating a set of partial sums for Z_n using progressively greater values of M. When the difference between two succeding Z_n values was less than 0.1%, the larger value was considered as the limit or sum of the series, and all previous partial sums normalized to this value. Percentage error was determined relative to the final Z_n for all partial sums and plotted as shown. If the first zero of $(\sin\theta_m/\theta_m)$ is chosen as the truncation point, (i.e., $\theta_M = \pi$) then $M = \frac{2}{w'}$ represents the number of modes to consider for error $\approx$ 1%. As $w \rightarrow 0$ the configuration approaches that of an infinitely thin post which is characterized by infinite inductance, i.e., the divergent series resulting from a $1/m$ term variation since $\lim_{\theta_m \rightarrow 0} \frac{\sin\theta_m}{\theta_m} = 1$.

Secondly, the parallel combination of an infinite number of sets is considered. From (2.17) the total admittance is the result of summing the admittances of the individual sets whose terms decrease for large values of n as

$$\lim_{n \rightarrow \infty} Y_R \longrightarrow K'\left(\frac{1}{n}\right)\left(\frac{\sin\frac{n\pi g'}{2}}{\frac{n\pi g'}{2}}\right)^2 \tag{3.2}$$

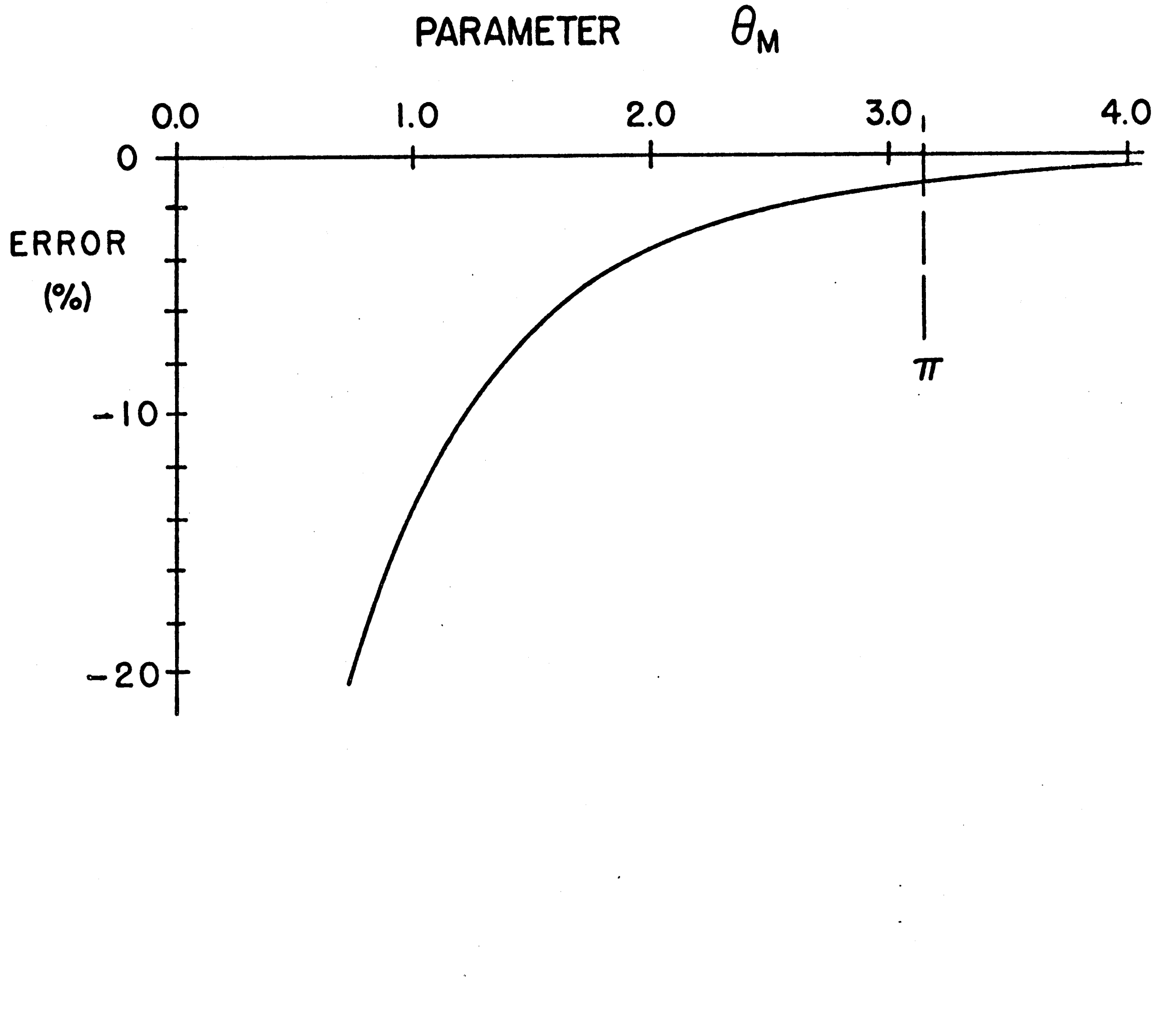

Fig. 3.1 Truncation error for Z_n.

This is obviously of the same form as (3.1), with different parameters involved. The dependence on the gap size is the controlling factor in the number of model sets N to include in the circuit, and similarly divergence is approached as $g \longrightarrow 0$. The divergent admittance would represent a short-circuited gap which is appropriate for $g = 0$. As with (3.1) consider the truncation point as the first zero of the $\sin \phi_n/\phi_n$ function. Therefore $N = \frac{2}{g'}$ represents the number of sets to include.

It should be noted that whenever dealing with a physically realizable mount, i.e., finite post and gap dimensions, the impedance functions are well behaved although slowly converging. The slow rate of convergence is not a problem however, since most precision analyses are carried out using a computer, as was done here.

3.3 Assumptions and Error

In (3.2) it is possible to see the consequences of the assumed y-distribution of the $\bar{E}$ - field in the gap. The rate of convergence for Y_R is controlled directly by the expansion coefficient S_p expressed in (2.12), and therefore will reflect any error in the distribution as error in the result. Then the approximate value Y_R' is related to the true value Y_R by

$$Y_R' = \sum_n \frac{1}{Z_n} = Y_R(1 + \Delta) \qquad (3.3)$$

where Δ is due to convergence error from the $(\sin \phi_n/\phi_n)$ description for the field distribution.

However from (3.1) it is seen that the approximate x-distribution assumed for the current on the post will produce similar errors resulting in Z'_n.

Then

$$Z'_n = Z_n(1 + \Delta') \tag{3.4}$$

where Δ' is due to convergence error from the $(\sin \theta_m/\theta_m)$ description for the current distribution. Reconsidering gives

$$Y'_R = \sum_n \frac{1}{Z'_n} = \frac{1}{(1 + \Delta')} \sum_n \frac{1}{Z_n} = \frac{(1 + \Delta)}{(1 + \Delta')} Y_R \tag{3.5}$$

or

$$Y'_R \approx Y_R$$

for $\Delta \approx \Delta'$, since both errors are due to comparable assumptions in parameter distribution. In fact, the error Δ can also be attributed to premature truncation of the $\sum_n$ summation. But quantitatively, if the $\sum_m$ summation is likewise cut short, the change in the error Δ' should follow Δ so that (3.5) is still good. This is demonstrated in Fig. 3.2. Use of the "first zero" criteria previously mentioned dictated $M = 20$, $N = 30$ for the limits of the respective

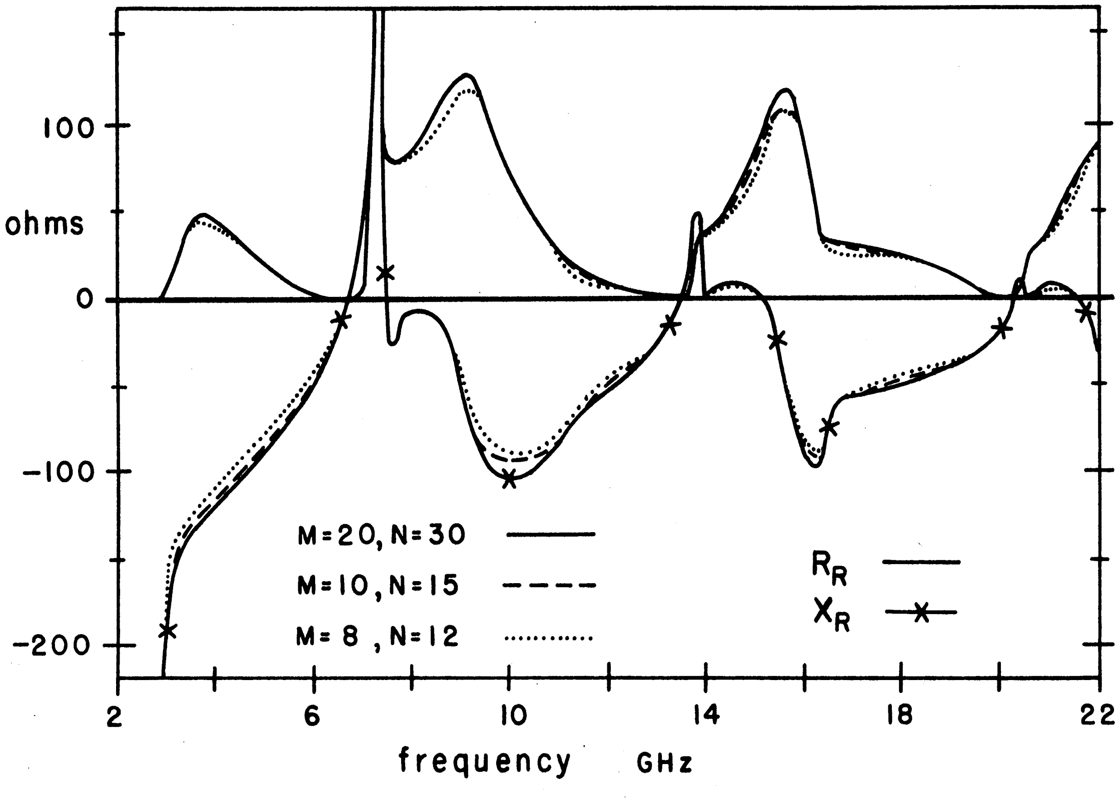

Fig. 3.2 Impedance comparison plot. C-Band waveguide a = 4.76 cm, b = 2.215 cm, s' = 0.500, h' = 0.0, w' = 0.115, g' = 0.069. M and N represent the number of terms retained in summing the respective series.

summations. This was first reduced to M = 10, N = 15 and then M = 8, N = 12 with the resulting impedances compared, indicating excellent agreement. The truncation criteria can then be reduced to $M = \frac{1}{w'}$, $N = \frac{1}{g'}$ without loss of accuracy.

This error compensation effect is due to the stationary nature of the impedance formulation with respect to the current and fields (Ref. 18, pp. 260-261).

3.4 Terminated Waveguide

The derivation presented so far has only considered infinite guide length or matched conditions. This was sufficient to establish the circuit representing the post mount as shown in Fig. 2.5. A more practical case would include the possibility of terminating the waveguide arms in something other than a match, e.g., sliding short, filter element, etc. To do this a new Green's function is required, which takes the terminating boundary conditions into account. To satisfy this requirement, $\bar{\bar{G}}_T(\bar{r}|\bar{r}')$ i.e., the Green's function for terminated waveguide, was derived. This derivation is presented in Appendix B. Fortunately $\bar{\bar{G}}_T(\bar{r}|\bar{r}')$ is directly related to the previous $\bar{\bar{G}}(\bar{r}|\bar{r}')$ by

$$\bar{\bar{G}}_T(\bar{r}|\bar{r}') = \bar{\bar{G}}(\bar{r}|\bar{r}') \quad \tau$$

where

$$\tau = \frac{1 + \rho_{1mn} e^{-2\Gamma_{mn}\ell_1} + \rho_{2mn} e^{-2\Gamma_{mn}\ell_2} + \rho_{1mn}\rho_{2mn} e^{-2\Gamma_{mn}(\ell_1+\ell_2)}}{1 - \rho_{1mn}\rho_{2mn} e^{-2\Gamma_{mn}(\ell_1+\ell_2)}} \tag{3.6}$$

representing the scattered energy effect of the terminations, and

$\rho_{1mn}, \ \rho_{2mn}$ = complex reflection coefficients for terminations 1 and 2.

$\ell_1, \ \ell_2$ = distances to terminations 1 and 2 from post mount plane.

This factor τ being independent of the x, y coordinates, is carried through all of the mathematics (equations 2.9 - 2.21) to act directly in determining a terminated mode pair impedance, Z_{Tmn} as

$$Z_{Tmn} = Z_{mn} \ \tau \tag{3.7}$$

This can be separated to represent the two arms of the waveguide with

$Z_{cmn} \ \tau_1$ - representing arm #1

and

$Z_{cmn} \ \tau_2$ - representing arm #2

where

$$\tau_j = \left(\frac{1 + \rho_{jmn} e^{-2 \Gamma_{mn} \ell_j}}{1 - \rho_{jmn} e^{-2 \Gamma_{mn} \ell_j}} \right) . \qquad (3.8)$$

An interesting and expected form of τ_j is

$$\tau_j = \frac{Z_{jmn} + \tanh \Gamma_{mn} \ell_j}{1 + Z_{jmn} \tanh \Gamma_{mn} \ell_j} \qquad (3.9)$$

with

Z_{jmn} = terminating impedance on arm #j normalized to Z_{cmn}

which is the impedance translation transmission line formula. Note that Z_{cmn} is imaginary for non-propagating mode pairs.

The denominator of τ accounts mathematically for the possible resonance between the two terminations; i. e.,

$$\left[1 - \rho_{1mn} \rho_{2mn} e^{-2 \Gamma_{mn}(\ell_1 + \ell_2)} \right] = 0$$

only when $|\rho_1| = |\rho_2| = 1$ and the proper phase exists with a propagating mode.

3.5 Multiport Characteristics

Since it was possible to isolate as terminal effects all of the various mode pair impedances, the equivalent circuit of the post mount was defined as a multiport coupling network. The plane $z = 0$ defines the position of all ports with respect to the waveguide; noting, as shown in the preceding section that mode terminations must be considered as the shunt combination of the two waveguide arms. For a propagating mode the plane $z = 0$ is accessible as an input port to the circuit so that the post mount may be considered as an obstacle in the waveguide. Normally only the H_{10} mode will be propagating so that all other mode ports will be terminated in Z_{cmn}. Termination of the opposite waveguide arm to the H_{10} mode, and knowledge of the characteristics Z_G of the particular device as placed in the gap, will permit accurate obstacle description. The circuit in Fig. 3.3 results from considering waveguide arm No. 1 as the input port to the post mount equivalent circuit for the H_{10} mode, with combined components specified as follows:

$$jX_L = \sum_{m=2}^{\infty} Z_{m0} \left(\frac{\kappa_{pm}}{\kappa_{p1}}\right)^2 (1 - w') \qquad (3.10a)$$

$$Y'_G = \kappa_{p1}^2 / Z_G \qquad (3.10b)$$

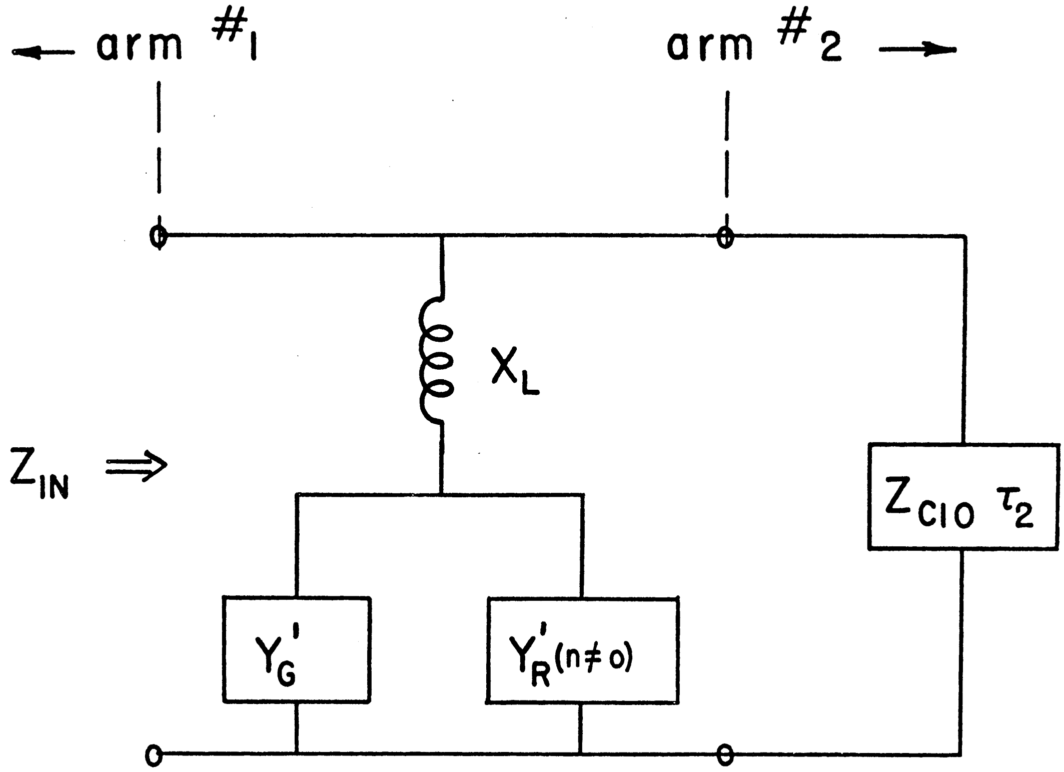

Fig. 3.3 Post obstacle circuit for incident H_{10} mode.

$$Y'_R(n\neq 0) = (\kappa_{p1}^2) \sum_{n=1}^{\infty} \left[\frac{1}{\sum_{m=1}^{\infty} Z_{mn} \left(\frac{\kappa_{pm}}{\kappa_{gn}} \right)^2} \right] \qquad (3.10c)$$

Since the formulation for the modified driving point admittance $Y'_R(n\neq 0)$ is the same as that discussed in Section 3.3 for Y_R, the less restrictive summation criteria $M = \frac{1}{w'}$, $N = \frac{1}{g'}$, may be used because of the compensating action. However this does not hold for the single summation of the inductive reactance X_L. Any error in the summation will directly affect X_L. Therefore it is necessary to use $M = \frac{2}{w'}$ for this special case. In fact it is also necessary to consider the error Δ' due to the assumption for the current distribution. While this has not been analyzed theoretically, the experimental work discussed in Section 5.3.1 indicates accurate results are obtained by use of the correction factor $(1 - w')$. Since $w' < 0.25$, this factor never becomes very large, simply adjusting for slight tendency due to the assumed current distribution to predict high values. The special case where the gap is shorted out, $Z_G = 0$, allows description of a post-in-waveguide. This holds for any incident mode by considering the proper input port of Fig. 2.5.

3.6 Impedance Characteristics

Using (2.17b), (2.21a), (2.22), (3.6), and (3.7) a concise form for the driving point impedance is found as

$$Z_R = \frac{1}{\sum_{n=0}^{\infty} \left[\frac{1}{\sum_{m=1}^{\infty} Z_{Tmn} \left(\frac{\kappa_{pm}}{\kappa_{gn}} \right)^2} \right]} \tag{3.11}$$

which is represented by the circuit in Fig. 2.5 with terminated impedance Z_{Tmn}. With this relationship established, it is desirable to take a closer look to determine what are the dominant and lesser characteristics, and how are they controlled by parameter values. A broad frequency range has been considered because of high interest in determining impedance characteristics for harmonics of pump and mixing frequencies in the design of parametric amplifiers and frequency converters (Refs. 24, 25). The dominant mode frequency range for the (C-Band) waveguide considered here is 4 - 6 GHz. Matched conditions are presumed in the following discussion so that $Z_{Tmn} = Z_{mn}$. It is clear from (2.21a) that once the waveguide dimensions a and b are chosen (as has been done in specifying C-Band waveguide), the characteristic impedances for all modes are established. In particular this means that the scaling and placement of the zero and pole for each mode impedance pair Z_{mn} (Ref. Fig. 2.3) has been fixed. Next the coupling to the gap must be considered. In general if arbitrary values are picked for s' and h', both κ_{pm} and κ_{gn} will be non-zero and all modes will have a non-zero contribution to Z_R. However special cases do exist where either one or both of the coupling factors may become zero for various specific values of m, n. The best recognized example of this is the lack of coupling to all m = even modes when the post is centrally located (s' = 0.500) in the guide since $\sin m\pi s' = 0$ for these conditions; i.e., $\kappa_{pm} = 0$. Other post positions can likewise decouple modes for specific values of m. More significant however to the general characteristic is the placement of the gap with h'; this parameter controls the coupling of the Z_n sets to the overall circuit. Equation (2.19) indicates a zero point for each Z_n which becomes the dominant characteristic seen by the gap because of the parallel nature of the sets. Fig. 3.2 shows this effect quite well with zeros present at f = 6.77, 13.54, and 20.31 GHz, corresponding to the zeros of Z_1, Z_2 and Z_3 respectively for the general case. It is however possible to choose h' such that $\cos n\pi h' = 0$. When this is done, the associated set Z_n is decoupled so the zero is not present. This is possible for the following conditions,

h'	decoupled sets for
0.500	n = 1, 3, 5 . . . ∞
0.250	n = 2, 6, 10 . . . ∞
0.166	n = 3, 9, 15 . . . ∞
0.125, 0.375	n = 4, 12, 20 . . . ∞
.	.

which represent the most significant cases. The strong effect of this change in h' on the impedance characteristic is shown in Fig. 3.4, drawn for the first three h' values in the list above. Note the lack or presence of zeros at 6.77, 13.54, and 20.31 GHz for each curve and how this feature predominantly sets the pattern.

In Fig. 3.5 the dependence upon waveguide height is shown. Here again the dominant characteristic is the placement of the zeros which shift to increasing frequency as b decreases. This shift produces an increase in the real part of the impedance in the H_{10} region because of reduced shunting by the higher order $n > 0$ modes.

Fig. 3.6 demonstrates the relatively slight effect produced by shifting the post sideways in the waveguide. The gap position chosen for this graph $h' = 0.250$ decoupled the Z_2 set which resulted in a more slowly varying impedance through the mid-frequency range.

Fig. 3.7 indicates what can be done with the mount circuit as an obstacle to the H_{10} mode. Plotted is a family of curves representing a "tuned post" in the waveguide. The gap size is varied from zero to slightly larger than 1/4 the guide height. The gap impedance Z_G is determined simply from the parallel-plate capacitance of the end of the post, which was centered to decouple the H_{20} mode. This extended the dominant mode region to 7.46 GHz

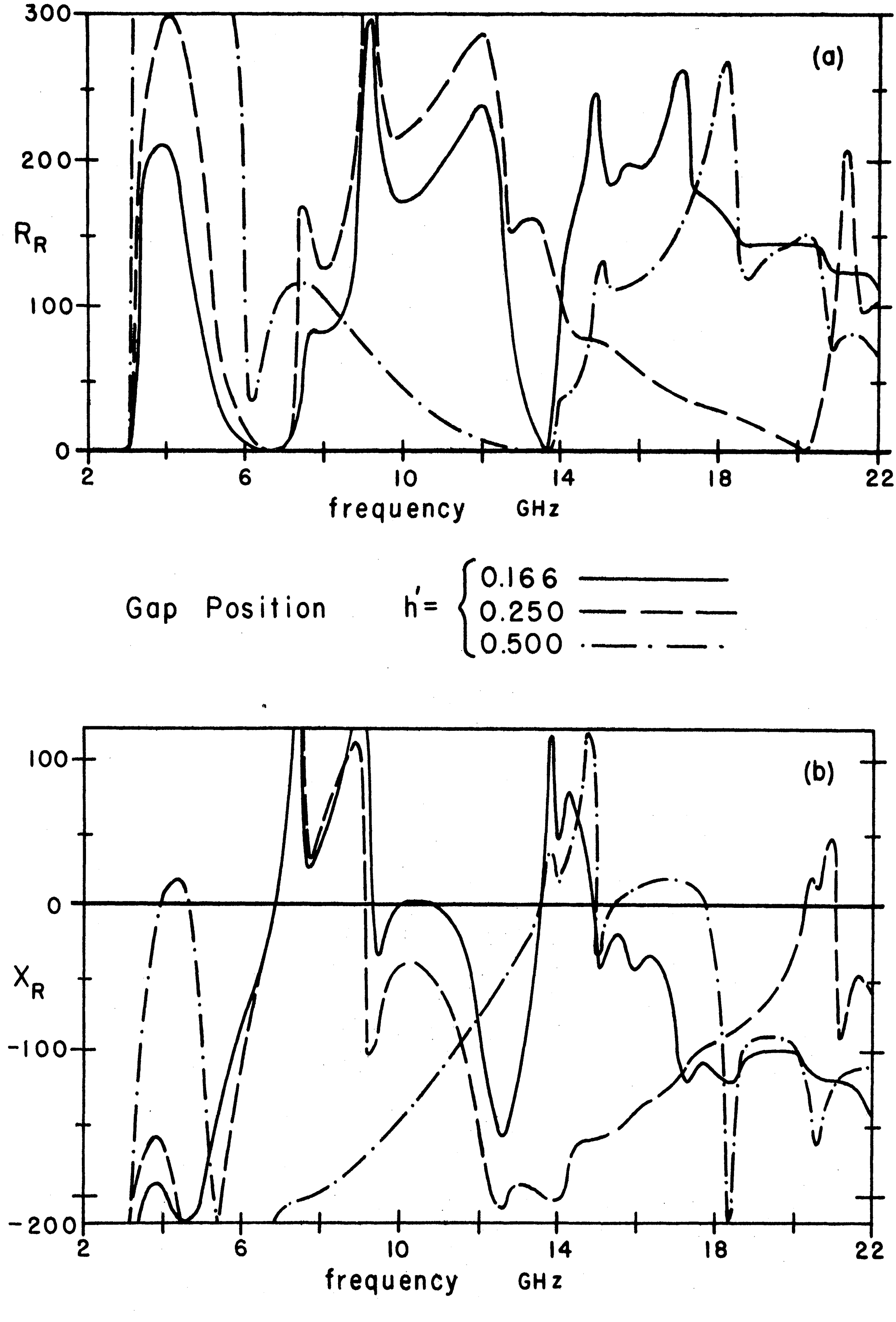

Fig. 3.4 Driving point impedance for gap position (h') variation with s' = 0.333, w' = 0.115, g' = 0.069, a = 4.76 cm, b = 2.215 cm.

(a) Resistive component.

(b) Reactive component.

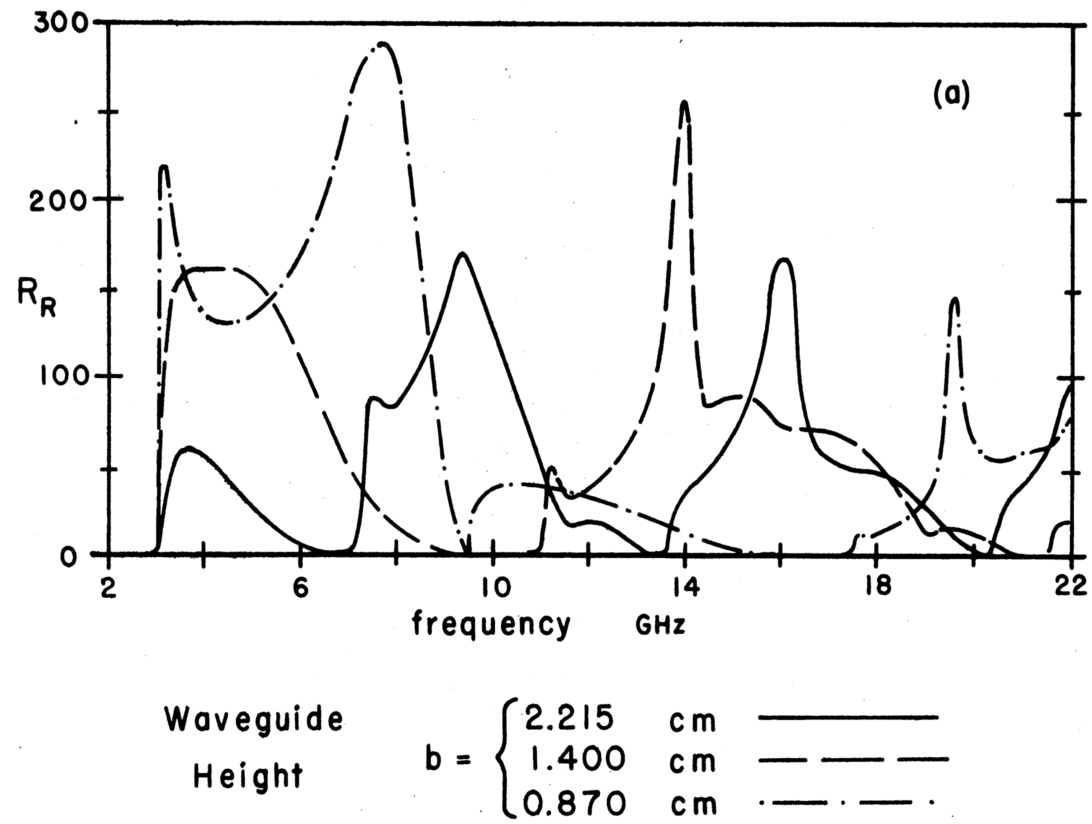

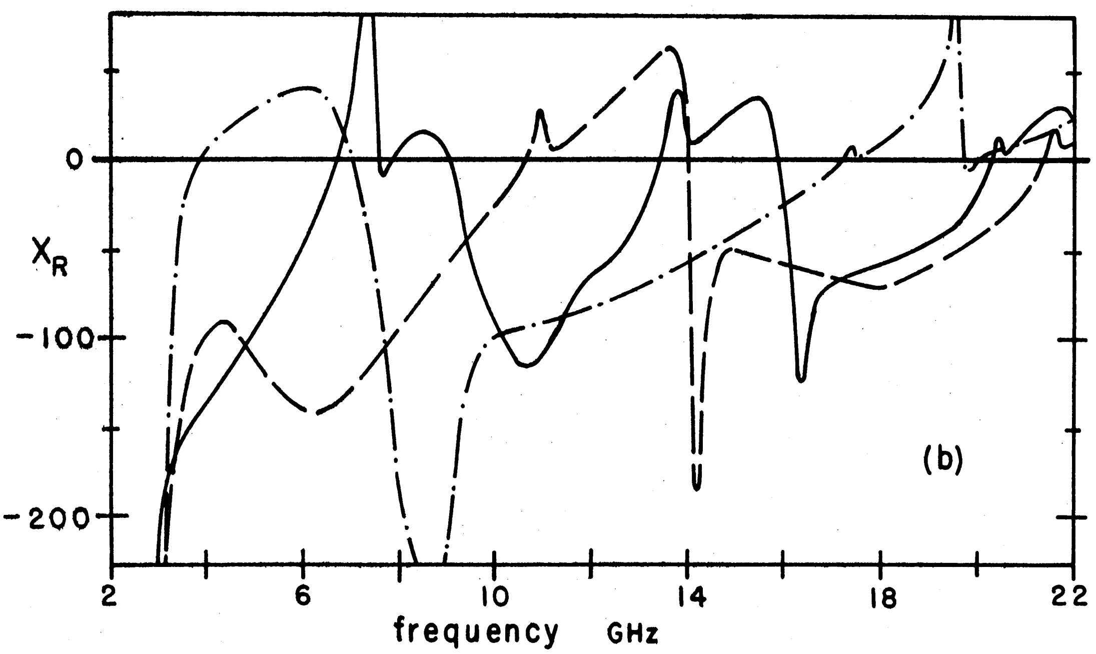

Fig. 3.5 Driving point impedance for waveguide height (b) variation with h = 0.076 cm, g = 0.152 cm, w' = 0.115, s' = 0.500, a = 4.76 cm. (Note: h' and g' vary for each curve since normalized to b).
(a) Resistive component.
(b) Reactive component.

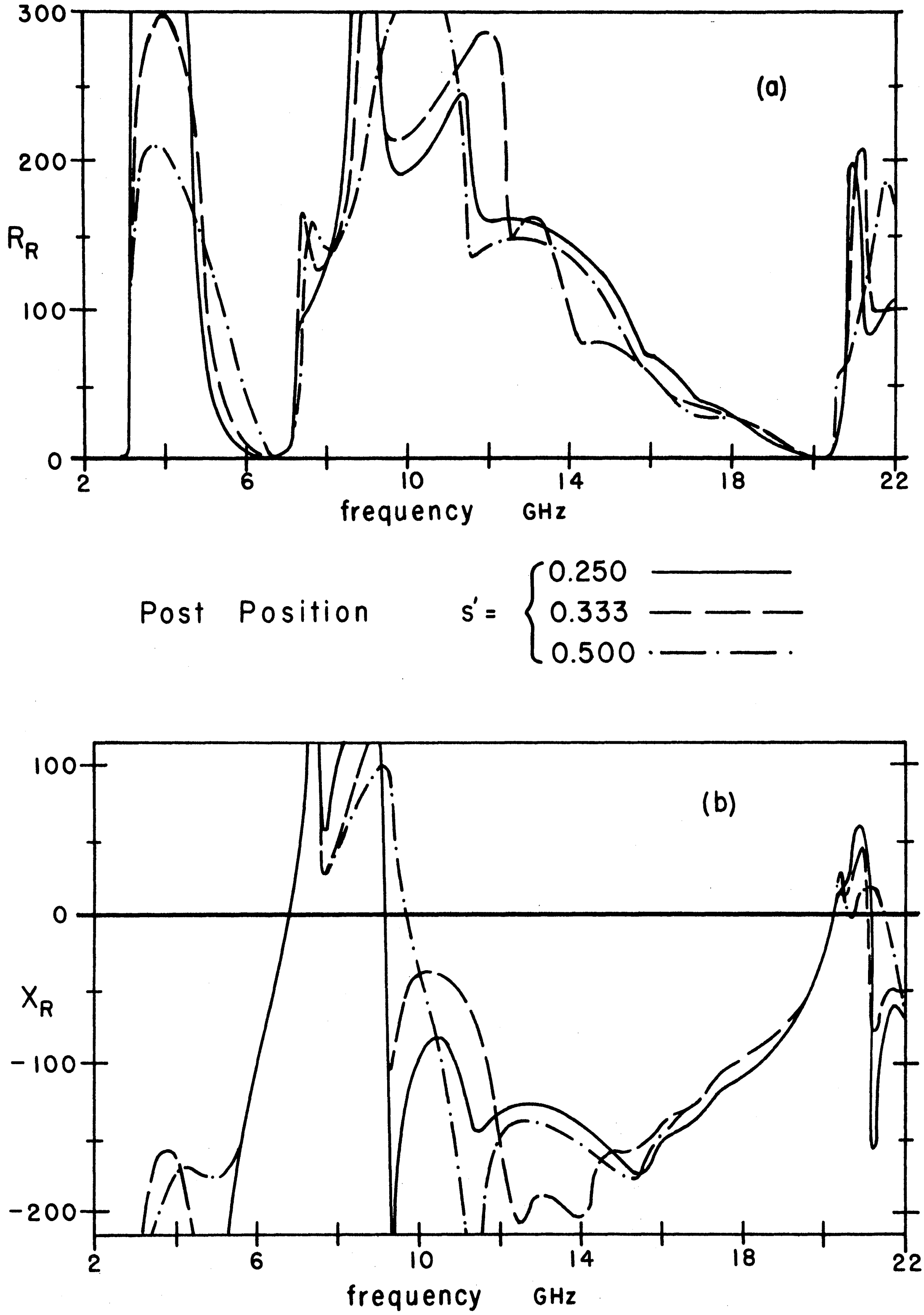

Fig. 3.6 Driving point impedance for post position (s') variation with h' = 0.250, w' = 0.115, g' = 0.069, a = 4.76 cm, b = 2.215 cm.
(a) Resistive component.
(b) Reactive component.

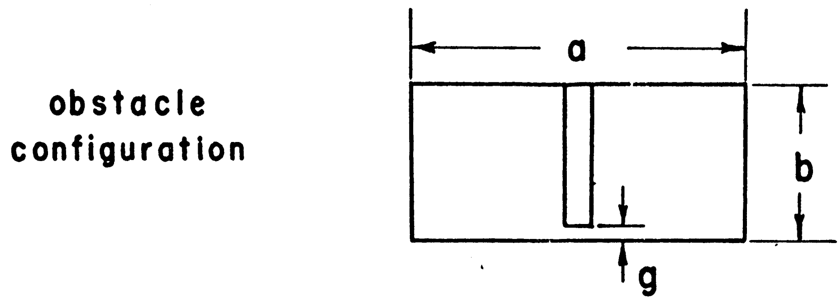

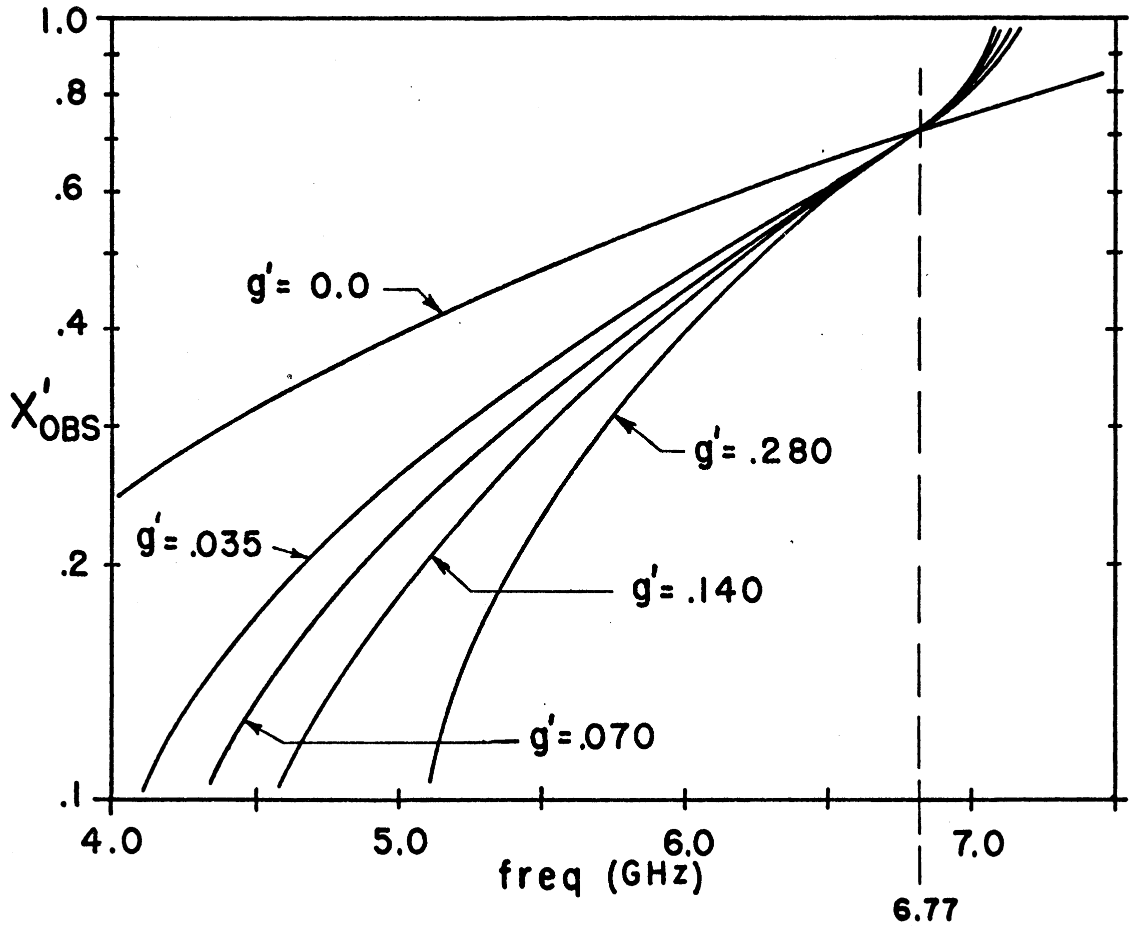

Fig. 3.7 Normalized obstacle reactance for gap size g variation in C-Band waveguide. a = 4.76 cm, b = 2.215 cm, s' = 0.500, w' = 0.115.

the cutoff frequency for the H_{11} and E_{11} modes, thus permitting observation of the characteristic at 6.77 GHz, where the reactance is independent of the gap size. Actually the reactance is independent of any impedance Z_G which happens to be present at 6.77 GHz because the admittance function $Y'_R(n \neq 0)$ is infinite at this frequency due to the zero of Z_1. This interesting feature would not be present if the gap were centered halfway up the post. Therefore a great variety of passive waveguide elements may be obtained through variation of the mount parameters.

The curves for Figs. 3.1 - 3.2, 3.4 - 3.7 were all determined using a special computer program developed for that purpose. This program is presented in Appendix C.

CHAPTER IV

EXPERIMENTAL DEVELOPMENT

4.1 Introduction

The purpose of this chapter is to discuss the work which went into the development of the equipment, techniques and procedures necessary to arrive at an accurate means of measuring the driving point impedance Z_R, of the waveguide mount shown in Fig. 4.1. This measurement information is desired to both aid and support the theoretical analysis discussed in the previous chapters.

4.2 Equipment Development

Measurement of this terminal impedance would not normally be considered possible because of the inaccessibility of the terminals, which probably accounts for the lack of published material dealing with the problem. However, with the advent of subminiature coaxial cable and connectors it is now possible to isolate the terminals electrically without affecting the surrounding field conditions, by running the measurement circuit cable inside the post.

Initially the equipment was designed for X-Band waveguide over the frequency range 6 - 22 GHz. This range proved insufficient to fully test the validity of the theoretical results in that the maximum number of propagating modes pairs was limited to five by the 22 GHz equipment limitation. Therefore it was necessary

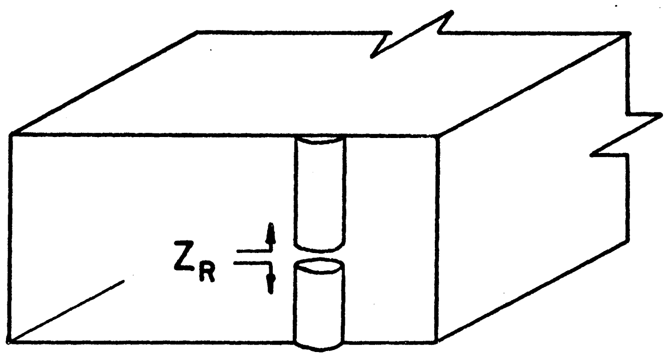

Fig. 4.1 General mount configuration

to reduce the lower limit by going to larger waveguide. The next lower standard waveguide band was considered (C-Band), increasing the frequency range to 3 - 22 GHz. For this range the C-Band waveguide would support up to nineteen propagating mode pairs (H_{mn} and E_{mn}), adequate for our purposes, thus leading to adoption of this range for the study.

4.2.1 Mount Design and Construction. The design and construction of the mount were considered as a single problem, because the two are so interrelated: in effect, designing to utilize the available construction capabilities while simultaneously skirting around construction difficulty. Most of this difficulty is due to the flexibility desired with the position parameters h and s, which is necessary to permit complete analysis. It is neither practical nor necessary to provide for variation with d and g as these values would normally be established by other criteria such as the size of the device to be mounted. Typical values are used here for d and g. Since excellent electrical contact is required at all junctions between movable parts, it is not feasible to have the parameters s and h continuously adjustable; rather these parameters occupy a set number of discrete values. In this manner it is possible to ensure adequate electrical and mechanical integrity within the system.

The mount described in Fig. 4.2 proved to work very well, demonstrating excellent symmetry in the data for values of h

a = 1.874" (4.760 cm)
b = 0.872" (2.215 cm)
d = 0.120" (0.305 cm)
g = 0.060" (0.153 cm)
$h' = h/b$ = variable
$s' = s/a$ = 0.250, 0.333 or 0.500

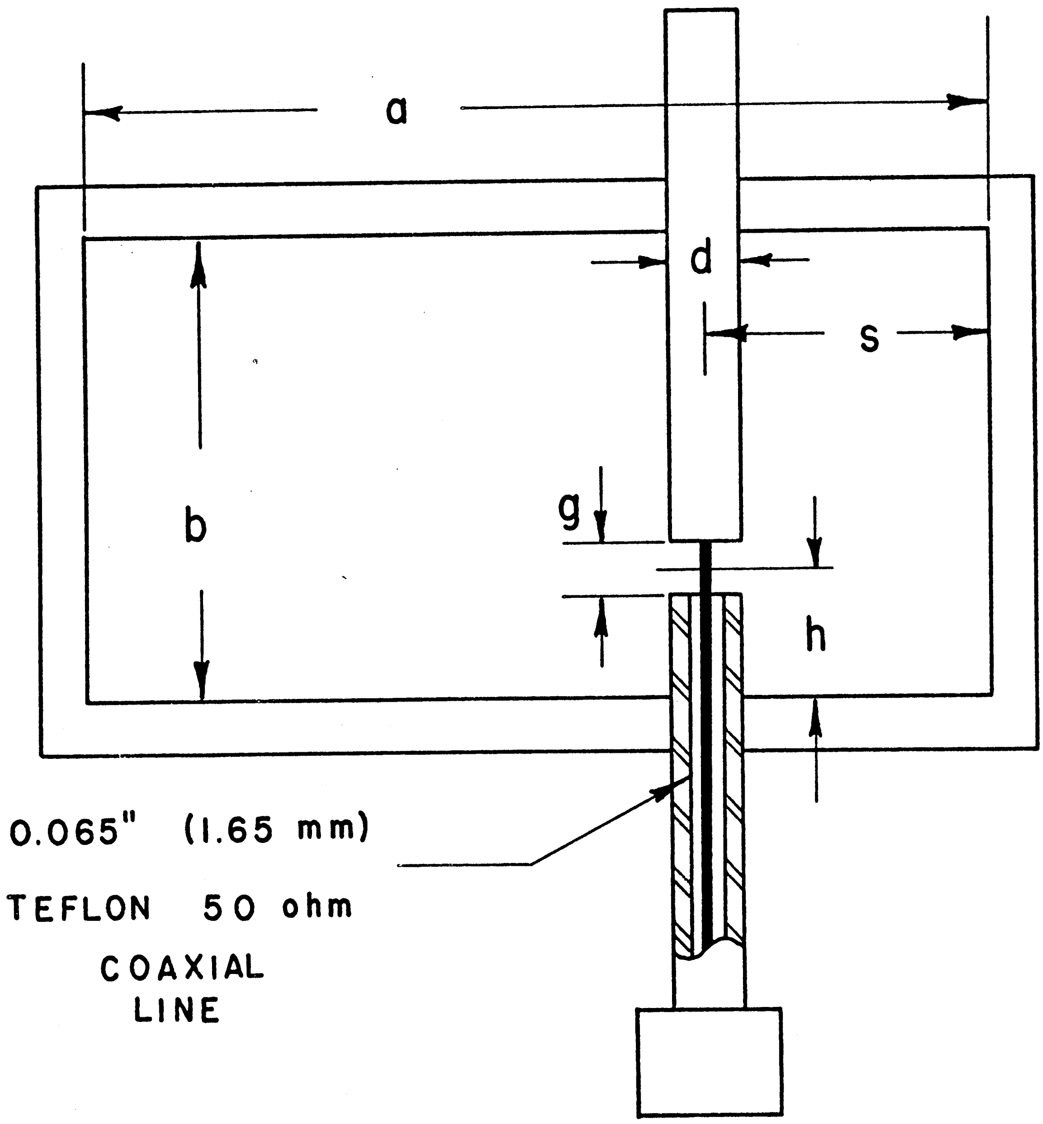

Fig. 4.2 Measurement mount

symmetrical about the center (b/2) of the guide. This data symmetry was sought as an indicator of proper construction, since differing fabrication methods were required for the top and bottom of the post.

The "measurement probe" was made by epoxy-soldering the subminiature coaxial line in a 0.120 inch sleeve and carefully attaching the center conductor to the center of the matching 0.120 inch rod. This is then held in place by a clamp around the coaxial portion, allowing vertical movement of the probe. Three sets of holes had to be drilled for the three positions across the guide. The holes were plugged when not in use.

The probe has a standard subminiature connector on the outside end on which was attached an adapter to precision 7 mm coaxial line.

4.2.2 Waveguide Terminating Considerations. Inherent in the objective to analyze this waveguide circuit over a wide frequency range is the necessity to describe accurately the terminating conditions for each of the propagating modes. From practical considerations only a short-circuit or a match could be provided for experimental purposes. The short-circuit was not used primarily because choosing its position would introduce another circuit parameter, adding undesirable complexity. Therefore a matched termination was required for both waveguide arms.

To satisfy this requirement, a standard H_{10} waveguide termination for C-Band was modified to improve its matching characteristics for higher order modes. This was done by supplementing the original load with four more tapers, providing a multiple load effect on the end wall similar to the configuration commonly used in anechoic chambers. Although equipment was not available to test the individual terminating characteristics for each mode (above H_{10}), it was possible to demonstrate the adequacy of the system by shifting the termination with respect to the mount while making Z_R impedance measurements. If reflections for any of the propagating modes were present, they would be seen as a change in the impedance at the mount. No changes were noted.

4.3 Measurement Circuit Modeling

To measure the desired impedance Z_R it was necessary to provide connectors and adapters to get from the subminiature cable up to the standard 7 mm size available on precision test equipment. These elements introduced irregularities into the measurement line which, if ignored, would produce errors in the data interpretation. Additional difficulty was created by the necessary transmission mode transformation from coaxial line to radial line at the gap. In order that a high degree of confidence could be put in the data and its interpretation, it was necessary to model these effects as an equivalent measurement circuit. A statistical comparison technique, described below, was used to arrive at values defining the assumed lumped discontinuities and line lengths involved. The resulting equivalent circuit is shown in Fig. 4.3.

The circuit loss was empirically determined to be

$$\text{attenuation} = 0.15 + 0.005\ f^{1.45}\ \text{dB}$$

where f is the frequency expressed in GHz. This effect was considered as a perturbation on the measured standing-wave-ratio rather than as additional elements in the equivalent circuit, because the overall effect was small and could be more conveniently handled this way. Modeling this loss in the measurement circuit would require the use of a complex characteristic impedance for the transmission line, complicating the analysis unnecessarily.

4.3.1 Statistical Comparision Technique. The analysis of the measurement circuit was based upon the concept that the source of error or inconsistency in a set of data could be separated statistically into two groups. First is the inherent inaccuracy in the measurement equipment, which has hopefully been minimized by proper measurement technique. The second is the interpretation error due to improper assumptions about the circuit. If a simple transmission line assumption is made for the circuit, this is in effect a "model" which, if different from the true circuit, will introduce interpretation error. As more complex models are

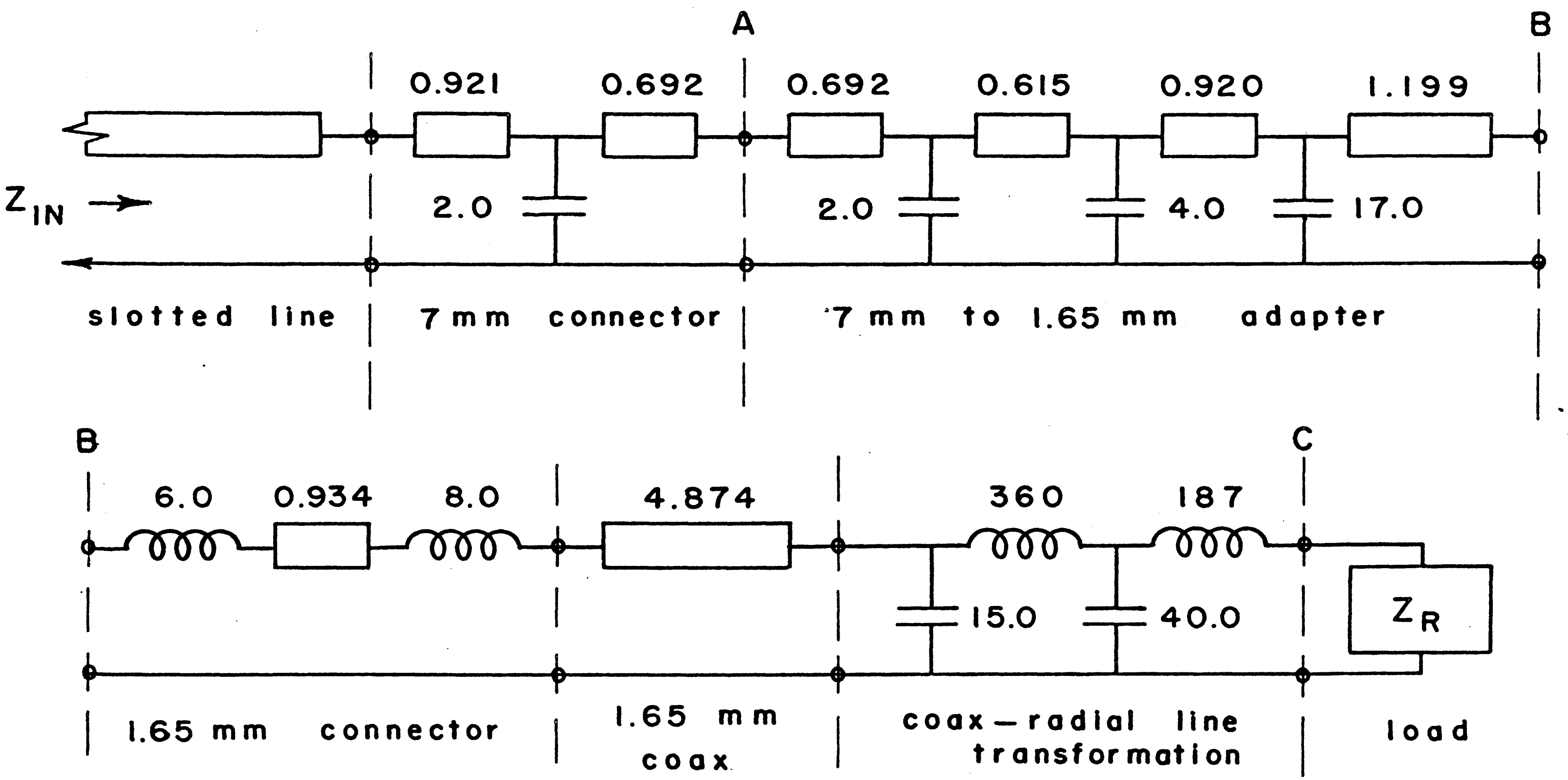

note:

a) capacitor values $\times 10^{-15}$ F

b) inductor values $\times 10^{-12}$ H

c) line lengths in cm

Fig. 4.3 Measurement circuit equivalent model.

assumed, effectively providing better approximation to the true circuit, the error due to the modeling decreases. In theory then, if a perfectly true model is assumed for the circuit, the total error will be minimized and the remaining error is due solely to the equipment (e.g., frequency drift, mechanical tolerances, etc.).

Initially a short-circuit was placed at plane A of Fig. 4.3. A set of data was taken to determine electrically the location of this short with respect to a given reference plane, assuming a simple airline case. By using a wide frequency range (8 - 18 GHz for 40 points) a certain amount of data scatter was present which could be defined by the mean value and average deviation from the mean for the short position. Approximate values for the discontinuity capacitances of the connector support bead were determined by physical considerations and used as initial values for modeling the circuit up to the short-circuit. The data was then interpreted through the new model and the scatter in the resulting short-circuit position compared. This trial and error procedure was followed, using a computer, until a stable minimum in the deviation was established. As expected only a small improvement of 3.0% was found by including this first capacitor. Next the adapter replaced the short-circuit at plane A and the short-circuit moved to plane B. A new data set was taken, and the whole procedure repeated considering only the element values between planes A and B as variables. This time a very substantial improvement, i.e., a 66.0% decrease in the average deviation, was noted. Finally the short-circuit was moved to plane C, which is actually a cylindrical surface across the gap at the surface of the post. A 35.0% improvement in the deviation resulted by using the values shown for the elements. The method used for determining the initial approximate and limiting values for the line elements is discussed in Appendix D.

The minimizing procedure was insensitive to changes in the values of the coaxial-radial line transformation elements because of their proximity to the short-circuit at plane C, with the result that these values could not be verified by measurement. Derivation of this transformation is discussed in the following section.

4.3.2 Coaxial-Radial Line Transformation. Determination of the transformation circuit was accomplished by following closely the concepts discussed by Getsinger (Ref. 13). A direct analogy is not possible however, because of the difference in configurations, i.e., the coaxial line here feeds the center of the radial line, not the outside. Fig. 4.4 shows the correspondence between the lumped element circuit and the actual circuit. C_{f1} and C_{f2} are fringing capacitances, with C_r the parallel plate capacitance in the radial line region. L_c is due to the region in the corner formed by extending the outer boundary of the coaxial line. L_r represents the volume in the radial line. This relatively simple equivalent circuit provides a good approximation as long as the dimensions involved are small with respect to wavelength.

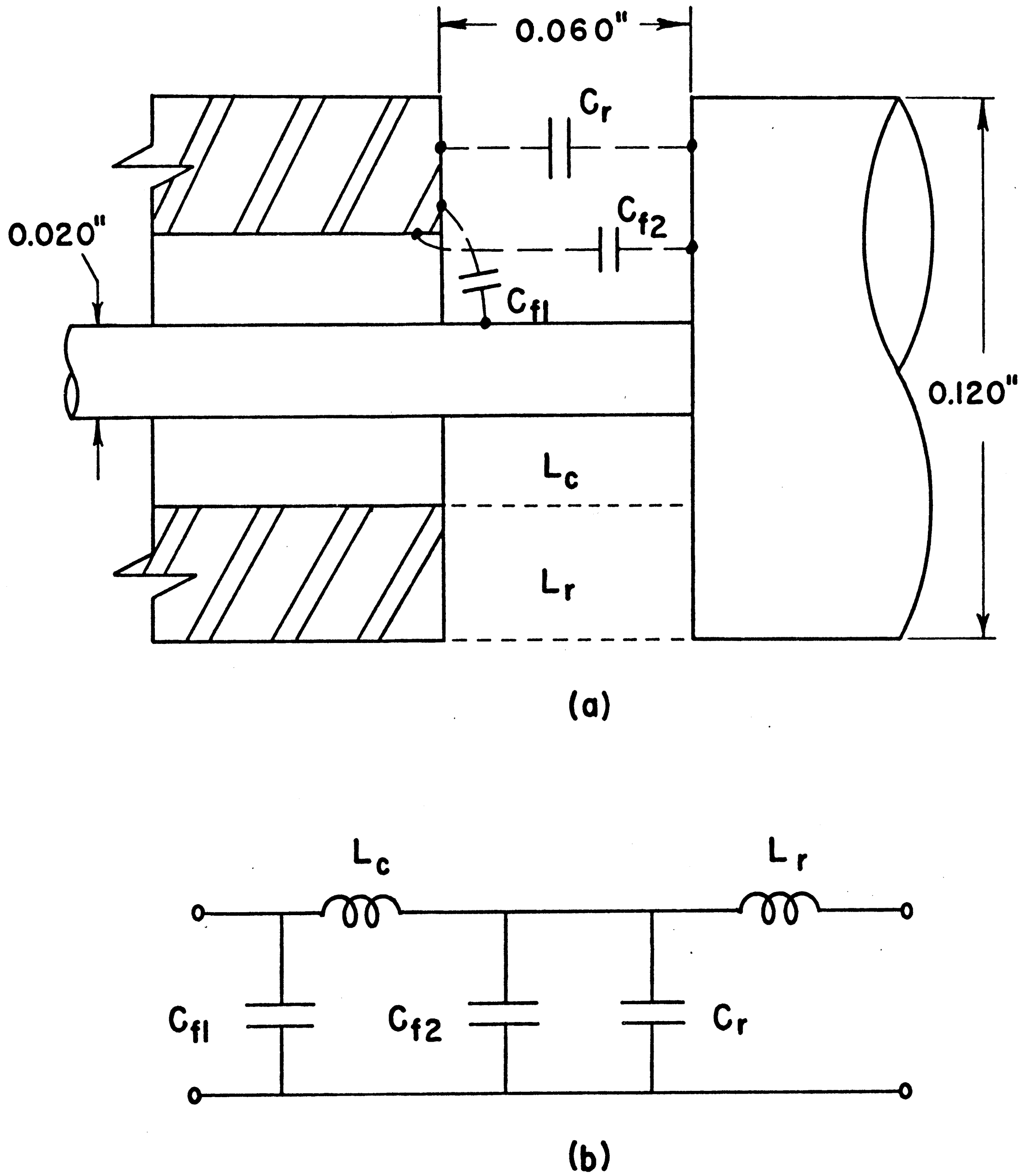

Fig. 4.4 Coaxial - radial line transformation
(a) Physical configuration.
(b) Equivalent circuit.

4.3.3 Effects of Circuit Modeling. To determine the usefulness of the measurement circuit model, comparisons were made of the various circuit effects on the data interpretation. Three situations were considered. First, a simple transmission line was assumed between the load and the measurement equipment; second, the coaxial-radial line transformation was introduced; and third, the complete circuit model was used. Fig. 4.5 indicates the differences in interpretation for the last two cases compared with the theoretical case for a typical data set. Lines are used here to represent the trends in the data interpretation. Data points are individually shown when the measurements are discussed in detail in the next chapter. The simple transmission line case is not shown because it bore so little resemblance to the other cases. Its only characteristic in common with the others was the placement of zeros at 6.77 and 20.3 GHz. Very worthwhile improvement is noted by including the total circuit model, justifying the effort involved.

4.4 Measurement Procedure

All of the impedance measurements were made using standard slotted-line techniques. The equipment was continually recalibrated to ensure precision and repeatability. Once the coaxial line adapter was placed on the probe and characterized, it was not removed. The data necessary to determine impedance, i.e., frequency, standing-wave-ratio (SWR), and standing-wave-minimum

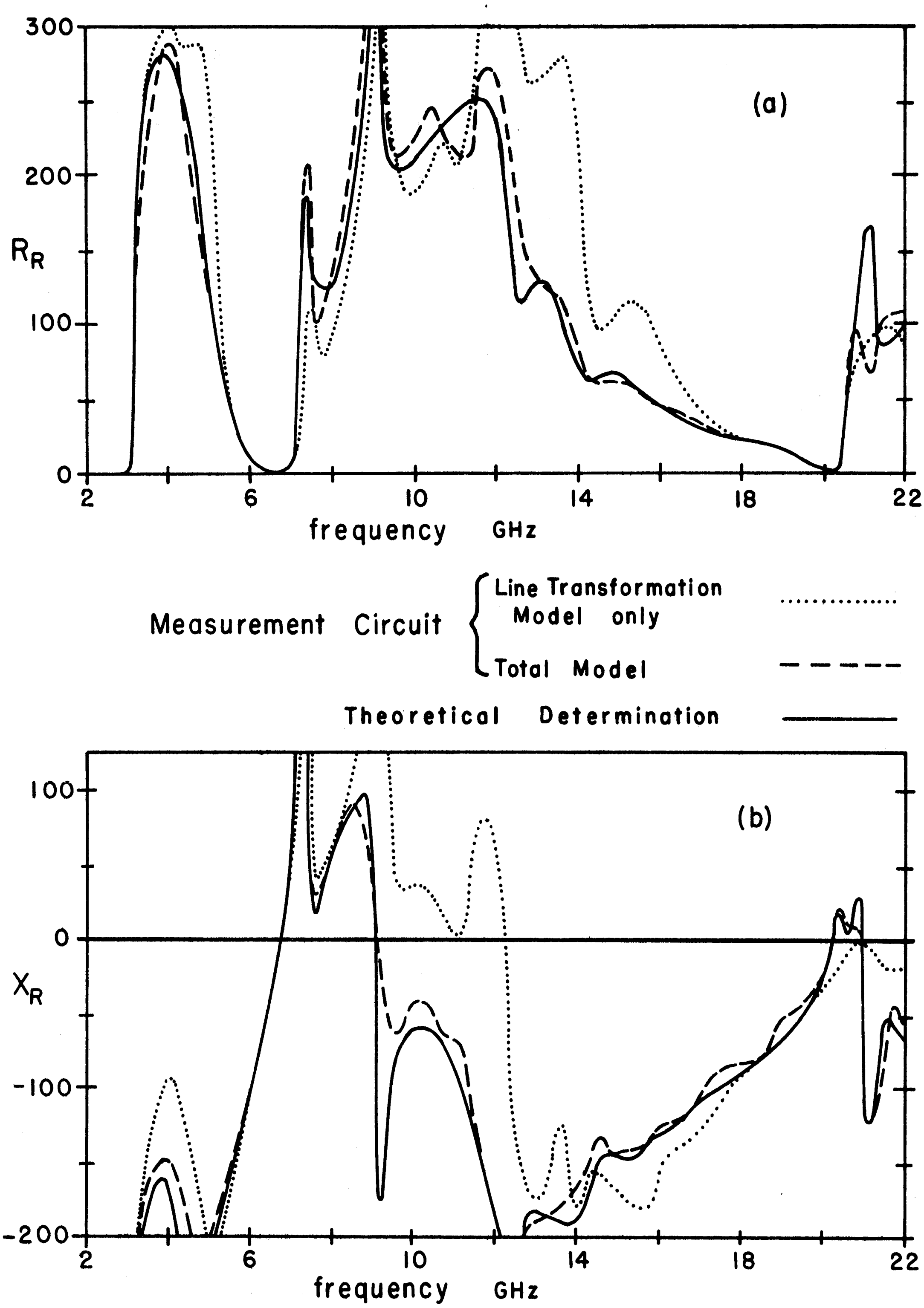

Fig. 4.5 Measurement circuit modeling comparison for the driving point impedance.
(a) Resistive component
(b) Reactive component

position, was processed through a computer program to be interpreted as Z_R versus frequency for each of the many configurations under test. This program is discussed in Appendix E.

CHAPTER V

COMPARISON OF THEORETICAL AND EXPERIMENTAL RESULTS

5.1 Introduction

This chapter brings together the results of the theoretical and experimental analyses, using the driving point impedance Z_R and the H_{10} obstacle reactance as points of comparison.

5.2 Driving Point Impedance Comparison

The driving point impedance of the mount shown in Fig. 4.2 is a function of the six dimensional parameters a, b, s', h', d, and g. Only the two here referred to as the position parameters s' and h' are varied in these measurements. Relatively standard values were chosen for the others to conform to a typical mount, i.e., a, b represent C-Band waveguide with d = 0.120" and g = 0.060", proper for mounting a "pill-type" device package. In addition all measurements were made under matched conditions on both waveguide arms. Theoretically-determined values are compared to those resulting from the measurements in Fig. 5.1 - 5.4.

Fig. 5.1 represents the impedance for the most typical mounting configuration, with the post centered and the gap at the bottom. Fig. 5.2 then shows the result of moving the gap halfway up the post. Since the post is centered, only coupling to the

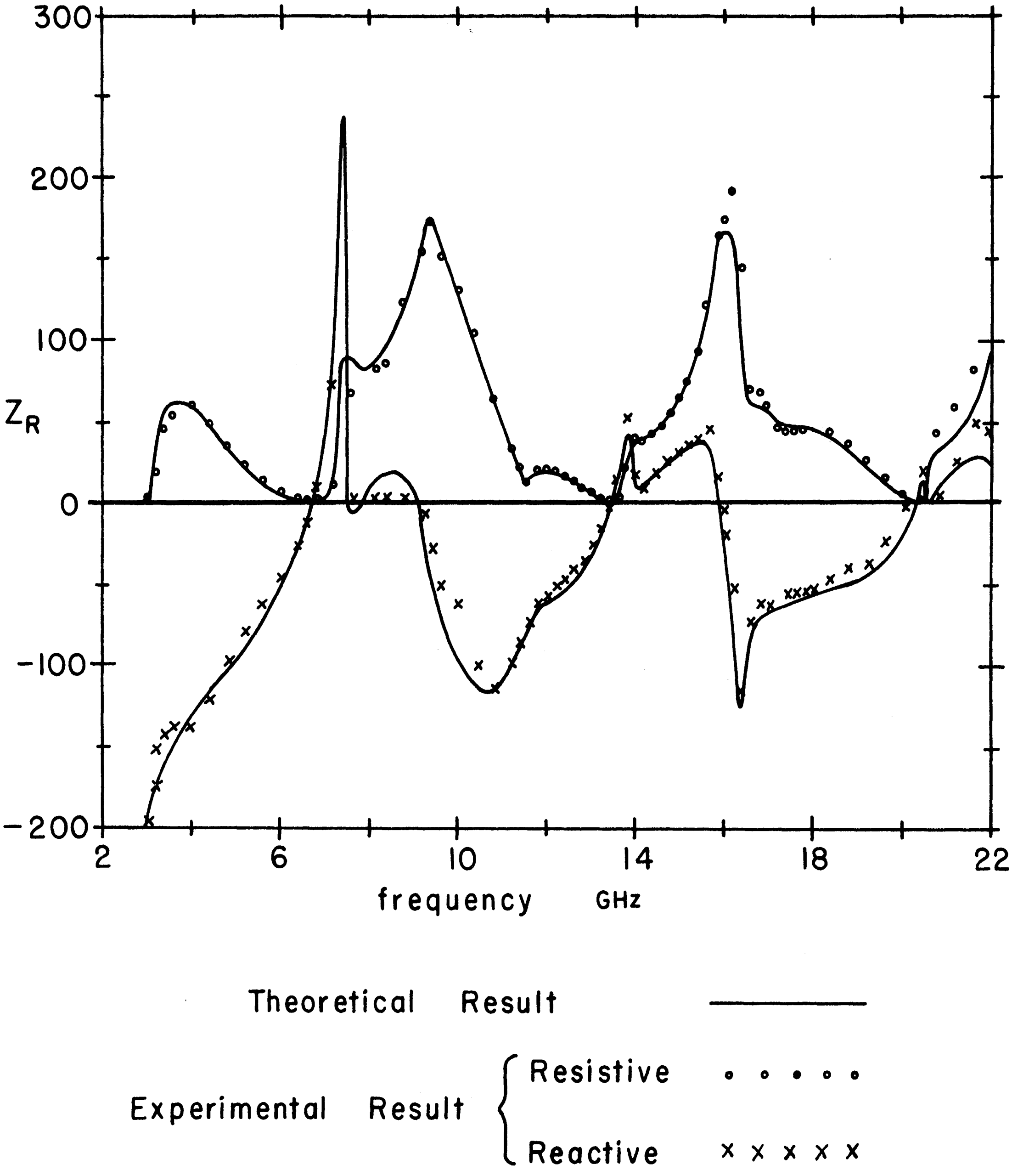

Fig. 5.1 Driving point impedance comparison - theoretical experimental s' = 0.500, h' = 0.035.

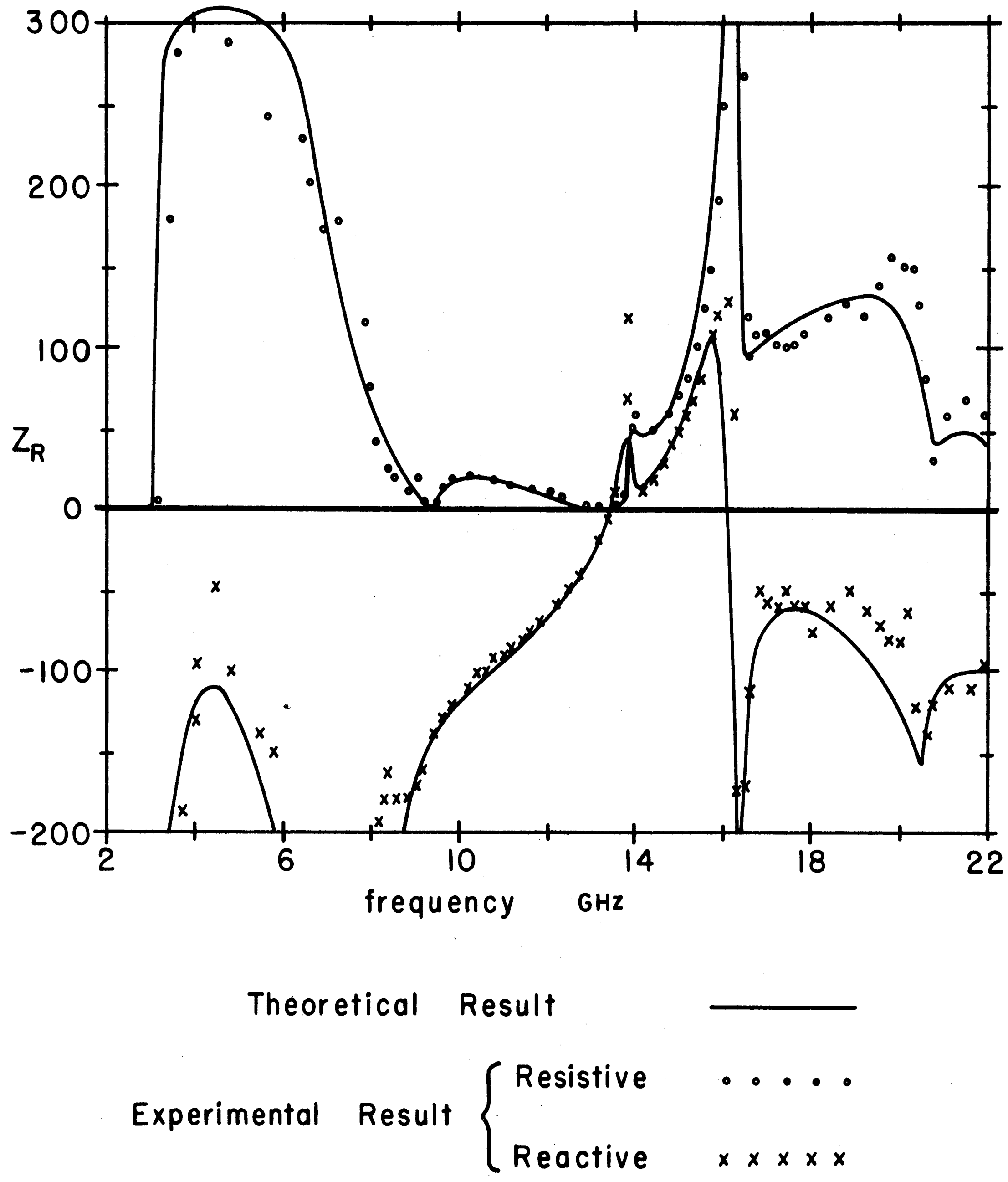

Fig. 5.2 Driving point impedance comparison - theoretical and experimental s' = 0.500, h' = 0.500.

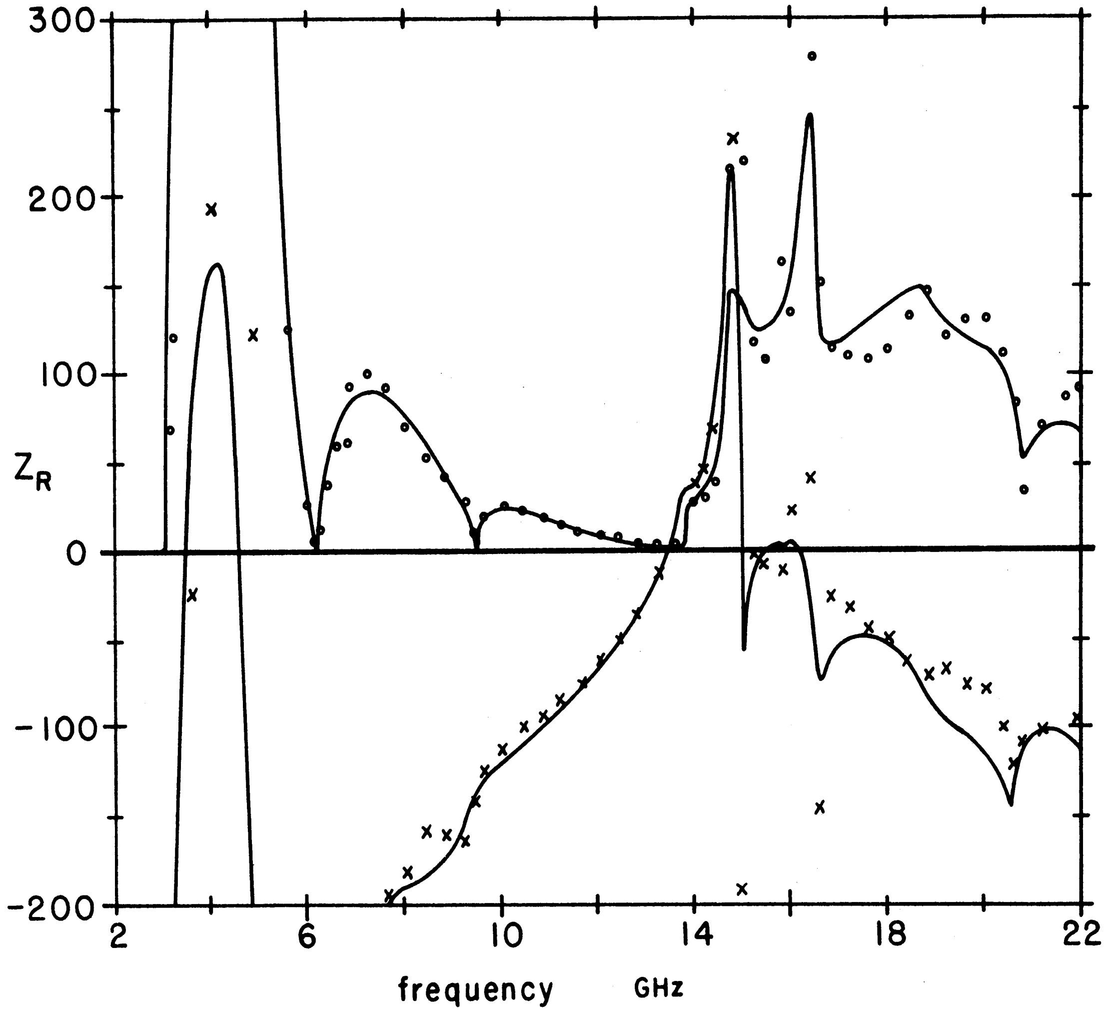

Theoretical Result ————————

Experimental Result { Resistive ∘ ∘ ∘ ∘ ∘ ; Reactive x x x x x }

Fig. 5.3 Driving point impedance comparison - theoretical and experimental s' = 0.250, h' = 0.500.

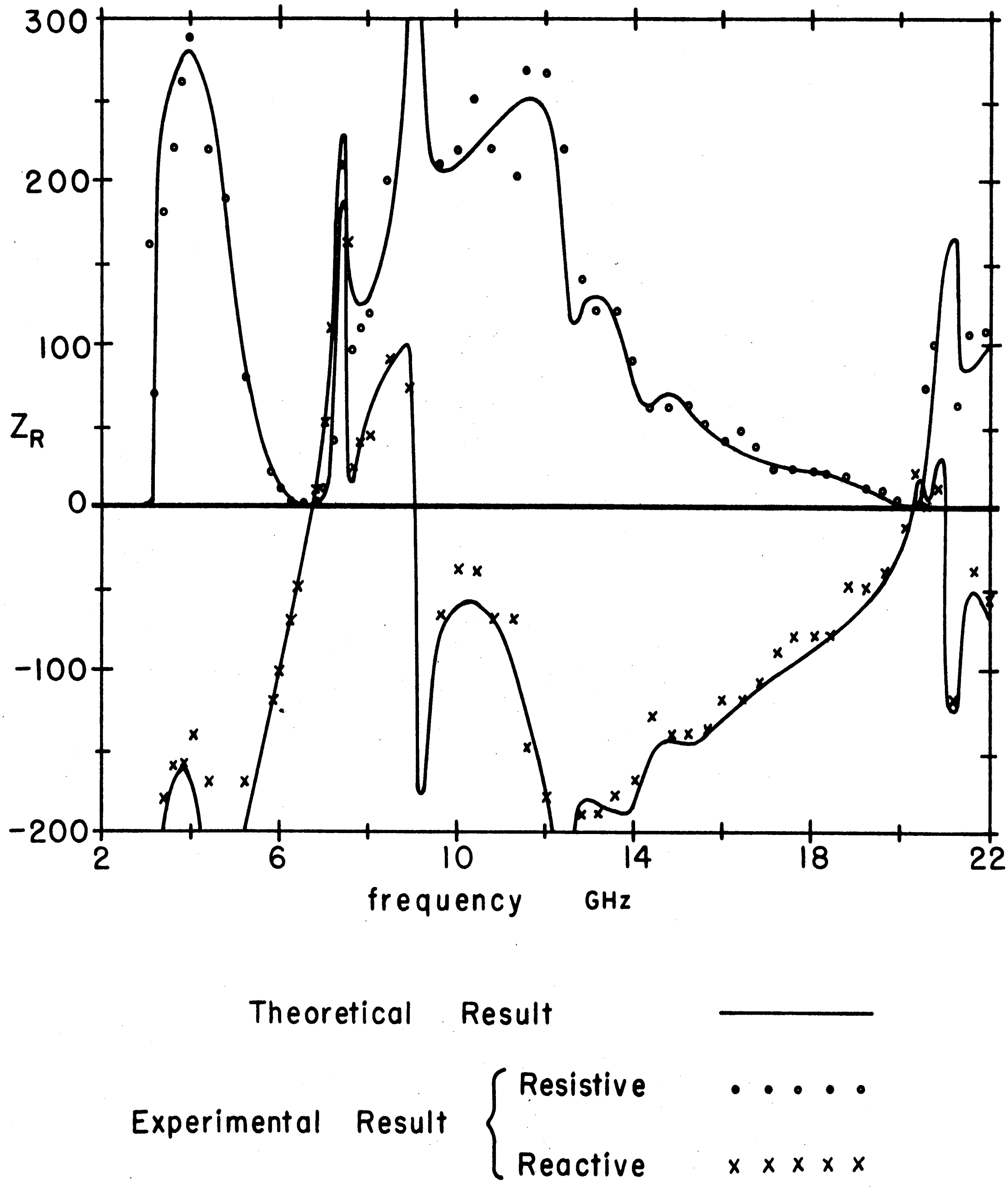

Fig. 5.4 Driving point impedance comparison - theoretical and experimental s' = 0.333, h' = 0.250.

m = odd modes exists. One of these modes, the H_{30} mode, having a pole at 9.45 GHz, causes the "resistive component" to have a zero at that frequency by decoupling energy to the H_{10} propagating mode. Leaving the gap centered in the post and shifting the post to s' = 0.250 results in Fig. 5.3. Note the additional "resistive component" zero at 6.3 GHz compared with Fig. 5.2. This is due to the H_{20} pole (cutoff frequency) which now must be considered for the off center post.

Fig. 5.4 was included to show a characteristic markedly different from the others, produced by choosing different position parameters, i.e., s' = 0.333, h' = 0.250. In all figures the data clearly shows the zeros and damped poles predicted by the theory, providing the verification desired.

5.3 Waveguide Obstacle Reactance Comparison

The measurements in this section consider the waveguide mount as an obstacle in the waveguide to an incident H_{10} mode, with a matched termination on the opposite arm. This condition is represented by Fig. 5.5, defining Z'_{OBS} as the normalized obstacle impedance in shunt across the waveguide. Z'_{OBS} includes the effects of the impedance Z_G placed in the gap plus all higher order modes, and is valid for all frequencies above H_{10} cutoff. Propagating higher order modes are seen as resistive elements in Z'_{OBS}.

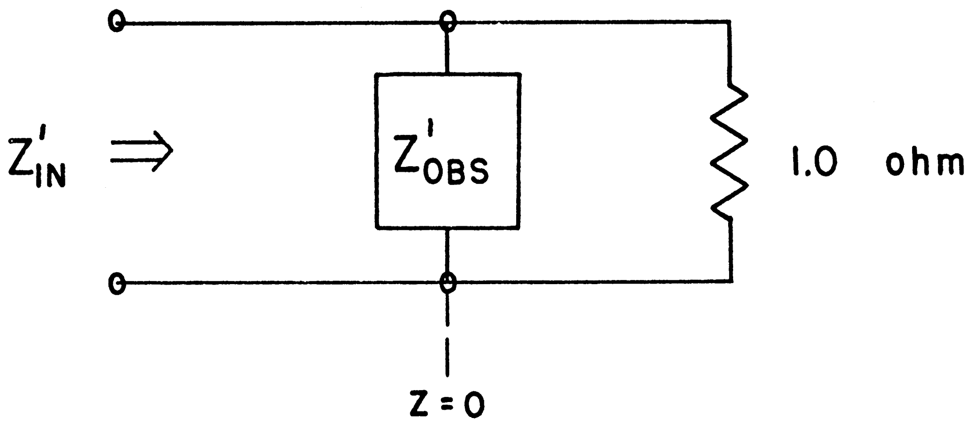

Fig. 5.5 Mount obstacle equivalent circuit.

5.3.1 Post Inductance. If the gap is shorted out (i.e., $Z_G = 0$), all coupling to $n > 0$ modes is removed, leaving only $m > 1$, $n = 0$ modes for consideration. These modes all exhibit inductive properties below cutoff so that in the dominant mode region the post will, as expected, appear inductive. This configuration allows isolated study of the post cross-section and lateral current distribution effects, leading to a general description of a post-in-waveguide.

Initially the relationship between a circular post (d = diameter) and a flat strip post (w = width) was considered. Although this relationship depends slightly on frequency, post size and location, good results are obtained by setting $w = 1.8\,d$ for the equivalent width of a circular post. Fig. 5.6 compares the measured values for a circular post with $d = 0.120$ inches and a flat post with $w = 0.216$ inches.

Next, the inductive reactances of flat posts, varying both size and position, were measured and compared against the predicted values. In general the predicted values were a little high, depending directly on the post width. This is due to the constant current assumption across the post width, which becomes more erroneous as the width increases. Therefore a small correction factor $(1 - w')$, was introduced to compensate for this error in the theory, resulting in the graphs shown in Figs. 5.7 - 5.9.

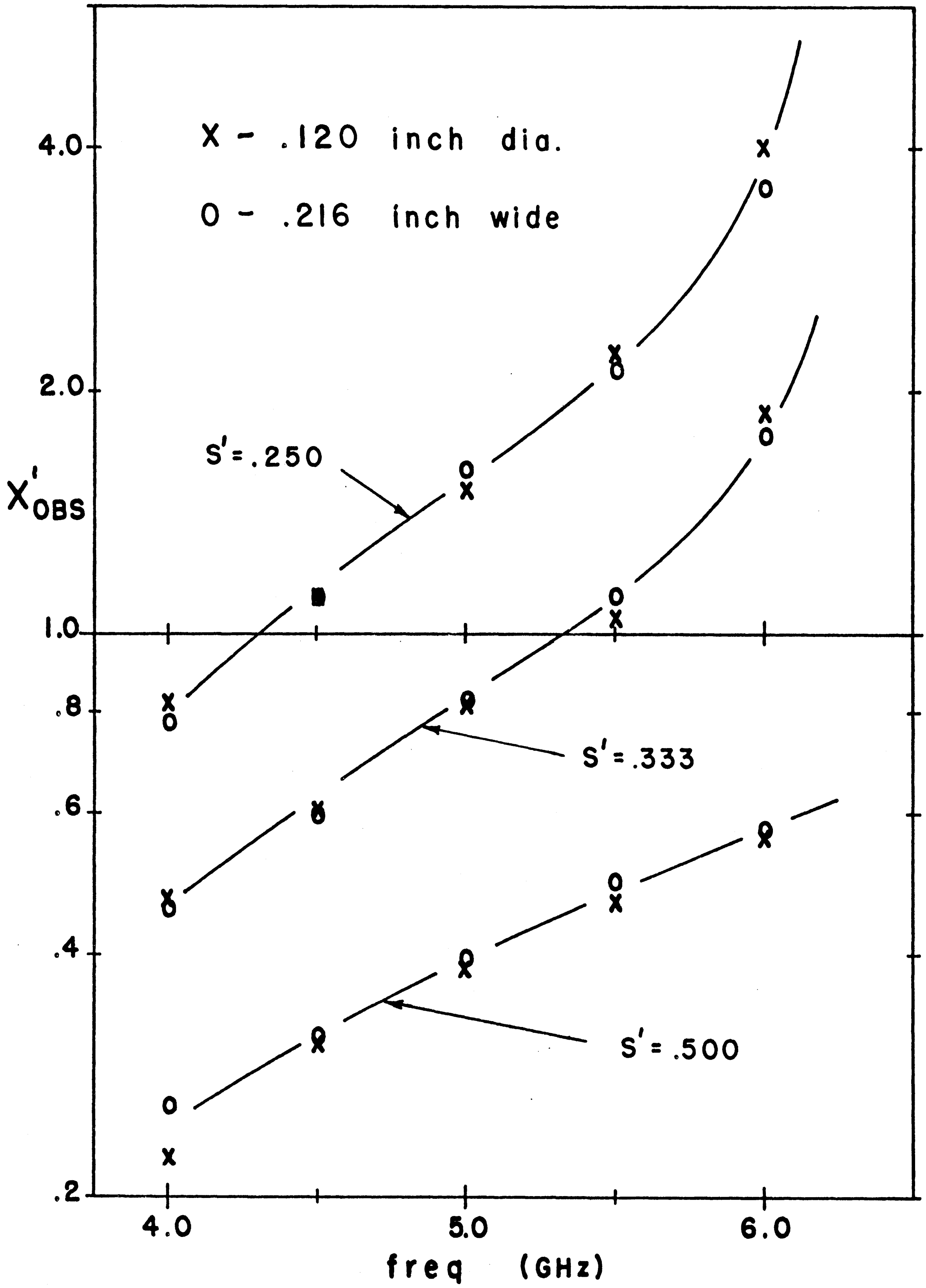

Fig. 5.6 Post cross-section comparison.

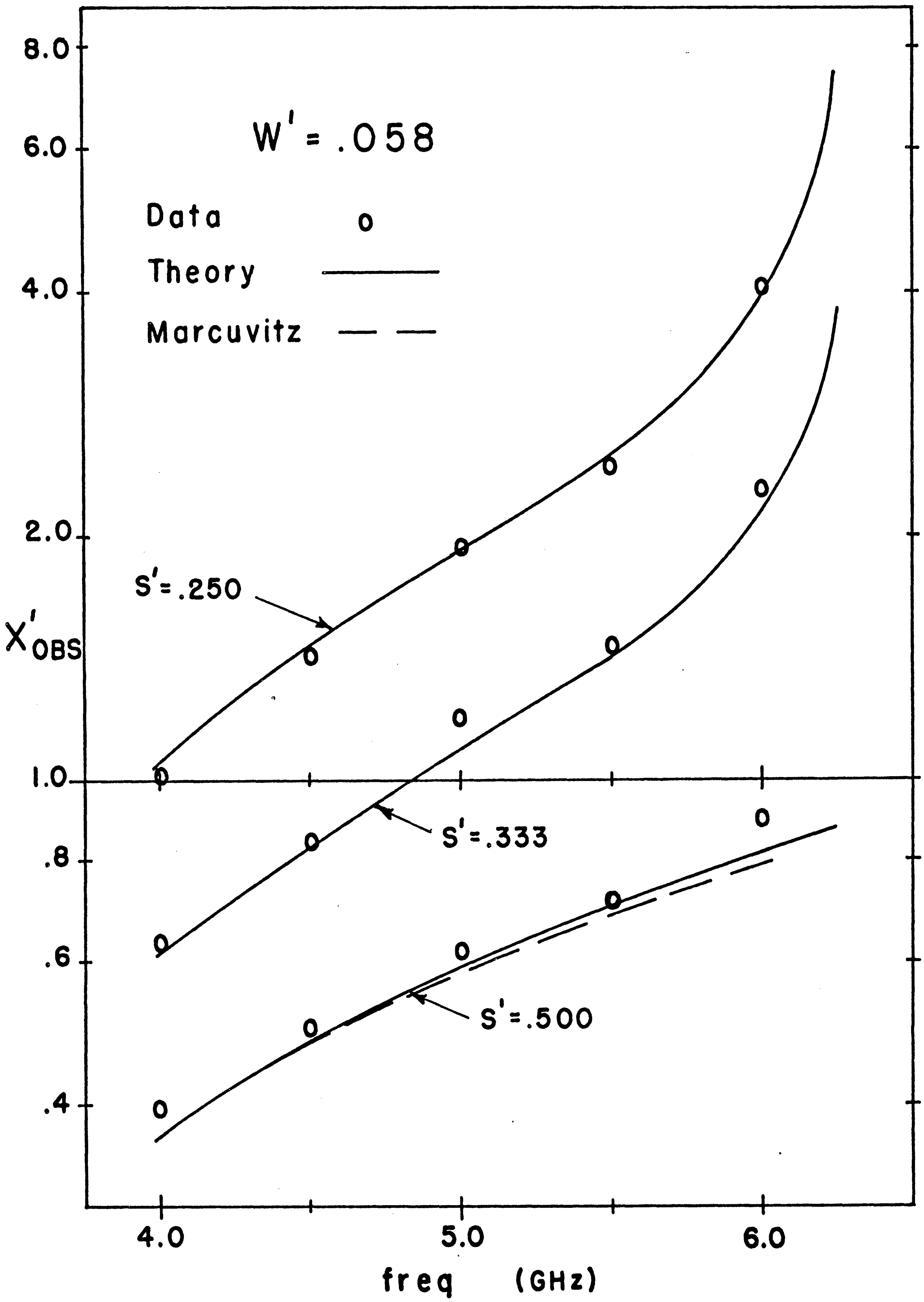

Fig. 5.7 Normalized flat post reactance w' = 0.058.

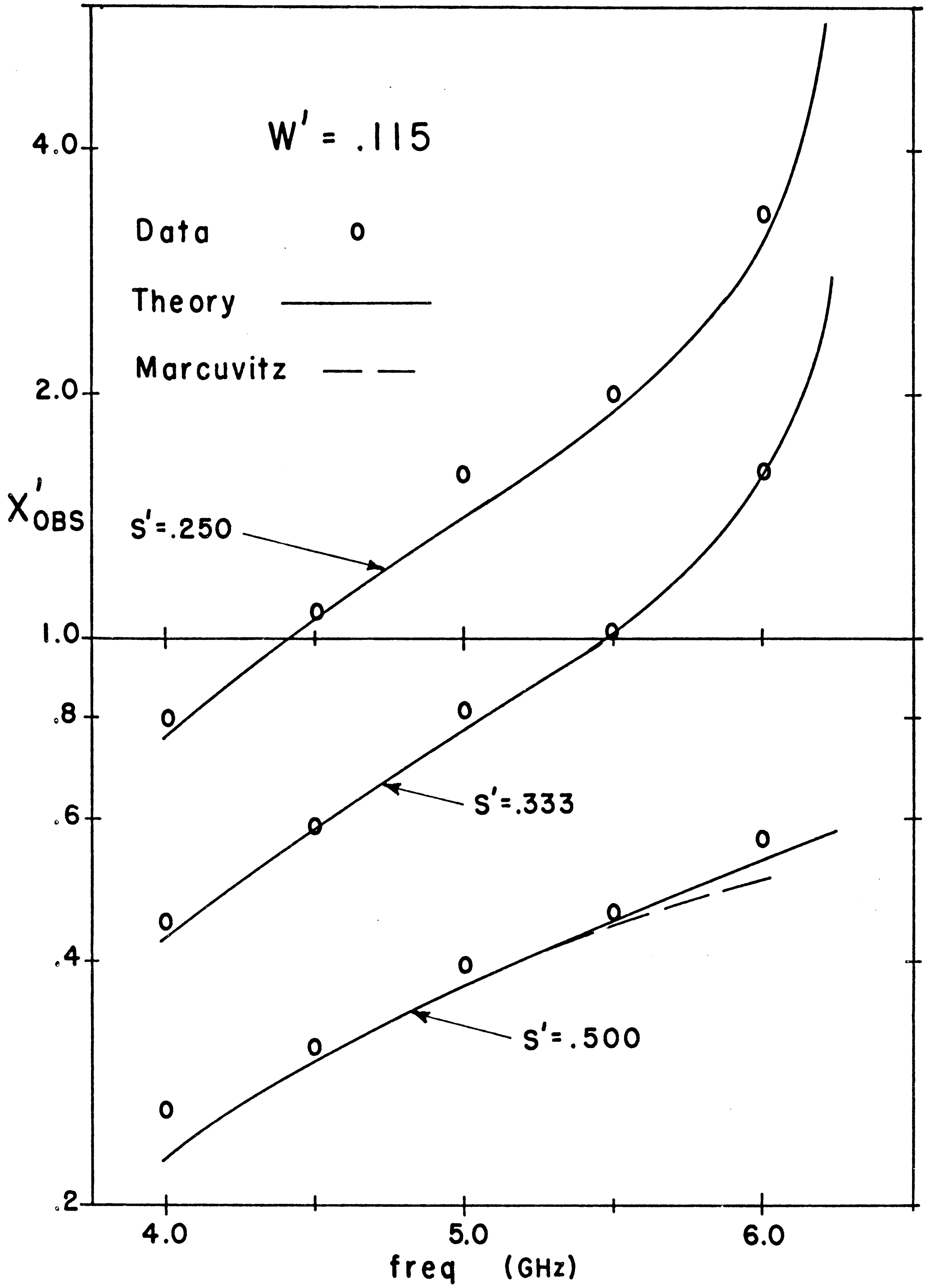

Fig. 5.8 Normalized flat post reactance w' = 0.115.

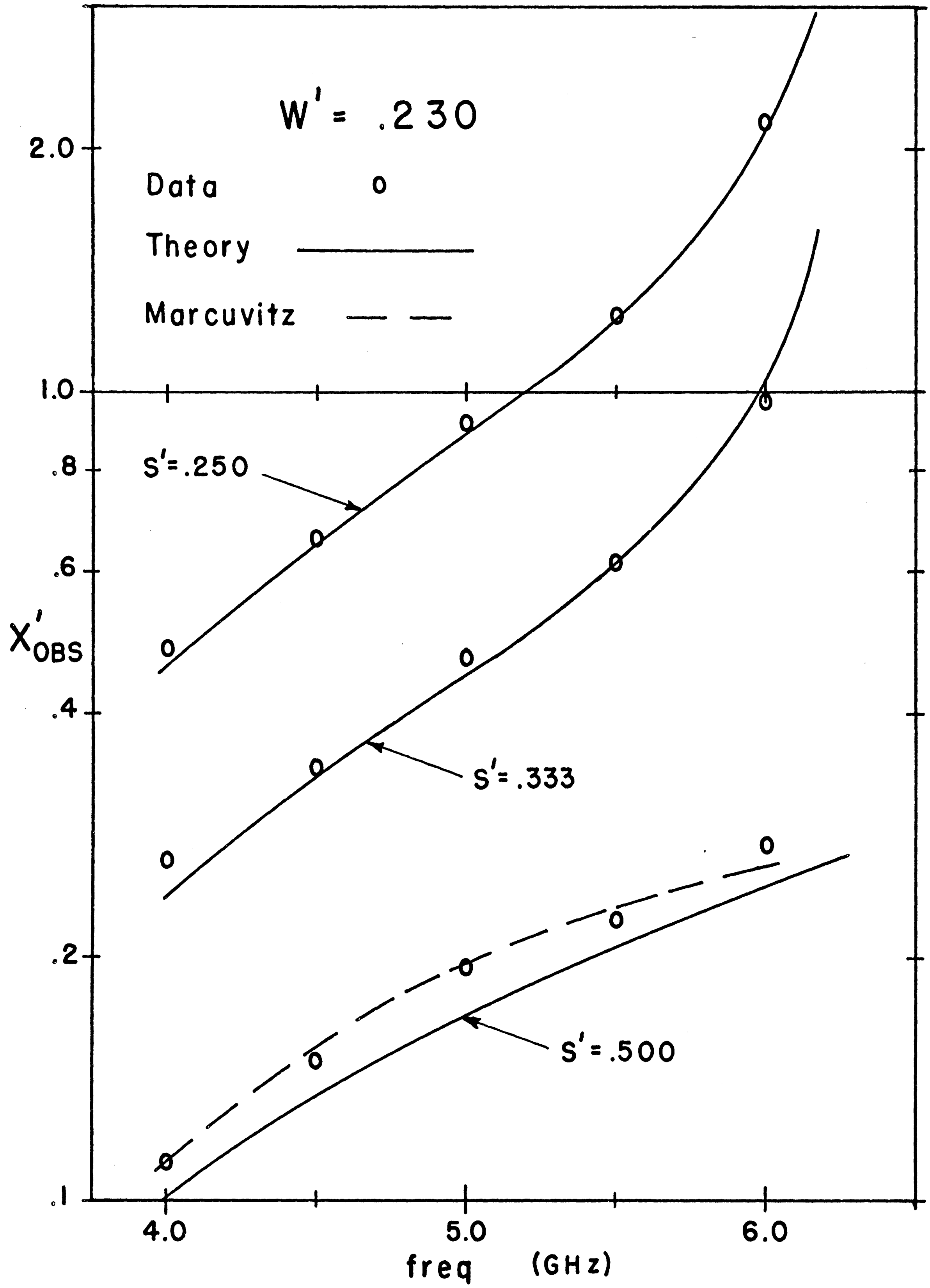

Fig. 5.9 Normalized flat post reactance w' = 0.230.

These graphs also include predicted values by Marcuvitz (Ref. 26) for the centered post position showing good correlation to the theory for Figs. 5.7, 5.8 while deviating approximately 10% for the wide case of Fig. 5.9. (Marcuvitz does not predict for off-centered flat posts.) The noticeable upswing of the off-centered curves of all three widths for the high frequency end is due to the action of the H_{20} mode impedance approaching infinity at 6.3 GHz.

5.3.2 Tuned Post. The final example considered is that produced by leaving the gap open, resulting in Z_G being the end capacitance of a circular post. This configuration is commonly called the tuned post and is described in Fig. 5.10 for different gap sizes. The gap dimensions are varied from zero to slightly larger than 1/4 the guide height. By centering the post, the H_{20} mode is decoupled so that the dominant mode region is extended to 7.46 GHz, the cutoff frequency for the H_{11} and E_{11} modes, thus allowing the observation and verification of the characteristic at 6.77 GHz where the reactance is independent of the gap size.

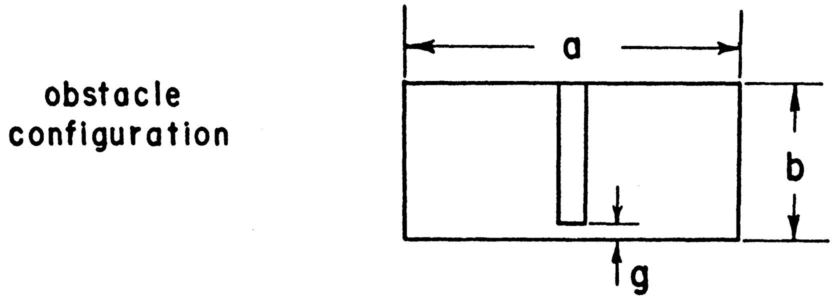

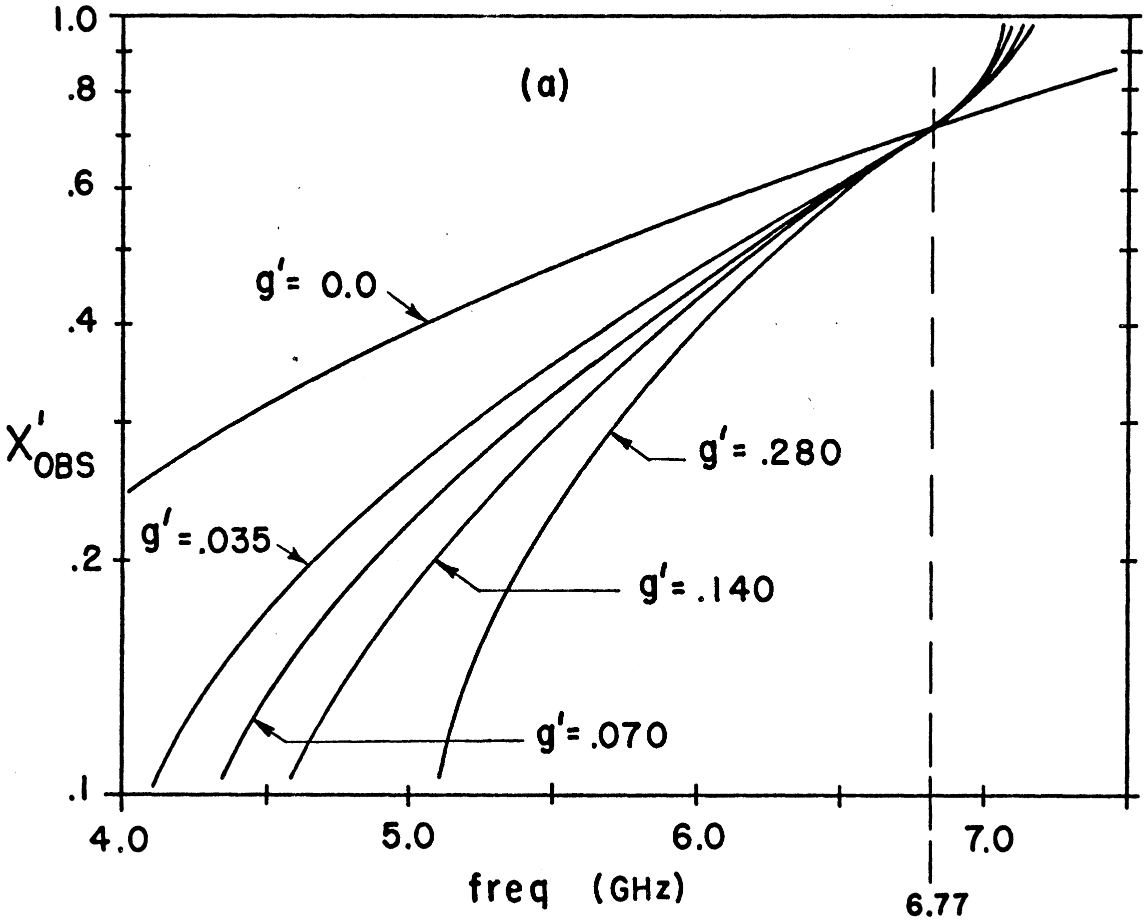

Fig. 5.10a Normalized obstacle reactance for gap size g variation, s' = 0.500, w' = 0.115.

(Theory)

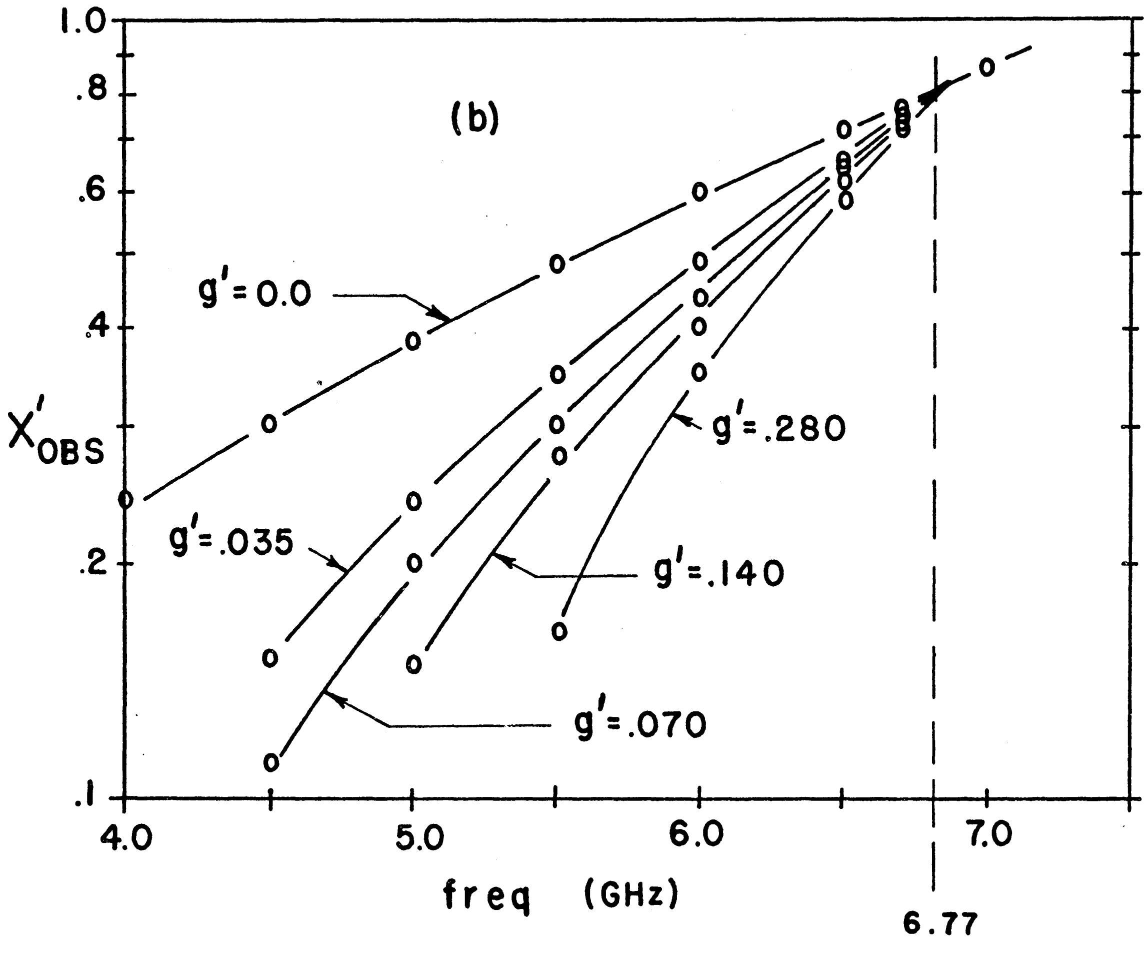

Fig. 5.10b Normalized obstacle reactance for gap size g variation, s' = 0.500, w' = 0.115.

(Experiment)

CHAPTER VI

REVIEW, CONCLUSIONS AND RELATED FUTURE STUDY

6.1 Introduction

All of the work is reviewed briefly, highlighting the prominent concepts and results introduced. Conclusions are drawn, followed by a short discussion of related future areas of study.

6.2 Review

The objective of this report was to characterize a common waveguide mount, resulting in a description which was convenient for use in circuit design. This goal has been satisfied. In the process, many additional thoughts have been introduced which either present an original idea or add support to a concept previously recognized. It is felt worthwhile to provide a short summary of these points, including the section number where each is discussed in more detail.

1) General Theoretical Analysis. By assuming a general expansion of the current density in the same orthogonal functions as the Green's function, it is possible to develop some knowledge about a radiating element without knowing the actual current distribution. Section 2.2 - 2.3.

2) Current Density y-dependence. As a consequence of the mathematics the y-dependence was easily developed, giving the current distribution on the post as a function of the mount parameters and the mode indices. It is most interesting how the phase information for current components associated with the H_{mn} and E_{mn} modes above and below cutoff is contained in the formulation. Section 2.3.6.

3) Mode Related Impedances. The development of the mode impedances Z_H and Z_E offer a strong case for adopting these formulations as the basis for waveguide characteristic impedances for all modes. Section 2.3.7.

4) Series Resonance of Mode Pairs. The resonant effect resulting from the series combination of Z_E and Z_H for the same m, n set is also interesting, particularly the fact that the resonant frequency is independent of m. Section 2.3.7.

5) Mount Equivalent Circuit. This circuit simply provides a means of defining the coupling between the impedance present in the gap and the mode impedances present in the waveguide arms. It is a linear, passive, reciprocal, doubly infinite network whose elements are a function only of the mount parameters. Section 2.3.7.

6) Impedance Measurement Technique. This simple concept of running a subminiature coaxial line inside the post to gain access to the gap was the heart of the thesis. All other attempts to measure Z_R failed. If the experimental effort had not produced such reliable and self-consistent results, the necessary insight to develop the theory would never have been obtained. Now that the technique has proven itself by measuring predictable impedance variations accurately, its real value will be in applications where the configuration cannot be handled theoretically, thus providing unique information. Section 4.2.1.

7) Measurement Circuit Modeling. Although the statistical method used was slow, tedious and expensive on the computer, it appeared to be the only way to isolate the extremely small effects due to the discontinuities in the line. The work was well justified by the resulting improvement in the data interpretation. Section 4.3.

6.3 Conclusions

The various graphs in Figs. 5.1 - 5.4 and 5.6 - 5.10 show a high degree of correlation between the theoretical plots and the measured data. Although only a limited number of situations were presented, they were of sufficient diversity to fully test the theory and the experimental procedure. The theory is further supported by the agreement with Schelkunoff (Ref. 21) and Marcuvitz (Ref. 26) for those special cases, as well as the low frequency formulation discussed in Section 2.4. On this basis it is reasonable to conclude that the theory presented is valid and that the measurement technique developed was highly successful.

6.4 Suggested Areas of Related Future Study

The following suggestions are submitted as areas in which investigations could be carried out using the information developed in this thesis as a basis upon which to expand.

6.4.1 Theoretical Study.

1) Application of the theoretical analysis to other physical configurations, e.g., gap driving point impedance for a gap in a circular post between two parallel ground planes. This configuration represents the feed point of a radial transmission line.

2) Removal of the current density x-distribution assumption in order to enhance accuracy and permit consideration of larger posts.

3) Removal of the gap voltage distribution assumptions in order to enhance accuracy and permit consideration of larger posts and larger gaps.

4) Application of the analysis to develop an equivalent circuit for a mount containing 2 independent gaps in the post.

5) Development of complex reflection coefficient descriptions for standard waveguide obstacles excited by higher order modes.

6.4.2 Experimental Study. Use the measurement technique on other types of mounting structures, including coaxial line, strip line, etc.; especially on configurations which cannot be handled theoretically.

6.4.3 Applications of the Circuit. The circuit developed to describe the mount can be used to improve the design of waveguide oscillators, amplifiers, frequency multipliers and converters, phase shifters, mixers, attenuators and various filter elements. Electronically tunable elements can also be designed using voltage-tunable devices mounted in this manner. An example of such an element is the common switching element employing a PIN diode as a variable Z_G.

APPENDIX A

DETERMINATION OF THE DYADIC GREEN'S FUNCTION FOR RECTANGULAR WAVEGUIDE

The following derivation was discussed in an advanced Electromagnetic Field Theory course given by Professor Tai, but the general method is not well known. For completeness a detailed description is given here.

We are interested in solving the vector wave equation

$$\nabla \times \nabla \times \bar{E}(\bar{r}) - k^2 \bar{E}(\bar{r}) = -j \omega \mu_o \bar{J}(\bar{r}') \qquad (A.1)$$

to develop a relationship for the electric field $\bar{E}(\bar{r})$ as a function of the current density $\bar{J}(\bar{r}')$. The method to be used is called the Green's Function method which is based on the proposition that a function $\bar{\bar{G}}(\bar{r}|\bar{r}')$ can be found which will satisfy the equation

$$\nabla \times \nabla \times \bar{\bar{G}}(\bar{r}|\bar{r}') - k^2 \bar{\bar{G}}(\bar{r}|\bar{r}') = \bar{\bar{I}} \delta(\bar{r} - \bar{r}') \qquad (A.2)$$

similar to (A.1), subject to the boundary condtions of the region of interest. Assuming such a $\bar{\bar{G}}(\bar{r}|\bar{r}')$ exists, (A.1) and (A.2) can be combined to develop an integral equation giving the necessary relationship between $\bar{E}(\bar{r})$ and $\bar{J}(\bar{r}')$. This result is

$$\bar{E}(\bar{r}) = -j \omega \mu_o \int_V \bar{\bar{G}}(\bar{r}|\bar{r}') \cdot \bar{J}(\bar{r}') \, dv' \qquad (A.3)$$

inviting interpretation of $\bar{\bar{G}}(\bar{r} \mid \bar{r}')$ as a coupling factor between $\bar{E}(\bar{r})$ and $\bar{J}(\bar{r}')$.

To solve (A. 2) let us investigate the solutions of the homogeneous equation

$$\nabla \times \nabla \times \bar{S} - \gamma^2 \bar{S} = 0 . \qquad \text{(A. 4)}$$

$\bar{S}$ in general can be represented by

$$\bar{M} = \nabla \times (\hat{z} \psi_1), \qquad \bar{N} = \frac{1}{\gamma} \nabla \times \nabla \times (\hat{z} \psi_2) \qquad \text{(A. 5)}$$

where ψ_1 and ψ_2 are two independent solutions satisfying the scalar wave equation

$$\nabla^2 \psi + \gamma^2 \psi = 0. \qquad \text{(A. 6)}$$

The region under consideration is the inside of a rectangular waveguide, described in Fig. A. 1. It is considered infinite in extent in the $\pm$ z-directions requiring Sommerfeld's radiation condition (Ref. 27) for the boundary conditions at large $|z|$. The waveguide is assumed to be perfectly conducting, consequently $\hat{n} \times \bar{E} = 0$ is the internal boundary condition on the guide wall surface. Since $\bar{\bar{G}}(\bar{r} \mid \bar{r}')$ is associated directly with $\bar{E}$, this boundary condition must hold for $\bar{\bar{G}}(\bar{r} \mid \bar{r}')$ in (A. 2), therefore requiring

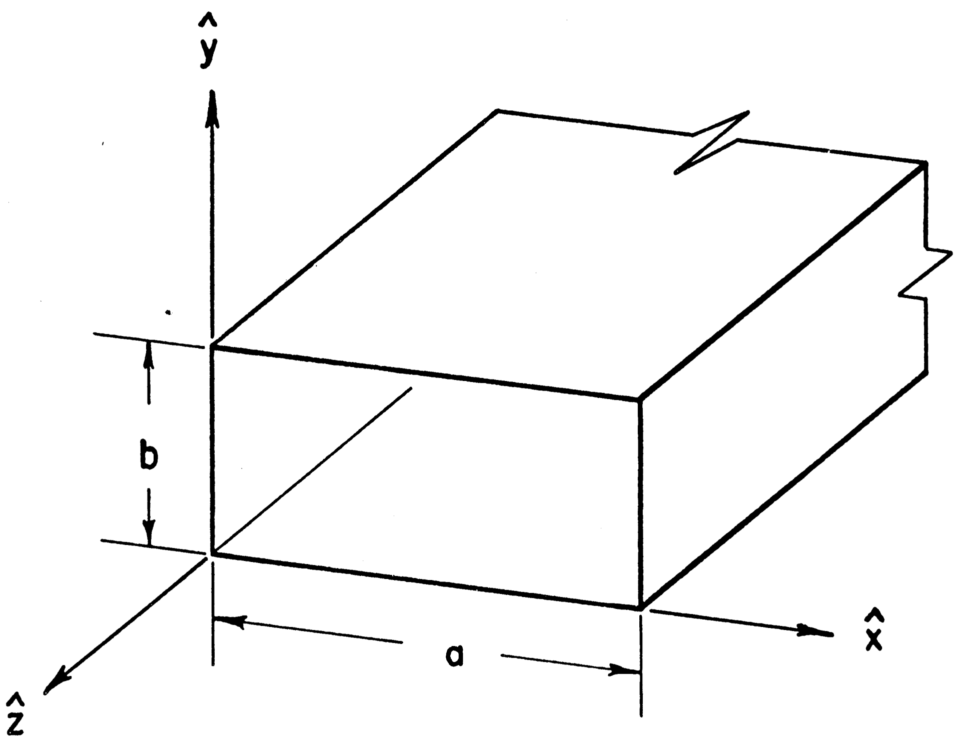

Fig. A.1 Coordinate description for the rectangular waveguide.

$$\hat{n} \times \begin{Bmatrix} \bar{M} \\ \\ \bar{N} \end{Bmatrix} = 0 \qquad \text{(A. 7)}$$

on the walls.

Equation (A. 6) can then be solved by separation of variables resulting in the functions

$$\psi_1 = \cos k_x x \cos k_y y \, e^{-j \zeta z} \qquad \text{(A. 8a)}$$

and

$$\psi_2 = \sin k_x x \sin k_y y \, e^{-j \zeta z} \qquad \text{(A. 8b)}$$

with

$$k_x = \frac{m\pi}{a}, \qquad k_y = \frac{n\pi}{b}$$

$$\zeta^2 = \gamma^2 - k_x^2 - k_y^2$$

which when substituted in (A. 5) satisfy these boundary conditions. The general solution is represented by

$$\bar{M}_{mn} = \bar{m} \, e^{-j \zeta z} \qquad \text{(A. 9a)}$$

$$\bar{m} = -\hat{x} \, k_y \cos k_x x \sin k_y y + \hat{y} \, k_x \sin k_x x \cos k_y y$$

and

$$\bar{N}_{mn} = \bar{n}\, e^{-j \zeta z} \qquad \text{(A. 9b)}$$

$$\bar{n} = \frac{1}{\gamma} \Big[-\hat{x}\, j\, \zeta\, k_x \cos k_x x \sin k_y y - \hat{y}\, j\, \zeta\, k_y \sin k_x x \cos k_y y$$

$$+ \hat{z}\, k_{mn}^2 \sin k_x x \sin k_y y \Big]$$

where

$$k_{mn}^2 = k_x^2 + k_y^2 .$$

We now assume an expansion of the delta function $\bar{\bar{I}}(\bar{r} - \bar{r}')$ in terms of these general functions allowing arbitrary vector coefficients $\bar{P}$, $\bar{Q}$. .

$$\bar{\bar{I}}\, \delta(\bar{r} - \bar{r}') = \sum_{m=0}^{\infty} \sum_{n=0}^{\infty} \int_{-\infty}^{\infty} d\zeta \left[\bar{M}_{mn}\, \bar{P} + \bar{N}_{mn}\, \bar{Q} \right]$$

(A. 10)

To determine $\bar{P}$, take the dot product of $\bar{M}_{m'n'}(\zeta')$ with both sides of (A. 10) and integrate over the enclosed volume, yielding

$$\int_{vol} \bar{M}_{m'n'}(\zeta') \cdot \bar{\bar{I}}\, \delta(\bar{r} - \bar{r}')\, dv = \bar{M}'_{m'n'}(\zeta')$$

$$= \int_{-\infty}^{\infty} d\zeta \int_{-\infty}^{\infty} T_{m'n'}\, \bar{P}\, e^{-j(\zeta + \zeta')z}\, dz \qquad \text{(A. 11)}$$

where

$$T_{m'n'} = \frac{ab}{4}\, k_{m'n'}^2\, (1 + \delta_o) \qquad \text{(A. 12)}$$

and $\overline{M}'$ indicates evaluation at the primed coordinates. Then knowing that

$$\delta[\zeta - (-\zeta')] = \frac{1}{2\pi} \int_{-\infty}^{\infty} e^{-j[\zeta - (-\zeta')] z} \, dz \qquad (A.13)$$

results in

$$\overline{M}'_{m'n'}(\zeta') = 2\pi \, \overline{P}(-\zeta') \, T_{m'n'}$$

or

$$\overline{P}_{mn}(\zeta) = \frac{\overline{M}'_{mn}(-\zeta) \, (2 - \delta_o)}{k^2_{mn} \, \pi \, a \, b} . \qquad (A.14)$$

Following the same procedure with $\overline{N}_{m'n'}(\zeta')$ we find that

$$\overline{Q}_{mn}(\zeta) = \frac{\overline{N}'_{mn}(-\zeta) \, (2 - \delta_o)}{k^2_{mn} \, \pi \, a \, b} . \qquad (A.15)$$

so that

$$\overline{\overline{I}} \, \delta(\overline{r} - \overline{r}') = \sum_{m=0}^{\infty} \sum_{n=0}^{\infty} \int_{-\infty}^{\infty} \frac{d\zeta}{2\pi T_{mn}} \left[\overline{M}_{mn}(\zeta) \overline{M}'_{mn}(-\zeta) + \overline{N}_{mn}(\zeta) \overline{N}'_{mn}(-\zeta) \right] \qquad (A.16)$$

Next assume an expansion of $\overline{\overline{G}}(\overline{r} \mid \overline{r}')$ in the same functions including necessary arbitrary scalar coefficients (α, β) to represent a general solution.

$$\overline{\overline{G}}(\overline{r} \; \overline{r}') = \sum_{m=0}^{\infty} \sum_{n=0}^{\infty} \int_{-\infty}^{\infty} \frac{d\zeta}{2\pi T_{mn}} \left[\alpha \overline{M}_{mn}(\zeta) \overline{M}'_{mn}(-\zeta) + \beta \overline{N}_{mn}(\zeta) \overline{N}'_{mn}(-\zeta) \right] \qquad (A.17)$$

Now by substituting (A.17) into (A.2) and carrying out the indicated operations we find that

$$(k_{mn}^2 + \zeta^2 - k^2)\,\bar{\bar{G}}(\bar{r}\,|\,\bar{r}') = \bar{\bar{I}}\;\delta(\bar{r} - \bar{r}'), \tag{A.18}$$

which specifies (α, β) as

$$\alpha = \beta = \frac{1}{(k_{mn}^2 + \zeta^2 - k^2)} \tag{A.19}$$

giving

$$\bar{\bar{G}}(\bar{r}\,|\,\bar{r}') = \sum_{m=0}^{\infty} \sum_{n=0}^{\infty} \int_{-\infty}^{\infty} \frac{d\,\zeta}{2\pi\, T_{mn}} \left[\frac{\bar{M}_{mn}(\zeta)\,\bar{M}'_{mn}(-\zeta) + \bar{N}_{mn}(\zeta)\,\bar{N}'_{mn}(-\zeta)}{(\zeta - k_g)\,(\zeta + k_g)} \right] \tag{A.20}$$

where $k_g^2 = k^2 - k_{mn}^2$ = (waveguide wave number)^2.

This is integrated by contour integration; by closing our contour in the lower half plane for the case $z > z'$ we include only the residue from the pole at $\zeta = k_g$. For $z < z'$ the contour includes the pole at $\zeta = -k_g$. This convention is the result of assuming $e^{j\omega t}$ time dependence.

We have then as a final result

$$\bar{\bar{G}}(\bar{r}\,|\,\bar{r}') = \sum_{m=0}^{\infty} \sum_{n=0}^{\infty} \frac{(2 - \delta_o)}{ab\, k_{mn}^2\, \Gamma_{mn}} \left[\bar{m}\,\bar{m}' + \bar{n}(\pm k_g)\,\bar{n}'(\pm k_g) \right] e^{-\Gamma_{mn}|z-z'|} \tag{A.21}$$

where we use $\begin{cases} \text{top sign for } z > z' \\ \text{bottom sign for } z < z' \end{cases}$

and $\Gamma_{mn} = j\, k_g$. The functional portion of (A. 21) is determined by substituting for $\overline{m}$, $\overline{n}$ from (A. 9) resulting in

$$\left[\overline{m}\ \overline{m}' + \overline{n}(\pm k_g)\ \overline{n}'(\pm k_g)\right]$$

$$\Longrightarrow \hat{y}\hat{y}\left[k_x^2 + \frac{(k^2 - k_{mn}^2)\, k_y^2}{k^2}\right] \sin k_x x \sin k_x x' \cos k_y y \cos k_y y' \tag{A. 22a}$$

or

$$\Longrightarrow \hat{y}\hat{y}\left[\frac{k_{mn}^2}{k^2}\,(k^2 - k_y^2)\right] \sin k_x x \sin k_x x' \cos k_y y \cos k_y y' \tag{A. 22b}$$

for the $\hat{y}\hat{y}$ component.

Equation (A. 22a) has two terms representing respectively the functional part of $G_H(\overline{r}\,|\,\overline{r}')$ and $G_E(\overline{r}\,|\,\overline{r}')$, while (A. 22b) is the combined form used in (2.5).

APPENDIX B

DETERMINATION OF THE GREEN'S FUNCTION FOR TERMINATED WAVEGUIDE

During the process of solving for $\bar{\bar{G}}(\bar{r}\,|\,\bar{r}')$ in Appendix A, the technique of separation of variables was used to solve the homogeneous equation (A. 6) in three dimensions. This concept can also be applied in interpreting $\bar{\bar{G}}(\bar{r}\,|\,\bar{r}')$ to determine dependence upon the spatial variables. In particular the y-dependence corresponds directly to that of a one dimensional transmission line situation with matched terminations. By considering the waveguide phase constant ($k_g = -j\,\Gamma_g$) as the phase constant of a hypothetical transmission line, it is possible to investigate the terminated properties of this one-dimensional line and apply the solution to the waveguide; thus resulting in a modified function of $\bar{\bar{G}}_T(\bar{r}\,|\,\bar{r}')$ which shall be called the Green's function for terminated waveguide.

Consider the one dimensional wave equation

$$\frac{d^2\, g_T(z\,|\,z')}{d\,z^2} + k_g^{\;2}\, g_T(z\,|\,z') = -\,\delta\,(z - z') \qquad \text{(B. 1)}$$

which has the solution

$$g_T(z|z') = \begin{cases} A^+ e^{jk_g z} + B^+ e^{-jk_g z} & z \geq z' \quad \text{(B. 2a)} \\ \\ A^- e^{jk_g z} + B^- e^{-jk_g z} & z \leq z' \quad \text{(B. 2b)} \end{cases}$$

where A^+, B^+, A^-, B^- are coefficients to be determined by application of boundary conditions. Here $g_T(z|z')$ is associated with the voltage on the line so that the appropriate termination or boundary condition is (Ref. 19),

$$g_T(\ell_1|z') = j \frac{Z_{\ell 1}}{Z_c k_g} \left. \frac{d\, g_T(z|z')}{d z} \right|_{z = \ell_1} \qquad \text{(B. 3)}$$

with

$Z_{\ell 1}$ = effective terminating impedance at ℓ_1

and

Z_c = characteristic impedance of the line.

A more convenient form for describing the termination is obtained using the concept of complex voltage reflection coefficient ρ where

$$\rho_1 = \frac{Z_{\ell 1} - Z_c}{Z_{\ell 1} + Z_c} \tag{B. 4}$$

Applying (B. 3) to (B. 2a) results in

$$A^+ = B^+ \rho_1 e^{-j\, 2k_g \ell_1} \tag{B. 5}$$

Similarly for (B. 2b) we have

$$B^- = A^- \rho_2 e^{j\, 2k_g \ell_2} \tag{B. 6}$$

where ρ_1, ρ_2 are reflection coefficients at planes 1 and 2 respectively and ℓ_1, ℓ_2, are the coordinate values at planes 1 and 2. At $z = z'$ the voltage must be continuous so that

$$g_T(z'_+ | z') = g_T(z'_- | z') \tag{B. 7}$$

resulting in a third relationship

$$B^+ e^{-j\, 2k_g z'} \left[1 + \rho_1 e^{-j\, 2k_g(\ell_1 - z')} \right] = A^- \left[1 + \rho_2 e^{j\, 2k_g(\ell_2 - z')} \right] \tag{B. 8}$$

The fourth and final condition requires a step discontinuity in the voltage derivative at $z = z'$ giving

$$B^{+} e^{-jk_g z'} \left[1 - \rho_1 e^{-j2k_g(\ell_1 - z')}\right] + A^{-} e^{jk_g z'} \left[1 - \rho_2 e^{j2k_g(\ell_2 - z')}\right] = \frac{-j}{k_g}$$

(B. 9)

Solving simultaneously (B. 5), (B. 6), (B. 8), and (B. 9), and substituting in (B. 2) results in

$$g_T(z|z') = \begin{cases} \dfrac{e^{-jk_g(z-z')}}{j2k_g} \left[\dfrac{\left(1+\rho_2 e^{j2k_g(\ell_2-z')}\right)\left(1+\rho_1 e^{-j2k_g(\ell_1-z)}\right)}{\left(1-\rho_1\rho_2 e^{-j2k_g(\ell_1-\ell_2)}\right)}\right] & z \geq z' \quad \text{(B. 10a)} \\[2em] \dfrac{e^{-jk_g(z'-z)}}{j2k_g} \left[\dfrac{\left(1+\rho_1 e^{-j2k_g(\ell_1-z')}\right)\left(1+\rho_2 e^{j2k_g(\ell_2-z)}\right)}{\left(1-\rho_1\rho_2 e^{-j2k_g(\ell_1-\ell_2)}\right)}\right] & z \leq z' \end{cases}$$

(B. 10b)

For $\rho_1 = \rho_2 = 0$ (matched conditions) this reduces to

$$g_o(z|z') = \frac{e^{-j\,k_g|z-z'|}}{j\,2k_g} = \frac{e^{-\Gamma_g|z-z'|}}{2\,\Gamma_g} \qquad \text{(B. 11)}$$

which is the one-dimensional free space Green's function. The multimode case must consider a summation of effects; therefore

$$\Gamma_g \longrightarrow \Gamma_{mn}$$

and

$$g_o(z|z') \longrightarrow G_z(z|z') = \sum_m \sum_n \frac{e^{-\Gamma_{mn}|z-z'|}}{2\,\Gamma_{mn}} \tag{B.12}$$

representing the portion of $G(\overline{r}|\overline{r}')$ which is a function of z. By direct association between (B.12), (B.11) and (B.10) we see that the modification necessary to consider terminations for the waveguide is the term in brackets in (B.10). However, this generalized form is unnecessary since the present application establishes both the source and observation points to be in the $z = 0$ plane of the waveguide, requiring the substitution $z = z' = 0$. In addition it is more convenient to define ℓ_1 and ℓ_2 as distances (magnitude only) from $z = 0$ to the termination planes. Therefore

$$\tau = \frac{\left(1 + \rho_{1mn} e^{-2\Gamma_{mn}|\ell_1|}\right)\left(1 + \rho_{2mn} e^{-2\Gamma_{mn}|\ell_2|}\right)}{1 - \rho_{1mn}\rho_{2mn} e^{-2\Gamma_{mn}\left(|\ell_1| + |\ell_2|\right)}} \tag{B.13}$$

which is the Green's function termination parameter allowing us to write

$$\overline{\overline{G}}_T(\overline{r}|\overline{r}') = \overline{\overline{G}}(\overline{r}|\overline{r}')\,\tau . \tag{B.14}$$

APPENDIX C

COMPUTER PROGRAM FOR THEORETICAL IMPEDANCE CALCULATION

The driving point impedance Z_R is calculated using (3.11) and the summation limit criteria developed in Section 3.3. Only the matched condition is considered so that $Z_{Tmn} = Z_{mn}$. Multiple loops are used in the program allowing variation of all configuration parameters plus frequency. Plots of impedance versus frequency are obtained along with individual value listings for each complete parameter set.

The obstacle impedance elements (3.10) can also be calculated but only relative to the H_{10} mode. A complex circuit is used to represent Z_G to allow great flexibility in program use. This is seen in Fig. C.1. Simpler circuits are represented by setting the appropriate elements in Fig. C.1 equal to zero or infinity.

The waveguide input impedance Z_{IN} (see Fig. 3.3), normalized to Z_{c10} is also determined for the terminating condition of a match, short, or open on the opposite waveguide arm.

All of the information concerning parameter values and iterations is contained in the necessary "data deck" which must follow the program. The description for this "data deck" format is given below. This is followed by a listing of the full program.

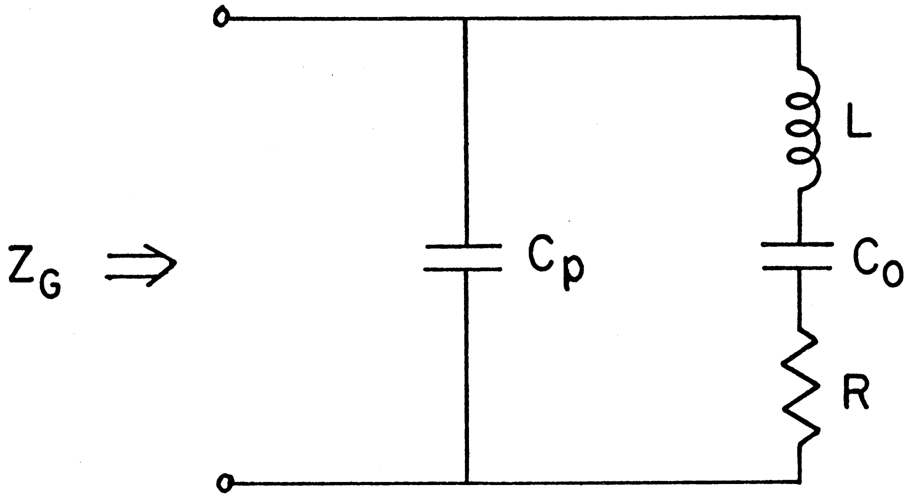

Fig. C.1 Gap impedance representation for use in the computer program.

Data Deck Format

Card	Format	Description
1	25I3	Fifteen numbers, all ≥ 1 representing the number of iterations for each variable; plus the branching code $ZQT = \begin{cases} 5 & \text{includes obstacle program} \\ 1 & \text{skips obstacle program} \end{cases}$ Order of variable iterations: M, N, H', G', S', W', A, B, C, D, CP, L, R, CO, ZQT
2	10F8.4	Values of H', $G'/2 \leq H' \leq 0.500$
3	10F8.4	Values of G', $0.0 < G' \leq 0.250$
4	10F8.4	Values of S', $0.0 < S' \leq 0.500$
5	10F8.4	Values of W', $0.0 < W' \leq 0.250$
6	10F8.4	Values of A, in centimeters (4.76/C, 2.286/X)
7	10F8.4	Values of B, in centimeters (2.215/C, 1.016/X)
8	10F8.4	Values of C, usually = 0.0, allows for external fringing fields at the gap, in 10^{-15} farads
9	10F8.4	RHO, values of D, RHO = -1, 0, +1 D in centimeters
10	10F8.4	Values of CP, in 10^{-12} farads
11	10F8.4	Values of L, in 10^{-9} henrys

12	10F8.4	Values of R, in ohms
13	10F8.4	Values of CO, in 10^{-12} farads
14	2F10.5, I4, 14A4	FSTART, FINT, FMAX, TITLE; where FSTART + FINT = 1st FREQUENCY value, FINT = frequency increment, FMAX = number of increments, and TITLE = describes frequency range

FORTRAN IV G COMPILER MAIN

```
             C     THIS PROGRAM IS DESIGNED TO GIVE GAP IMPEDANCE PLOTS (WITHOUT
             C     TERMINATIONS) AS A FUNCTION OF THE MANY MOUNT PARAMETERS.  IT
             C     WILL GIVE INDIVIDUAL MODE PLOTS ALSO IF MODIFIED SLIGHTLY..
             C     SECONDLY IT GIVES NORMALIZED INPUT IMPEDANCE VALUES AND PLOTS
             C     TO A H(10) MODE INCIDENT FROM ONE SIDE WITH A SHORT,OPEN OR
             C     MATCH ON THE OTHER, WITH COMPLEX LOAD IN THE GAP.
 0001              COMMON  RMN(10,15,101) ,XMN(10,15,101)
 0002              DIMENSION FREQ(110),D(1500),H(10),S(5),W(5),RN(15,101),
                  1 XN(15,101),GN(15,101),BN(15,101),RLOAD(110),XLOAD(110),A(5),
                  2 B(5),FTITLE(14),CAP(10),                          GLOAD(110),
                  3 BLOAD(110),BCAP(110),RPLT(110),XPLT(110),CF(51),G(5),DIST(20),
                  4 CP(5),L(5),R(5),C(5),RSN(22),XSN(22),RTN(22),XTN(22)
 0003              REAL  L
 0004              INTEGER F,FMAX,HMAX,SMAX,WMAX,BMAX,AMAX,CMAX,ZQT,GMAX,CPMAX,DMAX,
                  1 LMAX,RMAX,COMAX
 0005              MK = 99
 0006        1     FORMAT (25I3)
 0007        2     FORMAT (10F8.4)
 0008        3     FORMAT (2F10.5,I4,14A4)
 0009        4     FORMAT (1H1,10X,'FSTART = ',F10.5, 7X,'FINT =',F10.5, 7X,
                  1 'FMAX =',I4,10X,14A4)
 0010        5     FORMAT (1H0,4X,'MMAX =',I3,5X,'NMAX =',I3,5X,'HMAX =',I3,5X,
                  1 'GMAX =',I3,5X,'SMAX =',I3,5X,'WMAX =',I3,5X,'AMAX =',I3,5X,
                  2 'BMAX =',I3,5X,'CMAX =',I3/5X,'DMAX =',I3,5X,'CPMAX=',I3,5X,
                  3 'LMAX =',I3,5X,'RMAX =',I3,5X,'COMAX=',I3,5X,'FLAG =',I3)
 0011        6     FORMAT (1H0,10X,'GAP HEIGHT VALUES ARE =',10(F8.4,','))
 0012        7     FORMAT (1H0,10X,'POSITION   VALUES ARE =',10(F8.4,','))
 0013        8     FORMAT (1H0,10X,'POST WIDTH VALUES ARE =',10(F8.4,','))
 0014        9     FORMAT (1H0,10X,'G. WIDTH   VALUES ARE =',10(F8.4,','))
 0015       10     FORMAT (1H0,10X,'G. HEIGHT  VALUES ARE =',10(F8.4,','))
 0016       11     FORMAT (1H1)
 0017       12     FORMAT (10X,'M ='I2,10X,'N =',I2,10X,'GUIDE WIDTH (CM) =',
                  1 F8.4,10X,'GUIDE HEIGHT (CM) =',F8.4//)
```

```
0018      13    FORMAT (1H0,50X,'FREQUENCY IN GHZ')
0019      14    FORMAT (1H0,10X,'FREQ (GHZ)',10X,'RMN (OHMS)',10X,'XMN (OHMS)'//)
0020      15    FORMAT (10X,F10.5,12X,F8.3,12X,F8.3,12X,F8.3,12X,F8.3)
0021      16    FORMAT (1H0,10X,'FRINGE CAP VALUES ARE =',10(F8.4,','))
0022      17    FORMAT (10X,'M ='I2,10X,'N =',I2,10X,'GUIDE WIDTH (CM) =',
               1 F8.4,10X,'GUIDE HEIGHT (CM) =',F8.4,10X,' W =',F8.4/10X,'S =',
               2 F8.4//)
0023      18    FORMAT (10X,'M ='I2,10X,'N =',I2,10X,'GUIDE WIDTH (CM) =',
               1 F8.4,10X,'GUIDE HEIGHT (CM) =',F8.4,10X,' W =',F8.4/ 3X,'S =',
               2 F8.4,10X,'H =',F8.4,10X,'G =',F8.4,10X,'CAP =',F8.4//)
0024      19    FORMAT (10X,'M ='I2,10X,'N =',I2,10X,'GUIDE WIDTH (CM) =',
               1 F8.4,10X,'GUIDE HEIGHT (CM) =',F8.4,10X,' W =',F8.4/ 3X,'S =',
               2 F8.4,10X,'H =',F8.4,10X,'G =',F8.4,10X,'CAP =',F8.4,10X,'DIST =',
               3 F8.4,10X,'CP =',F8.4/ 3X,'L =',F8.4,10X,'R =',F8.4,10X,
               4 'C =',F8.4//)
0025      20    FORMAT (1H0,10X,'GAP SIZE VALUES ARE =',10(F8.4,','))
0026      21    FORMAT (1H0,10X,'RHO & DISTANCE TO LOAD =',10(F8.4,','))
0027      22    FORMAT (1H0,10X,'PACKAGE CAPACITANCE =',10(F8.4,','))
0028      23    FORMAT (1H0,10X,'LEAD INDUCTANCE =',10(F8.4,','))
0029      24    FORMAT (1H0,10X,'RESISTANCE VALUES =',10(F8.4,','))
0030      25    FORMAT (1H0,10X,'SERIES CAPACITANCE =',10(F8.4,','))
0031      26    FORMAT (1H0,10X,'FREQ (GHZ)',10X,'RSN (OHMS)',10X,'XSN (OHMS)',
               1 10X,'RTN (OHMS)',10X,'XTN (OHMS)'//)
0032      40    READ (5,1 ) MMAX,NMAX,HMAX,GMAX,SMAX,WMAX,AMAX,BMAX,CMAX,DMAX,
               1 CPMAX,LMAX,PMAX,COMAX,ZOT
0033            READ (5,2 )(H(K),K=1,HMAX)
0034            READ (5,2) ( G(K),K=1, GMAX)
0035            READ (5,2 )(S(K),K=1,SMAX)
0036            READ (5,2 )(W(K),K=1,WMAX)
0037            READ (5,2 )(A(K),K=1,AMAX)
0038            READ (5,2 )(B(K),K=1,BMAX)
0039            READ (5,2 )(CAP(K),K=1,CMAX)
0040            READ (5,2) RHO,(DIST(K),K=1,DMAX)
0041            READ (5,2) (CP(K),K=1,CPMAX)
0042            READ (5,2) ( L(K),K=1, LMAX)
```

```
      READ (5,2) ( R(K),K=1, RMAX)
      READ (5,2) ( C(K),K=1, CMAX)
      READ (5,3) FSTART,FINT,FMAX,(FTITLE(K),K=1,14)
      WRITE(6,4) FSTART,FINT,FMAX,(FTITLE(K),K=1,14)
      WRITE(6,5)  MMAX,NMAX,HMAX,GMAX,SMAX,WMAX,AMAX,BMAX,CMAX,DMAX,
     1 CPMAX,LMAX,RMAX,COMAX,ZQT
      WRITE(6,6) (H(K),K=1,HMAX)
      WRITE(6,20)( G(K),K=1, GMAX)
      WRITE(6,7) (S(K),K=1,SMAX)
      WRITE(6,8) (W(K),K=1,WMAX)
      WRITE(6,9) (A(K),K=1,AMAX)
      WRITE(6,10)(B(K),K=1,BMAX)
      WRITE(6,16)(CAP(K),K=1,CMAX)
      WRITE(6,21)RHO,(DIST(K),K=1,DMAX)
      WRITE(6,22)(CP(K),K=1,CPMAX)
      WRITE(6,23)( L(K),K=1, LMAX)
      WRITE(6,24)( R(K),K=1, RMAX)
      WRITE(6,25)( C(K),K=1, CMAX)
   50 DO 60 KK=1,FMAX
      FREQ(KK) = FSTART + FINT*KK
   60 CONTINUE
      DO 900 JA =1,AMAX
      DO 850 JB =1,BMAX
      DO 601 JN =1,NMAX
      N = JN-1
      DO 600 M =1,MMAX
   65 IF (N) 70,70,75
   70 DEL = 1.0
      GO TO 80
   75 DEL = 0.5
   80 DO 510 F =1,FMAX
      DEN1 =(M*14.986/A(JA))**2 +(N*14.986/B(JB))**2-FREQ(F)**2
      IF (ABS(DEN1) .LT. .0000001) GO TO 120
      Z=376.700*B(JB)*DEL*(FREQ(F)**2-(N*14.986/B(JB))**2)/(A(JA)*
     1 FREQ(F)*SQRT(ABS(DEN1)))
      IF (DEN1) 90,120,100
```

```
90      RMN(M,JN,F)  =  7
        XMN(M,JN,F)  =  0.0
        GO TO 500
100     RMN(M,JN,F)  =0.0
        XMN(M,JN,F)  =7
        GO TO 500

120     XMN(M,JN,F)  =  1000.
        RMN(M,JN,F)  =  1000.
500     CONTINUE
510     CONTINUE
600     CONTINUE
601     CONTINUE
        DO 800 JW =1,WMAX
        DO 750 JS =1,SMAX
603     DO 650 JN =1,NMAX
        N = JN-1
        DO 605 F =1,FMAX
        RN(JN,F) =0.0
        XN(JN,F) =0.0
605     CONTINUE
        DO 640 F =1,FMAX
        DO 630 M =1,MMAX
        IF (F .GT. 1) GO TO 627
        CF(M)=(SIN(M*3.1416*S(JS))*SIN(M*1.5708*W(JW))/(M*1.5708*W(JW)))
       1 **2
627     CONTINUE
        RN(JN,F)  =  RN(JN,F)+CF(M)*RMN(M,JN,F)
        XN(JN,F)  =  XN(JN,F)+CF(M)*XMN(M,JN,F)
630     CONTINUE
        DEN2 = RN(JN,F)**2 + XN(JN,F)**2
        GN(JN,F)  =  RN(JN,F)/DEN2
        BN(JN,F)  =-XN(JN,F)/DEN2
640     CONTINUE
650     CONTINUE
        DO 700 JH =1,HMAX
```

```
      DO 699 JG=1,GMAX
      DO 653 F=1,FMAX
      GLOAD(F) =0.0
  653 CONTINUE
      DO 695 JC =1,CMAX
      WRITE (6,11)
      WRITE (6,18) MK,MK,A(JA),B(JB),W(JW),S(JS),H(JH),G(JG),CAP(JC)
      WRITE (6,14)
      DO 655 F=1,FMAX
      BLOAD(F) = 0.0
  655 CONTINUE
      DO 690 F=1,FMAX
      DO 680 JN=1,NMAX
      N = JN- 1
      IF (JN .EQ. 1) GO TO 658
      CFN = (COS(N*3.1416*H(JH))*SIN(N*1.5708*G(JG))/(N*1.5708*G(JG)))
     1 **2
      GO TO 659
  658 CFN = 1.0
  659 IF(JC .GT. 1) GO TO 660
      GLOAD(F) = GLOAD(F) + CFN*GN(JN,F)
  660 IF (JN .GT. 1) GO TO 670
      BCAP(F) = 6.2832 *FREQ(F)*CAP(JC)/(10.**6)
      BLOAD(F) = BCAP(F) + CFN*BN(JN,F)
      GO TO 680
  670 BLOAD(F) = BLOAD(F) +CFN*BN(JN,F)

  680 CONTINUE
      DEN3 = GLOAD(F)**2 + BLOAD(F)**2
      RLOAD(F) = GLOAD(F)/DEN3
      XLOAD(F) = -BLOAD(F)/DEN3
      WRITE (6,15) FREQ(F),RLOAD(F),XLOAD(F)
  690 CONTINUE
      WRITE (6,14)
      WRITE (6,11)
      WRITE (6,18) MK,MK,A(JA),B(JB),W(JW),S(JS),H(JH),G(JG),CAP(JC)
```

```
      CALL PLOT2 (D,FREQ(FMAX),FREQ(1),300.0,-200.0)
      CALL PLOT3 ('R',FREQ,RLOAD,FMAX,4)
      CALL PLOT3 ('X',FREQ,XLOAD,FMAX,4)
      CALL PLOT4 (16,16HREAL & IMAGINARY)
695   CONTINUE
      IF (ZQT .LT. 3) GO TO 699
      DO 1500 KCP=1,CPMAX
      DO 1490 KL=1,LMAX
      DO 1480 KR=1,RMAX
      DO 1470 KC=1,COMAX
      DO 1460 KD=1,DMAX
      WRITE (6,11)
      WRITE (6,19) MK,MK,A(JA),B(JB),W(JW),S(JS),H(JH),G(JG),CAP(JC),
     1 DIST(KD),CP(KCP),L(KL),R(KR),C(KC)
      WRITE (6,26)
      DO 1300 F=1,FMAX
      PHI =2.*DIST(KD)*SQRT(ABS(.2096*(FREQ(F)**2-(14.986/A(JA))**2)))
      RMN(1,1,F)=376.7*B(JB)/(A(JA)*SQRT(ABS(1.-(14.99/(A(JA)*FREQ(F)))
     1 **2)))
      DEN10 = 1.0 + 2.0*RHO*COS(PHI) + RHO*RHO
      GL = (1.0-RHO*RHO)/(2.0*RMN(1,1,F)*DEN10)
      BL = RHO*SIN(PHI)/(RMN(1,1,F)*DEN10)
      OMEGA = 6.2832*FREQ(F)/(10.**3)
      DEN11 = (OMEGA**2*C(KC)*CP(KCP)*R(KR))**2 +(OMEGA*(C(KC)+CP(KCP))
     1 - OMEGA**3*C(KC)*CP(KCP)*L(KL)*10.**3)**2
      RG = (OMEGA*C(KC))**2*R(KR)/DEN11
      XG = -(OMEGA**5*C(KC)**2*CP(KCP)*(L(KL)*10.**3)**2 + OMEGA*(C(KC)
     1 + CP(KCP)) + OMEGA**3*(C(KC)**2*CP(KCP)*R(KR) - C(KC)**2*L(KL)*
     2 10.**3 -2.0*C(KC)*CP(KCP)*L(KL)*10.**3))/DEN11
      DEN12 = RG*RG + XG*XG
      GG = RG/DEN12
      BG = -XG/DEN12
      BCAP(F) = 6.2832 *FREQ(F)*CAP(JC)/(10.**6)
      GAPO = (SIN(1.5708*G(JG))/(1.5708*G(JG)))**2
      BG1 = BG + BLOAD(F) - BN(1,F)*GAPO + BCAP(F)
      DEN13 = GG*GG + BG1*BG1
```

```
      RP1 = GG*GAPO/DEN13
      XP1 = -BG1*GAPO/DEN13
      RS1 = RP1/CF(1)
      XS1 = ((XP1 + XN(1,F))/CF(1)) -XMN(1,1,F)
      RSN(F) = RS1/(RMN(1,1,F)*2.0)
      XSN(F) = XS1/(RMN(1,1,F)*2.0)
      DEN14 = RS1*RS1 + XS1*XS1
      GT = GL + RS1/DEN14
      BT = BL - XS1/DEN14
      DEN15 = GT*GT + BT*BT

      RTN(F) = GT/(DEN15*2.*RMN(1,1,F))
      XTN(F) = -BT/(DEN15*2.*RMN(1,1,F))
      WRITE (6,15) FREQ(F),RSN(F),XSN(F),RTN(F),XTN(F)
 1300 CONTINUE
      WRITE (6,26)
      WRITE (6,11)
      WRITE (6,19) MK,MK,A(JA),B(JB),W(JW),S(JS),H(JH),G(JG),CAP(JC),
     1 DIST(KD),CP(KCP),L(KL),R(KR),C(KC)
      CALL PLOT2 (D,FREQ(FMAX),FREQ(1),2.5,0.0)
      CALL PLOT3 ('R',FREQ,RSN,FMAX,4)
      CALL PLOT3 ('X',FREQ,XSN,FMAX,4)
      CALL PLOT3 ('S',FREQ,RTN,FMAX,4)
      CALL PLOT3 ('Y',FREQ,XTN,FMAX,4)
      CALL PLOT4 (16,16HREAL & IMAGINARY)
 1460 CONTINUE
 1470 CONTINUE
 1480 CONTINUE
 1490 CONTINUE
 1500 CONTINUE
  699 CONTINUE
  700 CONTINUE
  750 CONTINUE
  800 CONTINUE
  850 CONTINUE
  900 CONTINUE
      GO TO 40
      END
```

APPENDIX D

DETERMINATION OF APPROXIMATE AND LIMITING VALUES FOR SMALL COAXIAL LINE DISCONTINUITIES

The necessity to support the center conductor of a coaxial line generally results in the presence of small discontinuities in the line due to the supporting beads. The disruptive effect of such a support bead has been minimized considerably in the last few years with the development of precision 7 mm connectors; however the effect has not been totally removed. Additional discontinuities are introduced when the size or nature of the line is altered. Both of these types of discontinuities, when small, can be approximated by a lumped shunt capacitor. First order compensation is then possible by introducing a small inductance of the proper size adjacent to the discontinuity in series in the line.

In the measurement circuit there are many such discontinuities present, all somewhat compensated to reduce their effect. All of the discontinuities result from step changes in the diameter of the inner or outer conductor. The uncompensated effect can readily be characterized by the equivalent capacitance of such a step using the chart provided in the Microwave Handbook (Ref. 28). A compensated discontinuity will have a somewhat smaller effective capacitance, depending on the design of the circuit; the handbook value thus represents an upper limit.

Consider the circuit of Fig. D.1a where the shunt capacitance is small but fixed, we desire to choose the series inductance so that the input will see a match or Z_c, the characteristic impedance of the line. If

$$Z_{IN} = R_{IN} + j\,X_{IN} \tag{D.1}$$

then

$$X_{IN} \approx 0.0$$

and

$$R_{IN} \approx Z_c$$

for the condition

$$L_o = Z_c^{\,2}\, C_D \tag{D.2}$$

This is not totally unexpected since a differential length of transmission line satisfies the same relationship, e.g.,

$$Z_c = \sqrt{\frac{L_\ell}{C_\ell}} \tag{D.3}$$

where L_ℓ, C_ℓ are inductance and capacitance per unit length. With this in mind, it is possible to interpret the compensated discontinuity as a length of transmission line ℓ,

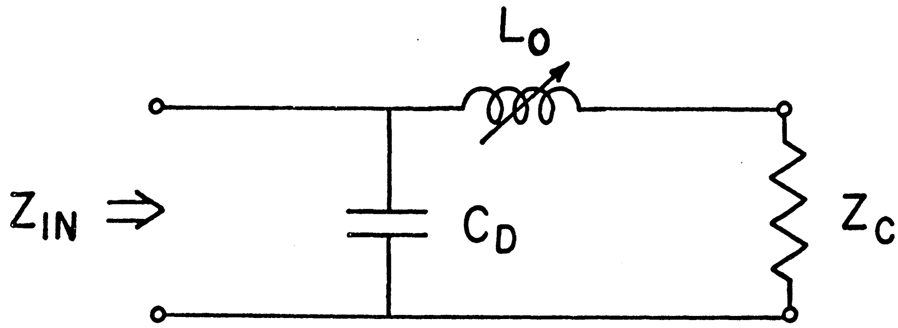

(a)

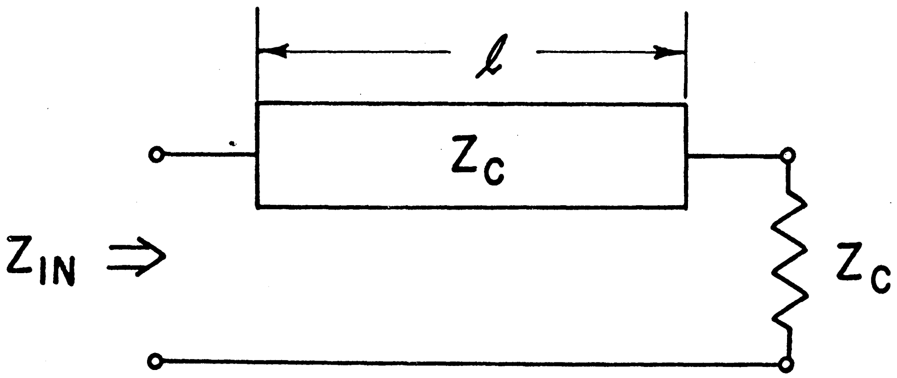

(b)

Fig. D.1 Line length equivalence for a compensated discontinuity.
(a) Discontinuity model.
(b) Equivalent length of Z_c line.

$$\ell = \frac{L_o}{L_\ell} \qquad \text{(D.4)}$$

as shown in Fig. D.1b.

A partially compensated shunt capacitance would result in a reduced capacitance with a short length of line; while an over compensated capacitance would look like an inductor in series. Both of these conditions are seen in the equivalent circuit of Fig. 4.3.

For an example let us consider one of the step discontinuities in the 7 mm to 1.65 mm adapter. The step considered results from changing the diameter of the inner conductor to match a 50 ohm airline to a 50 ohm Teflon line, as shown in Fig. D.2. To compensate, a short length of the Teflon side is without Teflon, thus increasing the characteristic impedance in order to appear inductive relative to 50 ohms. The discontinuity capacitance will be somewhere between 8.8 and 17.9 x 10^{-15} farads (Ref. 28) depending on the distribution of the fringing fields between the air and the Teflon. This distribution will depend on the length t of the high impedance section between the two 50 ohm sections. This short section of 65.2 ohm line can be considered as 50 ohm line with an excess inductance of 2.47 n H/inch. The required compensating inductance for C_D will be

$$L_o = (50)^2 \ (8.8 \times 10^{-15}) = 22.0 \text{ pH} \qquad \text{(D.5)}$$

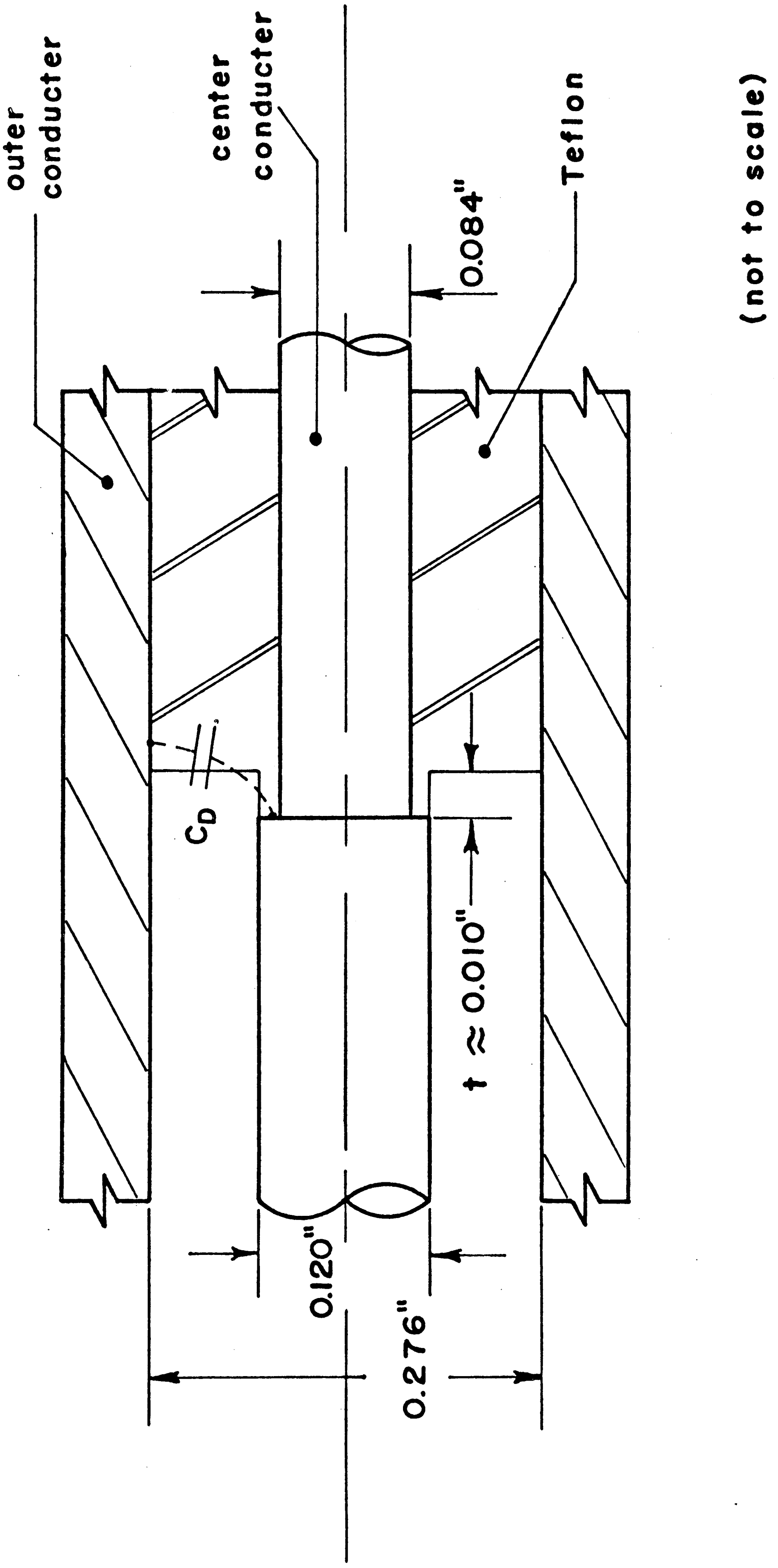

Fig. D.2 Compensated step discontinuity in coaxial line.

assuming all the fringe fields are in the air. Then from (D. 4),

$$t = \frac{22.0 \times 10^{-12}}{2.47 \times 10^{-9}} = 0.009 \text{ inch}$$

representing the minimum compensating length. If we had assumed all of the fringe fields were in the Teflon, then $L_0 = 44.8$ pH and $t = 0.018$ inch. In the adapter used, $t = 0.010$ inch by measurement, leading us to believe that the discontinuity might be slightly under compensated, since it is reasonable to expect that most of the fringe field will in fact be in the Teflon. As it turns out, the effective capacitance was 4.0×10^{-15} farads, determined by the statistical procedure outlined in Section 4.3.1, and is shown as the center capacitor in the 7 mm to 1.65 mm adapter in Fig. 4.3.

This procedure was used to establish approximate values for all of the various discontinuities in the measurement circuit.

APPENDIX E

COMPUTER PROGRAM FOR EXPERIMENTAL DATA INTERPRETATION

A computer program was written to provide an accurate and rapid means of interpreting the data from the impedance measurements. By knowing the standing-wave-ratio, minimum position and frequency, in conjunction with the measurement circuit, it is possible to specify the impedance terminating the circuit which would generate the measured data values.

For convenience, the measurement circuit is broken up into a number of smaller circuits, each of a standard form to simplify the mathematics. The impedance translation through the measurement circuit can then be accomplished by a repetitive operation through each of these standard circuits. Fig. E.1 describes the standard circuit used. Where appropriate various element values are set equal to zero to properly represent a given section of line. The measurement circuit in Fig. 4.3 is made up of eight such standard units.

The results of the program are both listed and plotted as real and reactive parts versus frequency.

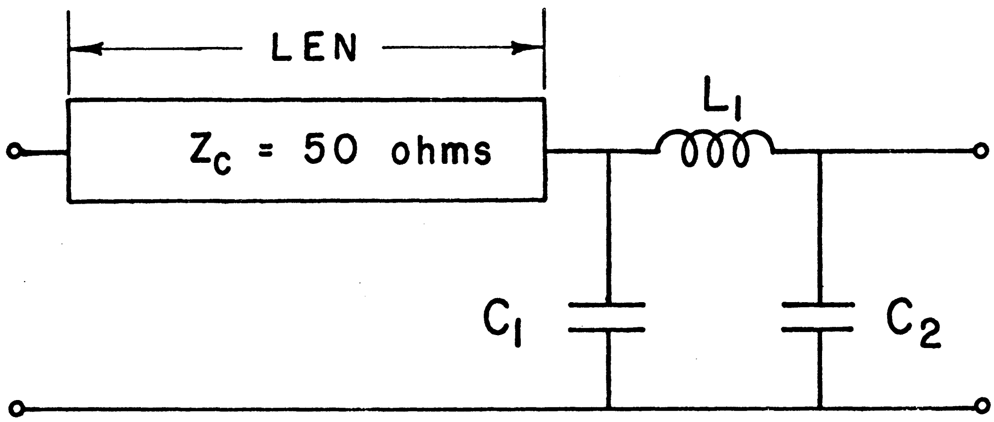

LEN = length of line in centimeters

C_1 , C_2 = capacitances in 10^{-15} Farads

L_1 = inductance in 10^{-12} Henrys

Fig. E.1 Standard circuit unit for data interpretation program.

```
C     THIS PROGRAM TAKES MEASUREMENT DATA AS MINL, SWR(DB),AND
C     FREQUENCY FROM SLOTTED LINE; FIRST CORRECTING THE SWR,THEN
C     TRANSLATING DOWN THROUGH LENGTHS OF LINE PLUS PI NETWORKS UNTIL
C     WE GET A RESULTANT IMPEDANCE.  PROVISIONS FOR VARIOUS PLOTS
C     ARE MADE.  WE GET OUT FREQ,WAVL,SWR(DB),SWR,SWRM,RHO,THETA,
C     RLOAD, AND XLOAD.
      DIMENSION  TITLE(20),FREQ(99),RLOAD(99),XLOAD(99),E(1500),RHO(99),
     1 THETA(99),TL(9),L(9),C1(9),C2(9),TI2(20)
      REAL MINL,L
    1 FORMAT (I2,2X,19A4)
    2 FORMAT(1H0,10X,'NUMBER OF DATA POINTS = ',I2,15X,19A4)
    3 FORMAT (1H0,2X,10HFREQ (GHZ),3X,15HWAVELENGTH (CM),4X,4HMINL,9X,
     1 7HSWR(DB),5X,3HSWR,5X,4HSWRM,5X,3HRHO,8X,5HTHETA,5X,5HRLOAD,
     2 5X,5HXLOAD//)
    4 FORMAT (5X,F7.3,6X,F7.4,7X,F7.4,8X,F6.2,4X,F6.2,4X,F6.2,3X,
     1 F6.4,4X,F7.2,4X,F8.3,3X,F8.3/)
    5 FORMAT (F8.3,2X,F8.4,2X,F5.2)
    6 FORMAT (1H1)
    7 FORMAT (1H ,10X,'NUMBER OF LINE SECTIONS = ',I2,5X,19A4)
    8 FORMAT (F7.3,3X,F6.1,4X,F6.1,4X,F6.1)
    9 FORMAT(1H0,60X,'FREQUENCY  IN  GHZ')
      READ (5,1)LMAX,(TITLE(J),J=1,19)
      WRITE (6,6)
      DO 20 I=1,LMAX
      READ (5,8) TL(I),C1(I),L(I),C2(I)
   20 CONTINUE
      WRITE (6,7) LMAX,(TITLE(J),J=1,19)
   45 READ (5,1) NN  ,(TI2  (J),J=1,19)
   46 WRITE(6,2) NN  ,(TI2  (J),J=1,19)
   47 WRITE (6,3)
   48 DO 50 JJJ=1,NN
      RLOAD (JJJ) =5000.
      XLOAD (JJJ) =5000.
   50 CONTINUE
      DO 200 K=1,NN
```

```
      READ (5,5) FREQ(K),MINL,DB
      WAVL = 29.875/FREQ(K)
      SWR = 10.0**(DB/20.0)
      ER = 0.3 + .01*(FREQ(K)**1.45)
      FAC = 10.0**(ALOG10((SWR+1.0)/(SWR-1.0))-ER/20.)
      SWRM = (FAC+1.0)/(FAC-1.0)
      G = SWRM
      B = 0.0
      PHI = 6.2832*(MINL-TL(1))/WAVL
      DO 75 KK=1,LMAX
      IF (KK .EQ. 1) GO TO 62
   60 PHI = 6.2832*TL(KK)/WAVL
   62 DEN1 = (B*SIN(PHI) +COS(PHI))**2 +(G*SIN(PHI))**2
      G1 = G/DEN1
      B1 = (B*COS(2.*PHI) +.5*SIN(2.*PHI)*(B*B+G*G-1.))/DEN1
      FTR = -(1.-(3.95E-8)*FREQ(K   )**2*C1(KK)*L(KK)+.00012566*FREQ(K
     1)*L(KK)*B1)
      DEN2 = (.00012566*FREQ(K   )*L(KK)*G1)**2 +FTR**2
      G2 = G1/DEN2
      B2 =(((3.95E-8)*FREQ(K   )**2*C2(KK)*L(KK)*B1-(1.24E-11)*FREQ(K   )
     1 **3*C1(KK)*L(KK)*C2(KK) +.00031416*FREQ(K   )*(C1(KK)+C2(KK))-
     2 B1)*FTR +.00012566*FREQ(K   )*L(KK)*G1**2*(1.-(3.95E-8)*FREQ(K   )
     3**2*L(KK)*C2(KK)))/DEN2
      G = G2
      B = B2
   75 CONTINUE
   80 DEN3 = G2*G2 + B2*B2
      RZ = G2/DEN3
      XZ = -B2/DEN3
      TEST = RZ*RZ + XZ*XZ -1.
      RHO(K   ) = SQRT(TEST**2 +4.*XZ*XZ)/((RZ +1.)**2 +XZ*XZ)
      IF (ABS(TEST) .LT. .001) GO TO 90
      THETA(K   ) = (180./3.1416)*ATAN2(2.*XZ,TEST)
      GO TO 92
   90 IF (XZ) 91,91,93
   91 THETA(K   ) = -90.0
```

```
92    IF (THETA(K  ))94,95,95
93    THETA(K  ) = 90.0
94    THETA(K  ) = THETA(K  ) + 360.0
95    RLOAD(K  ) = RZ*50.
      XLOAD(K  ) = XZ*50.
100   WRITE (6,4) FREQ(K),WAVL,MINL,DB,SWR,SWRM,RHO(K),THETA(K),
     1 RLOAD(K),XLOAD(K)
200   CONTINUE
      WRITE (6,3)
      WRITE (6,6)
300   CONTINUE
      CALL PLOT2 (E,22.0,2.0,300.0,-200.0)
      CALL PLOT3 ('R',FREQ,RLOAD,NN  ,4)
      CALL PLOT3 ('X',FREQ,XLOAD,NN  ,4)
      CALL PLOT4(16,16HREAL & IMAGINARY)
      WRITE (6,9)
      WRITE (6,6)
      GO TO 20
      END
```

REFERENCES

1. J. A. Copeland, "Theoretical study of a Gunn diode in a resonant circuit," IEEE Trans. on Electron Devices, Vol. ED-14, No. 2, February 1967, pp. 55-58.

2. W. J. Evans, "Circuits for high-efficiency avalanche-diode oscillators," IEEE Trans. on Microwave Theory and Techniques, Vol. MTT-17, No. 12, December 1969, pp. 1060-1067.

3. D. H. Steinbrecker, "Efficiency limits for tuned harmonic multipliers with Punch-Through Varactors," International Solid-State Circuits Conference Digest of Technical Papers, University of Pennsylvania, Philadelphia, February 15-17, 1967.

4. W. J. Getsinger and A. H. Kessler, "Computer-design of diode using microwave components, and a computer-dimensioned, X-band parametric amplifiers," Microwave Journal, March 1969, pp. 119-123.

5. MIT Radiation Laboratory Series, McGraw-Hill, New York Vols. 1-28, 1946-1948.

6. A. Uhlir, Jr., "The potential of semiconductor diodes in high frequency communications," Proc. IRE, Vol. 6, No. 6, June 1958, pp. 1099-1115.

7. D. Leenov, "Gain and noise figure of a variable-capacitance upconverter," B.S.T.J., July 1958, pp. 989-1008.

8. H. Heffner and G. Wade, "Gain bandwidth and noise characteristics of the variable-parameter amplifier," J. Appl. Phys., Vol. 29, No. 9, September 1959, pp. 1321-1331.

9. B. J. Robinson, "Theory of variable-capacitance parametric amplifiers," IEE Monograph, No. 480 E, November 1961.

10. K. Kurokawa and M. Uenohara, "Minimum noise figure of the variable-capacitance amplifier," B.S.T.J., May 1961, pp. 695-722.

11. D. Leenov and A. Ulhir, Jr., "Generation of harmonics and subharmonics at microwave frequencies with P-N junction diodes," Proc. IRE, Vol. 47, No. 10, October 1959, pp. 1724-1729.

12. D. B. Leeson and S. Weinreb, "Frequency multiplication with nonlinear capacitors - - A circuit analysis," Proc. IRE, Vol 47, No. 12, December 1959, pp. 2076-2084.

13. W. J. Getsinger, "The packaged and mounted diode as a microwave circuit," IEEE Trans. on Microwave Theory and Techniques, Vol. 14, No. 2, February 1966, pp. 58-59.

14. W. J. Getsinger, "Mounted diode equivalent circuits," IEEE Trans. on Microwave Theory and Techniques, Vol. MTT-15, No. 11, (Correspondence), November 1967, pp. 650-651.

15. E. Yamashita and J. R. Baird, "Theory of a tunnel diode oscillator in a microwave structure," Proc. IEEE, Vol. 54, No. 4, April 1966, pp. 606-611.

16. D. C. Hanson and J. E. Rowe, "Microwave circuit considerations of bulk GaAs oscillators," IEEE Trans. of Electron Devices, Vol. 14, No. 9, September 1967, pp. 469-476.

17. P. S. Carter, "Circuit relations in radiating systems and applications to antenna problems," Proc. IRE, Vol. 20, June 1932, pp. 1004-1041.

18. R. E. Collin, Field Theory of Guided Waves, New York: McGraw-Hill, 1960, pp. 39-40.

19. C. T. Tai, Dyadic Green's Functions in Electromagnetic Theory, International Text Book Company (in press).

20. H. Jasik, Antenna Engineering Handbook, McGraw-Hill, 1961, Chapter 3, p. 7.

21. S. A. Schelkunoff, "Impedance concepts in waveguides," Quart. Appl. Math., Vol. II, April 1944, p. 7.

22. M. K. McPhun, "Comparison of TEM with waveguide-below cutoff resonators," Electronic Letters, Vol. 5, No. 18, September 4, 1969, pp. 425-426.

23. S. B. Cohn, "Characteristic impedance of the shielded-strip transmission line," Trans. IRE, Vol. MTT-2, July 1954, pp. 52-57.

24. R. L. Eisenhart, "Derivation of parametric multifrequency coupling coefficients," Proc. IEEE (Letters), Vol. 58, No. 3, March 1970, pp. 495-496.

25. P. J. Khan, "Advanced phase-shift amplifier study," Tech. Report ECOM-0029-F, Contract No. DA 28-043 AMC-00029(E) Cooley Electronics Laboratory, The University of Michigan, Ann Arbor, May 1967.

26. N. Marcuvitz, Waveguide Handbook, Vol. 10, MIT Radiation Laboratory Series; 1951, McGraw-Hill, pp. 227-228.

27. A. Sommerfield, "Partial differential equations in physics," Lectures on Theoretical Physics, Vol. VI, Academic Press, New York, N.Y., 1967, p. 189.

28. Microwave Engineers Technical and Buyers Guide Edition, Horizon-House, Dedham, Massachusetts, 1969, p. 36.

DISTRIBUTION LIST

No. of copies	
20	National Security Agency Fort George G. Meade, Maryland 20755
1	Technical Library Dir. of Defense Research and Engineering Rm. 3E-1039, The Pentagon Washington, D.C. 20301
1	Defense Intelligence Agency Attn: DIARD Washington, D.C. 20301
2	Director National Security Agency Attn: C31 Fort George G. Meade, Maryland 20755
1	Naval Ships Systems Command Attn: Code 20526 (Technical Library) Main Navy Building, Rm. 1528 Washington, D.C. 20325
1	Naval Ships Systems Command Attn: Code 6179 B Department of the Navy Washington, D.C. 20360
2	Director U.S. Naval Research Laboratory Attn: Code 2027 Washington, D.C. 20390

DISTRIBUTION LIST (Cont.)

No. of copies	
1	Commanding Officer and Director U.S. Navy Electronics Laboratory Attn: Library San Diego, California 92152
1	Commander U.S. Naval Ordnance Laboratory Attn: Technical Library White Oak, Silver Spring, Maryland 20910
1	Dir. Marine Corps Landing Force Dev Ctr Attn: C-E Division Marine Corps Schools Quantico, Virginia 22134
1	Commandant of the Marine Corps (Code AO2F) Headquarters, U.S. Marine Corps Washington, D.C. 20380
1	Rome Air Development Center (EMTLD) Attn: Documents Library Griffiss Air Force Base New York 13440
1	U.S. Army Security Agency Test and Evaluation Center Fort Huachuca, Arizona 85613 Code IAOVT
2	Electronic Systems Division (ESTI) L. G. Hanscom Field Bedford, Massachusetts 01730

DISTRIBUTION LIST (Cont.)

No. of copies	
1	U.S. Air Force Security Service Attn: TSG, VICE Attn: ESD San Antonio, Texas 78241
1	ADTC (ADBRL-2) Eglin Air Force Base, Florida 32542
1	Headquarters, AFSC Attn: SCTSE Bolling AFB, D.C. 20332
1	Air University Library (3T) Maxwell Air Force Base Alabama 36112
1	HQ, USAF Tactical Air Recon Ctr (TAC) Department of the Air Force Shaw Air Force Base, South Carolina 29152
2	Chief of Research and Development Department of the Army Washington, D.C. 20315
2	Commanding General U.S. Army Materiel Command Attn: R&D Directorate Washington, D.C. 20315
3	Redstone Scientific Information Center Attn: Chief, Document Section U.S. Army Missile Command Redstone Arsenal, Alabama 35809
1	Headquarters U.S. Army Weapons Command Attn: AMSWE-RDR Rock Island, Illinois 61201

DISTRIBUTION LIST (Cont.)

No. of copies	
1	Commanding Officer U.S. Foreign Science & Tech Ctr Attn: AMXST-RD-R, Munitions Bldg Washington, D.C. 20315
1	Director, National Security Agency Attn: N-2, Mr. Sherwood Fort George G. Meade, Maryland 20755
2	Commanding Officer Aberdeen Proving Ground Attn: Technical Library, Bldg. 313 Aberdeen Proving Ground, Maryland 21005
2	Headquarters U.S. Army Materiel Command Attn: AMCMA-RM/3 Washington, D.C. 20315
1	Commanding General U.S. Army Combat Developments Command Attn: CDCMR-E Fort Belvoir, Virginia 22060
3	Commanding Officer U.S. Army Combat Developments Command Communications-Electronics Agency Fort Monmouth, New Jersey 07703
1	Commander U.S. Army Research Office (DURHAM) Box CM-DUKE Station Durham, North Carolina 27706

DISTRIBUTION LIST (Cont.)

No. of copies	
1	Commanding Officer U.S. Army Sec Agcy Combat Dev ACTV Arlington Hall Station Arlington, Virginia 22212
1	U.S. Army Security Agency Attn: OACofS, DEV Arlington Hall Station Arlington, Virginia 22212
1	U.S. Army Security Agcy Processing Ctr Attn: IAVAPC-R&D Vint Hill Farms Station Warrenton, Virginia 22186
1	Technical Support Directorate Attn: Technical Library Bldg 3330, Edgewood Arsenal Maryland 21010
2	U.S. Army Research and Dev Command Branch Library, Bldg 5695 Nuclear Effects Laboratory Edgewood Arsenal, Maryland 21010
1	Harry Diamond Laboratories Attn: Library Connecticut Avenue and Van Ness Street Washington, D.C. 20438
1	Commandant U.S. Army Air Defense School Attn: C&S Dept. MSL SCI DIV Fort Bliss, Texas 79916

DISTRIBUTION LIST (Cont.)

No. of copies	
1	Commanding General U.S. Army Electronic Proving Ground Attn: Technical Information Center Fort Huachuca, Arizona 85613
1	Asst. Secretary of the Army (R&D) Department of the Army Attn: Deputy Asst. for Army (R&D) Washington, D.C. 20315
1	Commanding Officer U.S. Army Limited War Laboratory Aberdeen Proving Ground, Maryland 21005
1	CH, Special Techniques Division Unconventional Warfare Department U.S. Army Special Warfare School Fort Bragg, North Carolina 28307
1	USAECOM Liaison Office U.S. Army Electronic Proving Ground Fort Huachuca, Arizona 85613
1	Office, AC of S for Intelligence Department of the Army Attn: ACSI-DSRS Washington, D.C. 20310
1	Chief, Mountain View Office EW Lab USAECOM Attn: AMSEL-WL-RU P.O. Box 205 Mountain View, California 94042
1	Chief, Intelligence Materiel Dev Office Electronic Warfare Lab, USAECOM Fort Holabird, Maryland 21219

DISTRIBUTION LIST (Cont.)

No. of copies	
1	Chief Missile Electronic Warfare Tech Area EW Lab, USA Electronics Command White Sands Missile Range, N.M. 88002
1	Headquarters U.S. Army Combat Developments Command Attn: CDCLN-EL Fort Belvoir, Virginia 22060
1	USAECOM Liaison Officer MIT, Bldg. 26, Rm. 131 77 Massachusetts Avenue Cambridge, Massachusetts 02139
18	Commanding General U.S. Army Electronics Command Fort Monmouth, New Jersey 07703 Attn: 1 AMSEL-EW 1 AMSEL-PP 1 AMSEL-IO-T 1 AMSEL-GG-DD 1 AMSEL-RD-LNJ 1 AMSEL-XL-D 1 AMSEL-NL-D 1 AMSEL-VL-D 1 AMSEL-KL-D 3 AMSEL-HL-CT-D 1 AMSEL-BL-D 3 AMSEL-WL-S 1 AMSEL-WL-S (office of records) 1 AMSEL-SC
1	Dr. T. W. Butler, Jr., Director Cooley Electronics Laboratory The University of Michigan Ann Arbor, Michigan 48105
24	Cooley Electronics Laboratory The University of Michigan Ann Arbor, Michigan 48105

Security Classification

DOCUMENT CONTROL DATA - R & D

(Security classification of title, body of abstract and indexing annotation must be entered when the overall report is classified)

1. ORIGINATING ACTIVITY *(Corporate author)*

Cooley Electronics Laboratory
University of Michigan
Ann Arbor, Michigan 48105

2a. REPORT SECURITY CLASSIFICATION

2b. GROUP

3. REPORT TITLE

Impedance Characterization of a Waveguide Microwave Circuit

4. DESCRIPTIVE NOTES *(Type of report and inclusive dates)*

Cooley Electronics Laboratory Technical Report No. 208

5. AUTHOR(S) *(First name, middle initial, last name)*

Robert L. Eisenhart

6. REPORT DATE	7a. TOTAL NO. OF PAGES	7b. NO. OF REFS
February 1971		28

8a. CONTRACT OR GRANT NO.	9a. ORIGINATOR'S REPORT NUMBER(S)
DAAB07-68-C-0138	01482-21-T TR208
b. PROJECT NO. 1H021101 A042.01.02	
c.	9b. OTHER REPORT NO(S) *(Any other numbers that may be assigned this report)*
d.	ECOM-0138-21-T

10. DISTRIBUTION STATEMENT This document is subject to special export controls and each transmittal to foreign governments or foreign nationals may be made only with prior approval of CG, U.S. Army Electronics Command, Fort Monmouth, N. J. Attn: AMSEL-WL-S.

11. SUPPLEMENTARY NOTES	12. SPONSORING MILITARY ACTIVITY
	U.S. Army Electronics Command Fort Monmouth, New Jersey 07703 Attn: AMSEL-WL-S

13. ABSTRACT The induced e.m.f. method has been extended and applied to derive the driving point impedance of a common waveguide structure used for mounting small microwave devices. The resulting mathematical relationship has been conceptually interpreted as an equivalent coupling circuit, terminated by a set of impedances which are associated with the many modes within the waveguide. Properties of this circuit and its terminations are discussed in detail. In addition the multilateral nature of the circuit allows consideration of the mount in the waveguide as an obstacle to any incident propagating mode. The driving point impedance of this mount was also considered from the experimental viewpoint. An investigation was carried out to check and support the results of the theoretical analysis. A novel measurement technique was employed, based upon the use of subminiature coaxial line to gain electrical access to a terminal pair located inside the waveguide. An extensive model of the measurement circuit was developed, which enhanced the accuracy of the data interpretation, and provided excellent agreement between these values and the theory. It is anticipated that this formulation will permit accurate design of many components which previously required empirical methods based on limited experimental data.

Security Classification

14. KEY WORDS	LINK A		LINK B		LINK C	
	ROLE	WT	ROLE	WT	ROLE	WT
Waveguide device mounting structure						
Driving point impedance						
Equivalent circuit						
Multimode						
Mode impedance						
Obstacle impedance						
Impedance measurement						